AN EXPERIMENTAL INVESTIGATION OF ELECTRIC FIELD INTENSITY AND WALL HEAT TRANSFER FOR THE HEATING REGION OF A CONSTRICTED ARC PLASMA

by

Larry Allan Lukens

AN EXPERIMENTAL INVESTIGATION OF ELECTRIC FIELD INTENSITY AND WALL HEAT TRANSFER

For The

HEATING REGION OF A CONSTRICTED ARC PLASMA

A Thesis

Submitted to the Faculty

of

Purdue University

by

Larry Allan Lukens

In Partial Fulfillment of the
Requirements for the Degree

of

Doctor of Philosophy

June 1971

To Charlie

ACKNOWLEDGMENTS

The author is grateful to have been afforded the opportunity to serve as a member of the HTGDL staff. He is particularly indebted to his major professor, Dr. Frank P. Incropera, for his generous offering of counsel, helpful suggestions, and encouragement during the course of the research.

For their participation in many provocative and informative discussions, the author extends sincere thanks to his colleagues in the High Temperature Gas Dynamics Laboratory. He is especially grateful to Messrs. Kim Clark, Bob Giannaris, and William Bower for their discussions relating to arc physics.

The author acknowledges N. Balasubramania for his invaluable assistance in the fabrication of the radiation gage.

He further acknowledges the technical staff of the School of Mechanical Engineering for assisting in the development of the experimental facility and diagnostic hardware.

For serving as advisory committee members, sincere thanks are extended to Professors J.G. Skifstad, P.W. McFadden, R. Goulard, and R. J. Schoenhals.

For permitting him the opportunity to pursue this course of study, the author is indebted to the United States Navy.

The author greatly appreciates the perseverance and quality of workmanship given by Mrs. Bette Freeman and Mrs. Karen Shively in the typing of the manuscript and by Mr. Jean Baladi in the preparation of the figures.

For providing him a constant source of encouragement and understanding, the author is forever grateful to his wife and children.

TABLE OF CONTENTS

TABLE OF CONTENTS (Cont'd.)

LIST OF TABLES

LIST OF FIGURES

LIST OF SYMBOLS

English Letter Symbols

Ag	Linearized relationship between the electrical conductivity and the heat flux potential, ϕ, used in the Stine-Watson model
C_2, C_3, C_4	Constants used in the Stine-Watson model
C_p	Specific heat at constant pressure
D,d	Duct diameter
e	Electronic charge
E	Duct wall potential
E_x	Electric Field intensity
h	Gas enthalpy, heat transfer conductance
H	Total irradiation
H_λ	Monochromatic irradiation
I	Arc current
I_a	Current drawn from duct wall
I_{ion}	Energy of recombination
k	Thermal conductivity, Boltzmann constant
k'	Translational thermal conductivity
k_{EFF}	Effective thermal conductivity ($k_{EFF} = k' + \lambda_R$)
L	Total (cathode to anode) duct length
M_A	Atomic weight

$\dot{m}$	Operating gas flow rate
n	Principal quantum number
Nu	Nusselt number
Oh	Ohmic heating parameter
p	Static pressure
P_R	Radiation source density
PLC	Power loss to the cathode cooling water
PLS	Power loss to the duct segment cooling water
q	Total wall heat flux
$\bar{q}$	Heat flux vector
Q_A	Anode total wall heat flux
q_{conv}	Convective wall heat flux
q_{rad}	Radiative wall heat flux
q_{rad}/q	Fraction of radiative to total wall heat flux
r	Radial coordinate
R	Duct radius
R_b	Ballast resistance
R_s	Internal resistance of the power supply
T	Temperature
T_e	Electron temperature
T_h	Heavy-particle temperature
T_w	Duct wall temperature
T_{inlet}	Operating gas inlet temperature

u	Axial velocity component
$U_A, U_{A'}$	Anode fall potential
x	Axial coordinate
Δx	Duct segment width (= 0.632 cm)

Greek Letter Symbols

α	Degree of ionization, total absorptance
α_λ	Monochromatic absorptance
ε	Total emittance
λ	Wavelength
λ_R	Reactive thermal conductivity
μ	Viscosity
π	3.14159 ...
ρ	Mass density, total reflectance
ρ_λ	Monochromatic reflectance
σ	Electrical conductivity
τ_v	Optical depth
ϕ	Heat flux potential (= $\int k dT$)
ϕ_A	Work function of anode material

Subscripts

a	Asymptotic Conditions
A	Anode conditions
m	Properties evaluated at the temperature corresponding to the mixed-mean enthalpy, h_m

Subscripts

a	Asymptotic Conditions
A	Anode conditions
m	Properties evaluated at the temperature corresponding to the mixed-mean enthalpy, h_m

Subscripts

a	Asymptotic Conditions
A	Anode conditions
m	Properties evaluated at the temperature corresponding to the mixed-mean enthalpy, h_m

ABSTRACT

Lukens, Larry Allan, Ph.D., Purdue University, March 1971. An Experimental Investigation of Electric Field Intensity and Wall Heat Transfer for the Heating Region of a Constricted Arc Plasma. Major Professor: Frank P. Incropera.

Electric field intensity and total wall heat transfer measurements have been performed for the inlet, asymptotic, and anode regions of a laminar, atmospheric cascade arc. In addition to the diagnostics required for these measurements, a unique radiation gage has been developed and used to obtain radiative wall heat flux data. While the majority of the measurements have been made for an argon arc, some data are reported for helium and nitrogen arcs.

Comparisons between the experimental data and available equilibrium and nonequilibrium numerical solutions are presented in an attempt to ascertain the adequacy of single-fluid models to accurately describe overall arc energetics. For the most part, the equilibrium theory predictions for the asymptotic region in an argon arc agree with the experimental results to within the combined experimental and theoretical uncertainties. However, there is a small, but discernable nonequilibrium

effect at both the lower and higher arc currents in argon. In contrast, the nonequilibrium theory predictions are in excellent agreement with the experimental results over the entire range of asymptotic conditions investigated in argon. Further comparisons are presented which indicate that atmospheric helium arcs are characterized by a significant departure from local thermodynamic equilibrium.

On the basis of comparisons between experiment and theory for the anode region, it is shown that anode heat balance models are ill-suited for providing design estimates for the total heat flux to the anode of the arc constrictor.

CHAPTER I INTRODUCTION

I.1 General Objectives of This Study

Owing to interest in space flight technology, MHD systems, and thermonuclear energy conversion, considerable effort has been devoted to the study of high temperature gas flows. Of particular interest to this study is that portion of this effort which deals with a device which has long served as a versatile tool in generating high temperature gases for both industrial and laboratory use - the plasma arc generator.

Designed initially by Maecker[1], the operation of the Gerdien, or constricted tube, arc generator is based upon the conversion of electrical to thermal energy. In the most common configuration (Figure I.1), this conversion is accomplished by passing a gas through an electric arc which is established by applying a d-C potential between the electrodes.

The constricted tube arc produces a continuous and well-defined plasma flow which, in addition to its use in certain technological applications, is particularly useful for the experimental determination of high temperature gas transport properties and the development of high

temperature diagnostic techniques. Irrespective of its use, however, the constricted tube arc is distinguished by extremely high heat fluxes to the containing walls and these walls are often destroyed if sufficient cooling is not provided. Accordingly, an understanding of the electrical and thermal characteristics of arc constrictors is important to the designer as well as to those with a general interest in arc physics. The objective of this study is to enhance this understanding through an experimental investigation of the electrical and thermal effects in an atmospheric cascade arc and through an interpretation of these effects in terms of available theoretical studies. While the major portion of the experimental work has been performed for an argon plasma, some measurements have also been made for nitrogen and helium arcs.

The regions of interest for the cascade arc are depicted schematically in Figure I.1. The arc column, which is a composite of individually water-cooled and electrically isolated copper discs, is divided into three distinct regions: inlet, asymptotic, and anode. The gas flow in each region is subjected to an externally applied electric field, and the inlet and asymptotic regions are generally bounded by non-current-carrying surfaces. In contrast, the anode surface is electrically conducting.

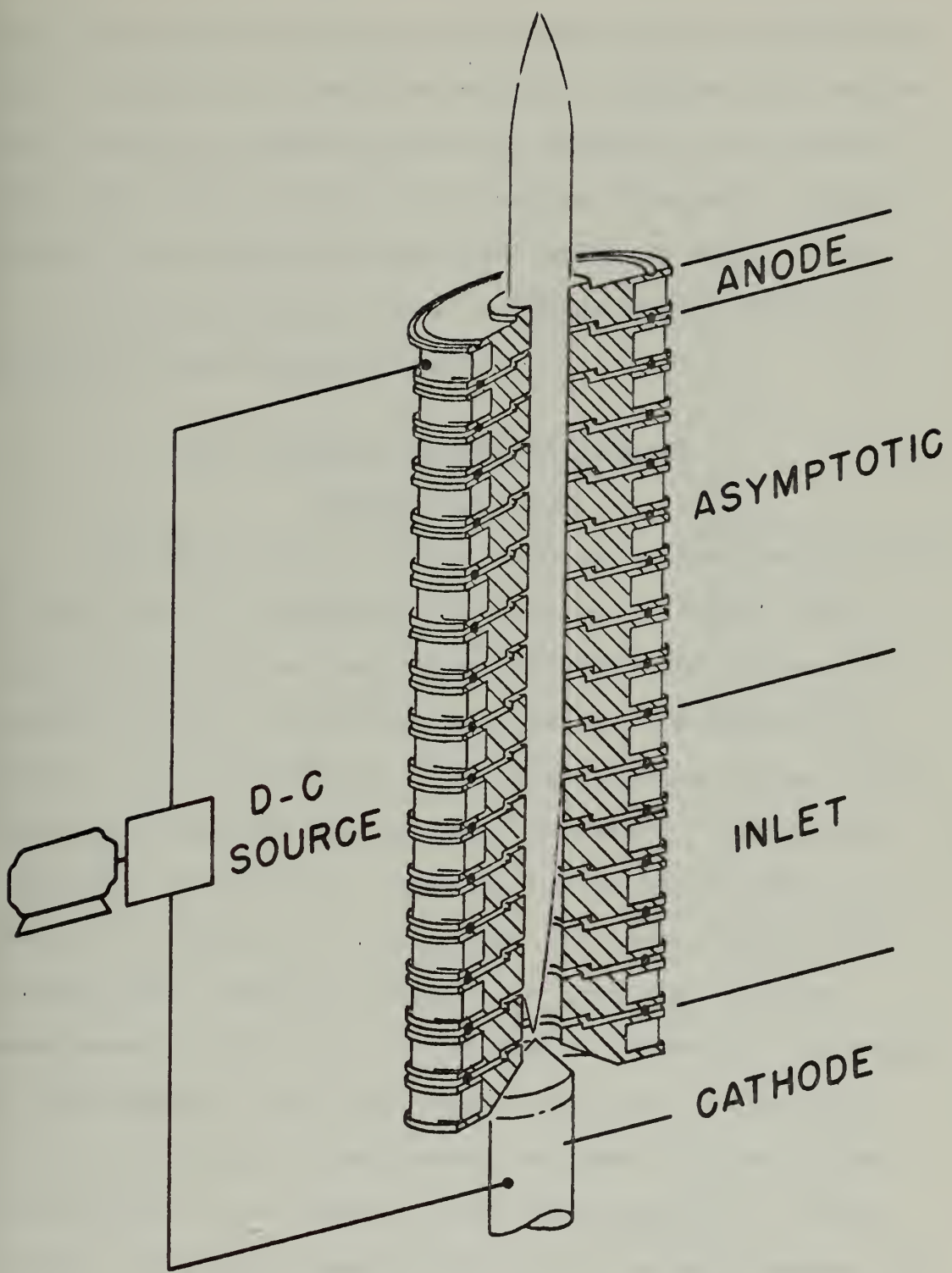

Figure I.1 Designation of Arc-Heating Regions

The inlet region is further distinguished by a significant axial variation of the flow variables, whereas the asymptotic region is characteristic of thermally fully-developed flow. As a matter of convention, the axial location at which the mean (mass averaged) enthalpy attains 90% of its fully-developed value is chosen to mark the beginning of the asymptotic region.

I.2 Previous Investigations of Plasma Tube Flow

Although the literature devoted to theoretical study of the inlet and asymptotic regions is extensive, few experimental studies have been performed for purposes of determining the overall arc energetics. Of particular scarcity are experimental studies pertaining to the inlet region of the water-cooled duct. Skifstad[2] performed electrical potential and wall heat flux measurements in the inlet region of a helium arc, and investigators at the NASA-AMES Research Center[3-5] have made similar measurements in air and nitrogen arcs. However, the range of experimental conditions (gas flow rate, arc current, and duct geometry) investigated in these studies differ significantly from those of this investigation. Consequently, meaningful comparisons cannot be made between the data of this study and the experimental results reported

by these investigators. Similarly, Pfender, et al.[6,7] report results for the local wall heat flux in the inlet region of an argon cascade arc; however these measurements were for turbulent flow and were used primarily for the support of anode heat transfer studies.

A greater number of experimental investigations have been performed for the asymptotic region of the arc[8-15]. While these studies are primarily concerned with the use of an inversion method to determine plasma transport properties, they necessarily include measurement of the arc-column electrical characteristics and are therefore germane to this study*. In addition, Morris, et al.[14] present asymptotic wall heat flux data and Emmons[13] and Maecker[15] report on the percentage contribution of radiation to the total energy balance.

In view of the excellent reviews given by Skifstad[16] and, more recently, by Bower[17], the present discussion of theoretical investigations is limited to those studies which are to be used for comparison with experiment in Chapter IV.

The approximate analytical solution by Stine and Watson[18] was one of the first reported theoretical treatments of the inlet region of the cascade arc. This

---

* The inversion method of property determination will be discussed further in Chapter IV.

solution is based upon a reduced form of the governing energy equation, obtained by neglecting radiation, radial convection, and viscous dissipation. In addition, the Stine-Watson model assumes a uniform mass flux throughout the constrictor and uses linearized relationships between the enthalpy and related properties (T, k/C_p, and σ). The primary weakness of this model is its failure to properly account for the variation of the transport properties with temperature and, particularly when applied to the higher temperature argon and nitrogen arcs, its failure to account for radiative losses.

To remove the need for the above assumptions, detailed numerical solutions for the inlet region have been carried out by Watson and Pegot[19] and by Bower and Incropera[20]. Of the two, the latter will be used for the comparisons of this study since it gives greater consideration to pertinent thermal effects. Specifically, Bower and Incropera formulate a rigorous equilibrium model for the laminar, steady, and axially symmetric (without swirl) flow of an atmospheric argon plasma through the heating region of a constricted tube arc. An implicit finite-difference scheme[17] is then used to solve the resulting conservation equations (mass, momentum, and energy) consistent with the thermal and caloric equations

of state, Ohm's law, and the temperature dependence of the required thermodynamic and transport properties. Implicit in the final form of the equations are the boundary layer approximations and the assumptions of negligible radial current density, quasi-neutrality, and local thermodynamic equilibrium. The results of this numerical solution are presented in the form of wall heat transfer and shear stress (as predicted from energy and momentum balances) and correlations between the mean Nusselt number and an Ohmic heating parameter.

As a result of the evolution of the aforementioned numerical solutions, it would appear that the theoretical treatment of the inlet and asymptotic regions of arc constrictors has reached a practical limit. However, the variable tube diameter experiments performed by Emmons[13] and, more recently, the spectroscopic measurements conducted by Bott[21] and by Incropera and Giannaris[22] provide strong experimental evidence of the presence of nonequilibrium in confined plasmas. Accordingly, the validity of the local thermodynamic equilibrium assumption which is implicit in the single-fluid model is subject to question.*

---

* A comprehensive discussion of local thermodynamic equilibrium in confined plasmas is given in references[22] and [23].

In an attempt to account for the nonequipartition of species translational energies (thermal nonequilibrium), Pytte and Winsor[24] formulated a nonequilibrium theory for the asymptotic region of a helium arc. This attempt, however, is at best, semi-empirical, for its solution relies upon experimentally determined arc-column characteristics. In addition, the Pytte-Winsor model suffers from use of the Saha (equilibrium) equation to compute the plasma composition.

While accounting for both thermal nonequipartition and chemical nonequilibrium, Clark[25] has formulated a rigorous multifluid (electrons, ions, and neutral atoms) model for the steady, laminar flow of a nonequilibrium argon plasma in the inlet and asymptotic regions of a constricted tube arc. After applying the boundary layer approximations, the governing set of species and global conservation equations, along with the thermally perfect gas equation of state and Ohm's law, are solved numerically using finite-difference techniques[25]. Of particular interest to this study are the predictions for the asymptotic electric field intensity, total wall heat flux, and ratio of radiative to total wall heat flux which result from the nonequilibrium solution.

The need for extended operating times for the most severely heated component of the arc constrictor, the

anode, has prompted considerable research on the complex energy exchange mechanisms occurring at this surface. Energy transfer models have been proposed in which the various contributions to the total anode heat flux are delineated. For the most part, these models are based on a heat balance across the anode surface[6,7,26-29]*. In addition, extensive studies of the electrical characteristics of anodes have been conducted by researchers at Dartmouth[31-33]. For purposes of comparison with the anode heat transfer measurements of this study, primary emphasis will be placed upon the widely used model which is described by Pfender, et al.[6].

I.3 Scope and Specific Objectives of This Study

The primary objective of this study is the measurement of the axial distribution of the electric field intensity and the total wall heat flux for the inlet, asymptotic, and anode regions of an atmospheric argon cascade arc. These measurements are made for a wide range of laminar flow operating conditions. Additional measurements are made to determine the ratio of radiative to total wall heat flux for the asymptotic region of an argon arc**. An important secondary objective includes

---

* A review of the subject of anode heat transfer for various electrode geometries is given by Eckert and Pfender[30].

** A review of the literature pertinent to this subject is presented in the Appendix.

comparison of the asymptotic wall heat transfer and electric field intensity measurements with the experimental data of other investigators and with the analytical and equilibrium and nonequilibrium numerical solutions described previously. With respect to the latter, particular attention is given to ascertaining both the validity of existing Nusselt number correlations and the adequacy of single-fluid models for the description of arc energetics. Pursuant to gaining additional information on anode physics and the suitability of anode heat transfer correlations, further comparisons are made with existing anode heat transfer models. The measurements are also of value in providing an improved understanding of the development length characteristics of the constricted tube, laminar arc. In order to ascertain the influence of operating gas, additional experimental results are presented for nitrogen and helium arcs.

This study, which is the first serious attempt to experimentally verify existing equilibrium and nonequilibrium theoretical predictions of thermal parameters for the arc heating region, is intended to provide information useful to the arc designer and to contribute to an improved understanding of arc physics and flow modeling.

CHAPTER II ARC GENERATOR AND DIAGNOSTIC TECHNIQUES

II.1 Arc Generator and Supporting Systems

A well-defined, stable plasma flow is achieved through use of a constricted tube plasma arc generator manufactured by Creare Inc.[34] (Figure II.1). The constrictor is formed by stacking together a series of individually water-cooled copper segments (discs), each of which is 0.632 cm wide with a 1.0 cm central bore. Each segment is electrically insulated from adjoining segments by cool O-ring seals which further provide for alignment and hermetic sealing of the duct. The lengths of the arc heating and field-free regions may be varied according to the anode location and the number of segments used to form the stack (up to a maximum of 40). The thoriated tungsten cathode is water cooled and may be precisely centered with respect to the initial nozzle-shaped segment through micrometer adjustment. The cathode-nozzle geometry provides for a high degree of flow symmetry which, along with water cooling, provides for extended cathode life. If the tungsten tip of the cathode is periodically (every 20 hours) re-shaped on a lathe such that the proper

Figure II.1 Plasma Generator Assembly

LEGEND

1. Axial Micrometer
2. Lateral Micrometer
3. Cathode Plenum Window
4. Cathode
5. Sintered Ring
6. Coolant Manifold Seal Plate
7. Duct Segments
8. Segment Water Tubes
9. Anode
10. Stack Cooler
11. Coolant Distribution Manifold
12. Exhaust Collector
13. Vacuum Lock
14. Cooling Water Connections

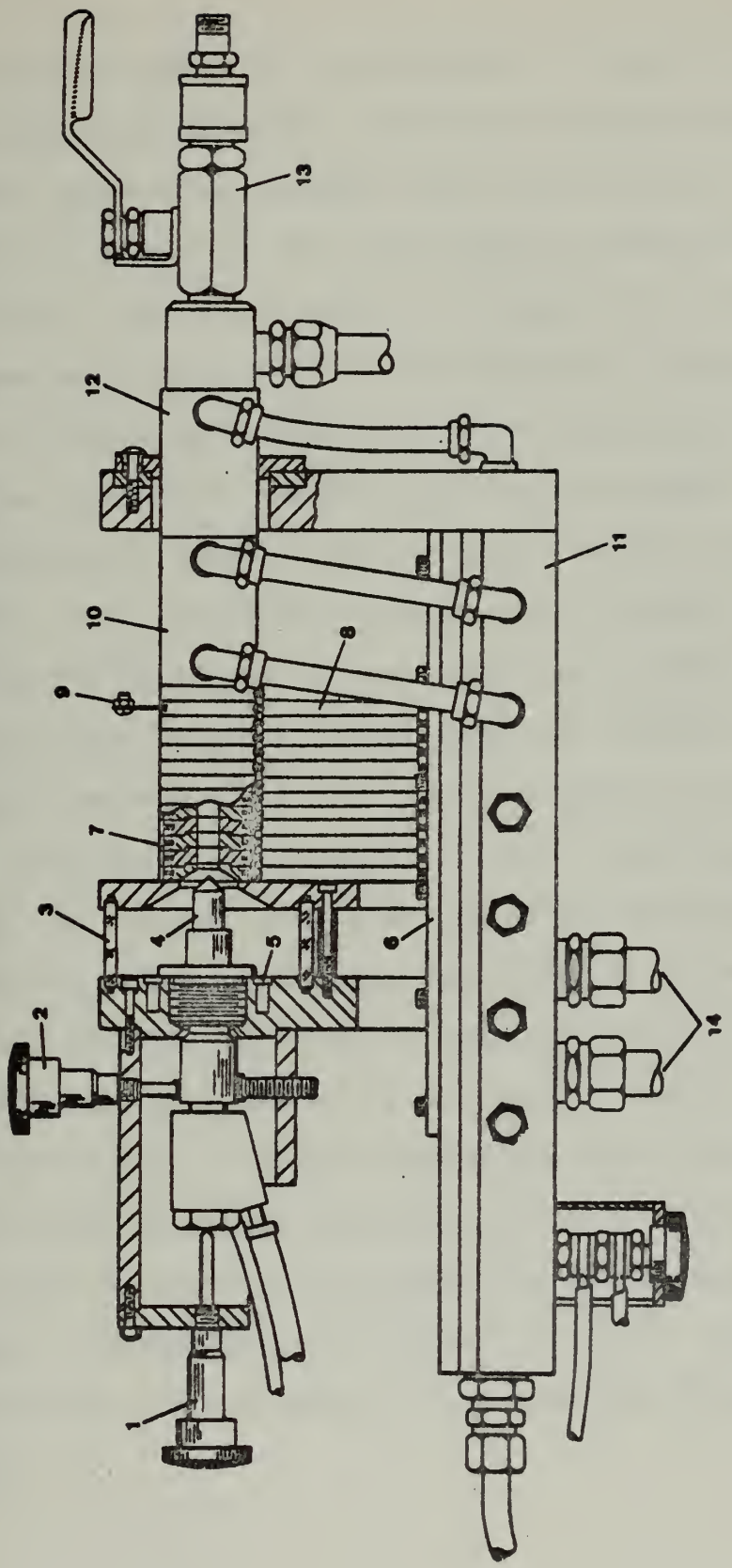

Figure II.1

cathode-nozzle geometry is maintained, a single cathode will provide approximately 100 hours of operation.

The supporting systems which are necessary to sustain the arc generator are illustrated schematically in Figure II.2. Electrical power is supplied by a D-C motor-generator set capable of delivering 75 kw at 300 amperes. Stable operating conditions are achieved through use of two, step-wise variable ballast resistors which are connected in series with the power supply and arc generator. The electrical system will allow for the use of either r-f discharge or prod starting procedures.

The main coolant system supplies cooling water to the plasma generator coolant manifold and to the main ballast resistor. The manifold in turn distributes cooling water to the cathode, the starting prod, those segments which do not serve as calorimeters, and to the additional downstream ducting required to cool the gas for discharge. A secondary coolant system is employed to reduce flow demands on the main coolant system and to provide a means of selectively monitoring and controlling the coolant flow rates through those duct segments for which wall heat transfer measurements are desired. This system also supplies cooling water to the auxiliary ballast resistor.

Figure II.2 Supporting Systems

LEGEND

1. Plasma Generator
2. Coolant Storage Tank
3. Main Coolant Pump
4. Heat Exchanger
5. Main Coolant Booster Pump
6. Filter
7. Main Coolant Flowmeter
8. Surge Tank
9. Filter
10. Duct Segment Coolant Distribution Manifold
11. Motor-Generator Set
12. Main Ballast Resistor
13. Auxiliary Ballast Resistor
14. r-f Oscillator
15. Gas Cylinders
16. Gas Flowmeters
17. Liquid Nitrogen Cold Trap
18. Vacuum Pump

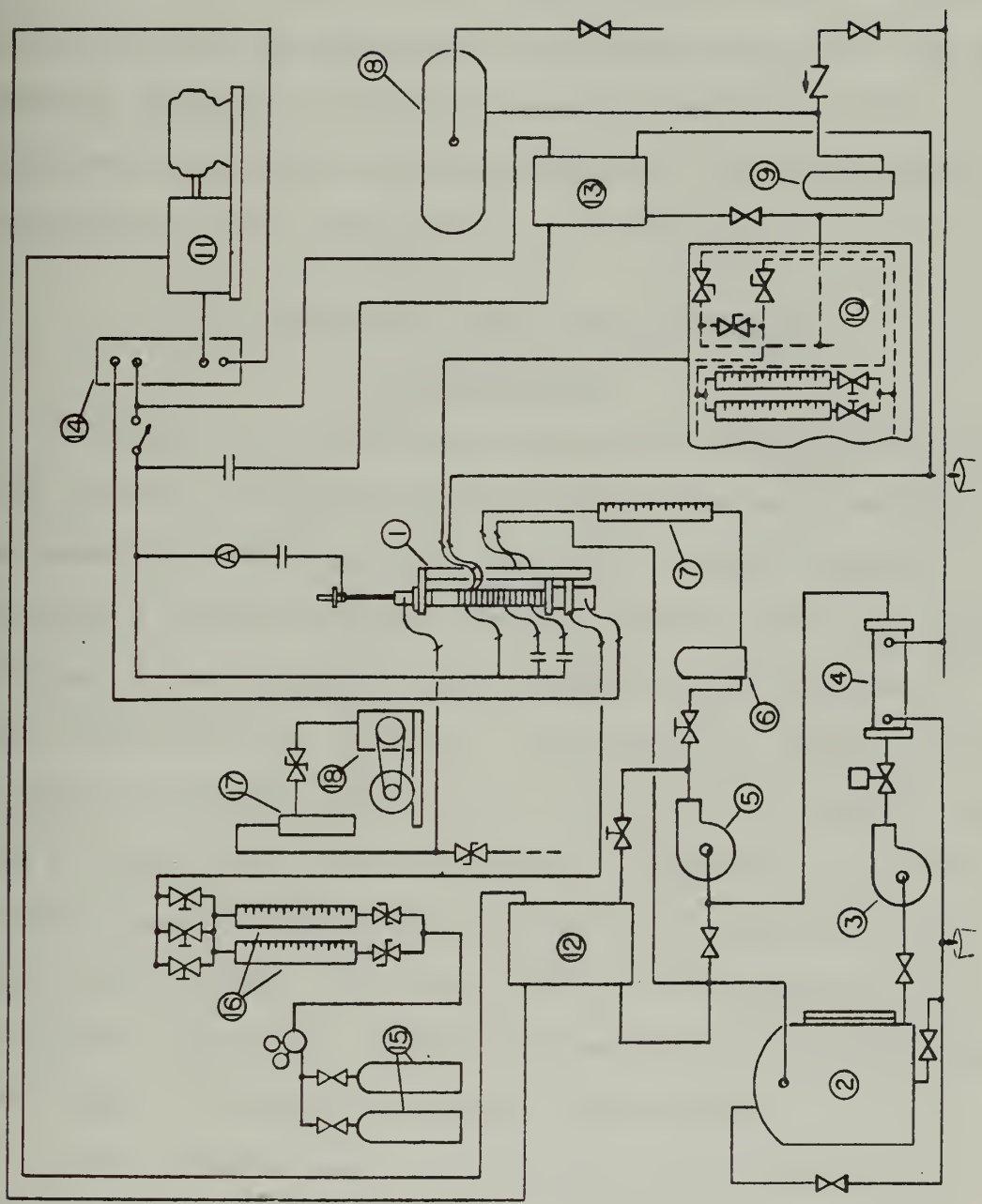

Figure II.2

Receiving its supply from commerical gas cylinders, the gas system facilitates control and measurement of the operating gas flow rate. Stringent purity requirements are maintained throughout the gas system including use of research grade gas, prior ultrasonic cleaning of all components exposed to the plasma stream, and continuous outgassing of the system prior to operation.

II.2 Particular Operating Procedures and Limitations

Despite the aforementioned purity requirements, the level of duct contamination resulting from arc operation has steadily increased over the past two year period. During the earlier stages of this research, when the major portions of the electric field intensity and total wall heat flux data were acquired, there were no visible indications of surface contamination, even after extended periods of operation (up to 40 hours). However, during the latter phases of the research, when the radiative wall heat flux data were acquired, the level of contamination continually increased in spite of special precautions that were taken in addition to those listed above.

The contamination is evidenced by a thin deposit which coats the duct walls in a distinct and repetitive pattern. The deposit, which appears to be a dark oxide

layer, forms on the leading (upstream) edge of each of the segments in the arc heating region and diminishes in the axial direction, leaving the downstream half of the segment surfaces free of visible contamination. The deposit, which at times has a bluish cast, has not been observed in the field-free region, not even on the segment immediately downstream of the anode.

Similar deposits have been observed by other investigators[13,32,33]; however opinions differ concerning the effect of surface contamination on experimental results. Emmons[13] claims that the overall arc characteristics are virtually unaffected by small amounts of contamination. On the other hand, Runstadler[33] reports a reduction in the electric field intensity for helium of some 10% when data are acquired under contamination-free conditions. Throughout the course of this study, both electric field intensity and total wall heat flux measurements have been consistently reproducible to within their respective experimental uncertainties, irrespective of the level of contamination. None the less, it was assumed initially that contamination would render the proposed radiation gage completely useless, since the dark deposits would significantly alter the optical properties of the gage surface. While useful data were acquired from the

radiation gage, the contamination level within the duct still prevented the gage from being used as it was originally intended (see the Appendix).

As reported by McKee, et al.[32], the difficulties associated with obtaining reproducible measurements of anode characteristics are most likely due to the pronounced affect that surface contamination has on electrode performance. In connection with this problem, a number of investigators[27, 32-35] have devoted considerable effort to the elimination and investigation of surface contamination within constricted tube arcs. In summarizing work performed in this area at Dartmouth, Runstadler[33] suggests a number of procedures which may be used to reduce the level of contamination within the duct. These recommended procedures include use of ultra-pure grade gas, elimination of possible cathode contaminants through use of a sonic orifice, outgassing of the duct surfaces, and nickel plating of all copper surfaces exposed to the plasma stream. The plating procedure was found necessary in order to eliminate outgassing from the copper surfaces during arc operation.

Similar, yet considerably less involved, measures were taken in this study in an attempt to eliminate the contamination of the duct surfaces. Ultra-pure grade (as opposed to commercial grade) gas was used; however

its use did not result in a significant reduction in surface contamination. This is not to say, however, that use of commercial grade gas will not result in surface contamination. After a thorough cleaning of the gas system failed to effect any change in the degree of surface contamination, the inlet portion of the gas system was virtually eliminated by connecting the gas cylinder directly to the plasma generator (a short piece of plastic tubing was connected between the gas inlet to the plasma generator and the gas regulator and the regulator was connected directly to the gas cylinder). In addition, the gas regulator (a two-stage, metal diaphram type) was completely disassembled, cleaned ultra-sonically with acetone and isopropyl alcohol, and allowed to degas at 10^{-6} mm Hg for a period of 24 hrs. Several hours prior to starting the plasma generator, the combined generator and gas system was evacuated to approximately 40 microns and the metal components, particularly the duct segments, were heated to accelerate degassing. Unfortunately, none of, or any combination of, these procedures led to any significant reduction in the level of surface contamination. In addition, the possible influence of prod and r-f discharge starting techniques was investigated, as were the procedures used to mechanically and chemically clean the duct segments. Special care was taken in

positioning the cathode within the initial nozzle segment so as to minimize possible contamination from erosion of the tungsten cathode tip. Again, there were no perceptable changes in the level of surface contamination with any of these additional measures.

On the basis of these results, it is tentatively concluded that the surface contamination is an oxide layer which is formed by a chemical reaction between the copper duct walls and the gases which escape from these walls during operation of the arc. This conclusion is supported by the observations of Runstadler[33] concerning the nickel plating of the copper surfaces, and also by the experiments performed in this study with the thin film aluminum surface on the radiation gage (Appendix). Further support of this conclusion is provided by the x-ray diffraction analysis conducted by McKee, et al.[32] which identified the surface contaminants as copper-oxide and carbon. While not fully understood, the form of the axial distribution of the surface contamination on segments in the arc heating region and the absence of surface contamination in the field-free region indicate that certain electrical effects must also influence the contamination.

In addition to experiencing contamination problems, some difficulties arose in connection with generating He and N_2 arc plasmas. The maximum current-carrying capabilities of the starting prod (75 amp) and r-f discharge (50 amp) circuits, while adequate for initiating argon arcs, are insufficient to permit starting in either nitrogen or helium. Accordingly, a special pre-start procedure was devised. This procedure involves use of a dual gas supply manifold whereby both Ar and either N_2 or He can be supplied to the arc generator simultaneously. Following initiation of a stable, 50 amp Ar arc, the proportion of N_2 or He to Ar is slowly increased from 0 to 100% while the open-circuit voltage is steadily increased to maintain a stable operating condition. While this procedure is adequate for initiating N_2 and He arcs, the maximum obtainable open-circuit voltage of the power supply is nonetheless insufficient to sustain stable operation of these gases over as wide a range as is possible with Ar.

The restrictions which are placed upon both high and low current operation of the arc generator are a result of certain physical limitations of the power supply and external ballast resistor. Specifically, high current operation is limited by the maximum open-circuit voltage capability of the power supply. In contrast, low current operation is restricted by the lower limit of electrical

stability which, in turn, is a function of the available ballast resistance as well as the maximum obtainable open-circuit voltage of the power supply.

These limits of operation can be explained by considering a set of hypothetical (yet typical) load line characteristics for an arc generator and its associated D-C power supply (Figure II.3). As indicated by the electrical circuit which accompanies Figure II.3, the power supply load line characteristic is a plot of the voltage available to the arc generator versus the available arc current. Generally, the power supply characteristic is represented by a straight line which intersects the voltage axis at the value of the open-circuit voltage and which has a slope equal to the negative of the sum of the constant internal resistance of the power supply (R_s) and the variable external ballast resistance (R_b). The arc generator load line, on the other hand, represents a plot of the current conducted by the arc versus the voltage required to sustain that current. On the whole, the arc generator is characterized by a wide spectrum of load lines which result from various combinations of the operating gas, the operating gas flow rate ($\dot{m}$), the operating pressure (p), the overall (cathode to anode) duct length (L), and the duct radius (R).

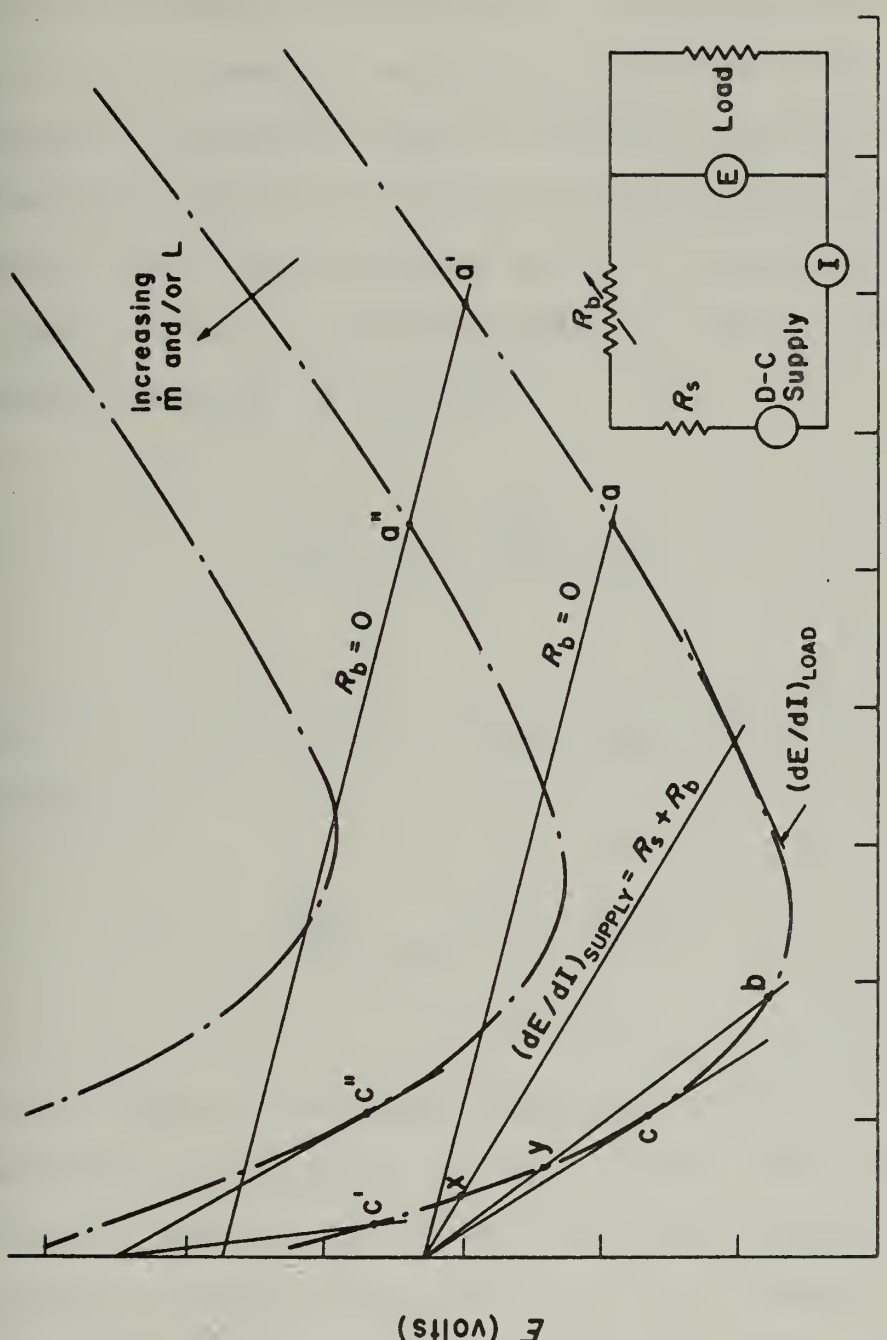

Figure II.3 Hypothetical Load and Supply Characteristics

The actual operating state (for a specified gas, $\dot{m}$, p, L, and I) of a constant diameter arc generator is uniquely determined by the point of intersection of the load (arc generator) and supply characteristics. The degree of electrical stability which exists for a given operating state is a function of the relative slopes of the two load lines at their point of intersection. The criterion that must be satisfied in order to achieve stable operation is given by

$$\left(\frac{dE}{dI}\right)_{LOAD} - \left(\frac{dE}{dI}\right)_{SUPPLY} \geq 0 \qquad \text{(II.1)}$$

which, in the case of a linear supply characteristic, reduces to

$$\left(\frac{dE}{dI}\right)_{LOAD} + R_s + R_b \geq 0 \qquad \text{(II.2)}$$

It is noted at this point that, while Equation II.2 establishes, in principle, the criterion for stable operation, in practice the slope of the load characteristic must always be greater than the slope of the supply characteristic if stable operation is to be realized. That is,

$$\left(\frac{dE}{dI}\right)_{LOAD} + R_s + R_b >> 0. \qquad \text{(II.3)}$$

Since R_s is constant and since $\left(\frac{dE}{dI}\right)_{LOAD}$ is dictated by the desired arc operating condition, improved electrical stability at each condition can be effected only by increasing R_b. This, in turn, necessitates an increase in the open-circuit voltage. Accordingly, for stable arc operation, it is generally advisable to use the highest possible settings of both the ballast resistor and the open-circuit voltage of the power supply.

Irrespective of the value of R_b, Equation II.3 will be satisfied as long as operation is confined to the positive slope portions of the arc generator load lines*. Nevertheless, the maximum open-circuit voltage capability of the power supply can place a restriction on high current operations. For example, if all of the ballast resistance has been removed in order to operate in condition-a (Figure II.3), further operation at higher arc currents (position-a') or operation at greater values of $\dot{m}$ and/or L (position-a") can be achieved only by increasing

---

* Note that operation at the initial point of intersection (e.g., points x and y in Figure II.3) is not likely since, according to Equation II.2, the arc would be inherently unstable at this condition.

the open-circuit voltage. Therefore, aside from possible over heating of the electrodes, high current operation is limited by the maximum obtainable open-circuit voltage of the power supply.

According to the stability requirement expressed by Equation II.3, operation on the negative slope portions of the arc generator load lines (e.g., position-b) is inherently less stable than operation in the positive slope regions. In addition, a lower limit for stable operation exists at the current for which the slopes of the load and supply characteristics are equal (e.g., position-c). In practice, the arc will extinguish prior to this lower limit; however, lower current operation (position-c') or operation at higher valves of $\dot{m}$ and/or L (position-c") can be achieved by increasing the open-circuit voltage and increasing R_b. This procedure can be continued until the maximum open-circuit voltage of the power supply (or the maximum value of R_b) is reached.

For the duct lengths and operating gas flow rates employed in this study, the point at which the slope of the load characteristic is equal to zero ($(\frac{dE}{dI})_{LOAD} = 0$) occurs at an arc current of approximately 25 amp for Ar, 150 amp for N_2, and at a current in excess of 400 amp in He. Therefore, according to the previous arguments, low current operations in all three gases and high current

operations in N_2 and He are limited by the power supply. High current operation in Ar is limited by the maximum power that can be dissipated by the main ballast resistor. It is further noted that over heating of the anode (as evidenced by ablation of the anode surface) occurred at the higher arc currents in N_2 ($I > 200$ amp) and in He ($I > 100$ amp).

II.3 Diagnostic Methods and Related Instrumentation

The overall and local arc-column characteristics are determined by measuring the potential difference between the "floating" duct segments and the cathode. The arc voltage measurements are used both to determine the axial distribution of the electric field intensity and, along with the arc current and calorimetric measurements, to determine the mixed-mean enthalpy of the gas at each segment location. The arc voltages are measured with a high input impedance (4 megaohm) strip-chart recorder (Electronik-19 by Honeywell). The arc current is determined by monitoring the voltage drop across a calibrated shunt resistor with a digital voltmeter (Dana, model # 54030). As shown schematically in Figure II.4, further circuitry is available to permit up to 400 ma of current to be drawn from a duct segment while its potential (with respect to the cathode) is monitored.

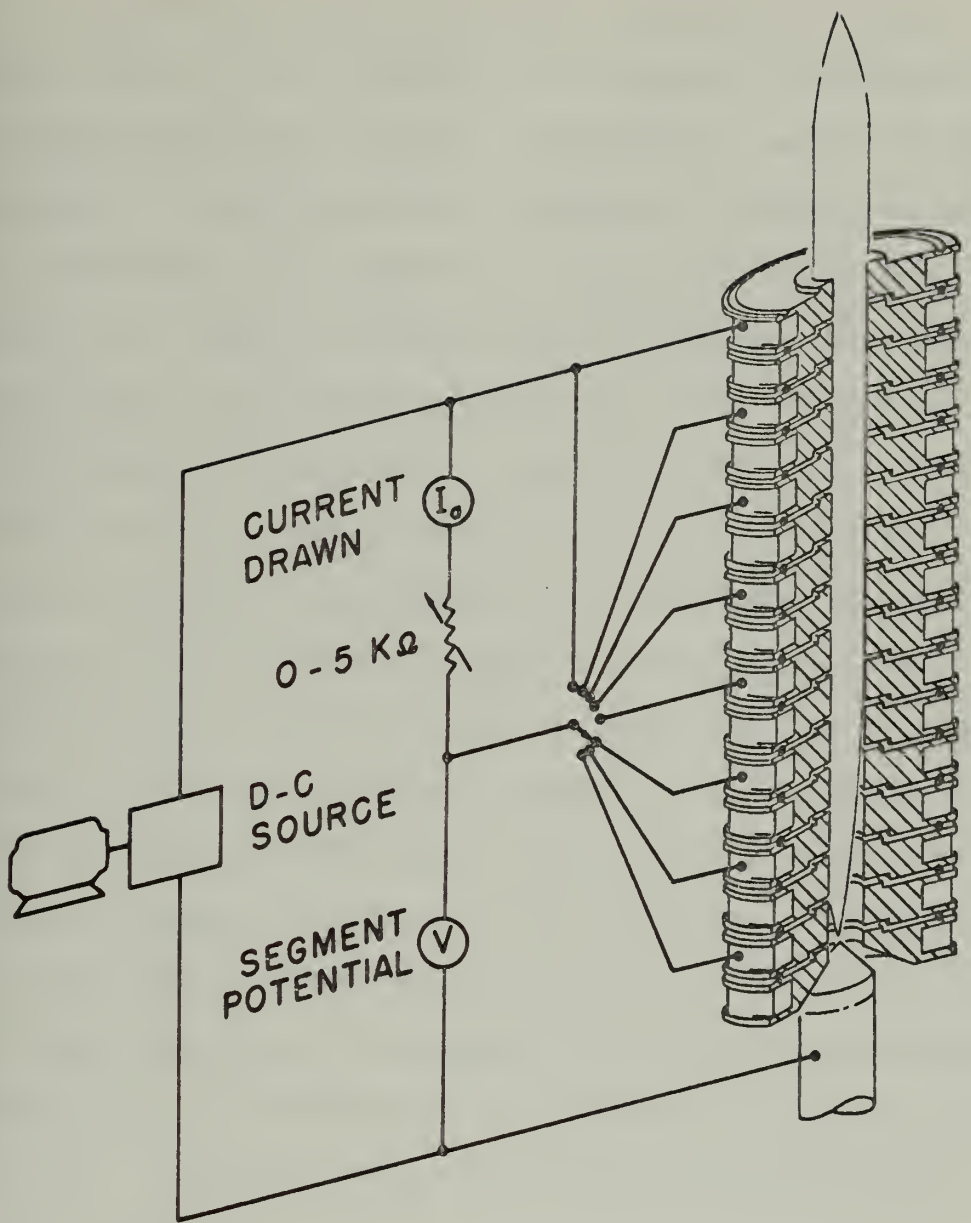

Figure II.4 Circuit Used for Impressed-Current (I_a) Method of Wall Potential Measurement

The energy loss to the duct segments, to the cathode, and to the remaining arc generator components is determined calorimetrically. Accordingly, each of these components is equipped with a specially designed temperature difference (ΔT) transducer. The ΔT transducers (Figure II.5) employ a single pair of copper-constantan thermocouples, mounted in plexiglass inlet and outlet plenum chambers, and wired in series to provide a voltage signal which is directly proportional to the coolant temperature rise. Considerable care was taken in the shielding and calibration (against mercury-in-glass thermometers) of these transducers and they are accurate to within 5% of the indicated reading. The transducer output voltages are amplified (Dana model #3850-V2) prior to being displayed on the digital voltmeter. The absolute temperature of the operating gas at both inlet and discharge locations is measured with a copper-constantan thermocouple (as referenced to a copper-constantan ice-junction). The gas temperatures are monitored by the digital voltmeter.

A unique radiative heat transfer gage is used to delineate the radiative contribution to the total wall heat flux. As shown in Figure II.6, the radiation gage consists of two semicylindrical copper segments which are thermally isolated from one another, individually

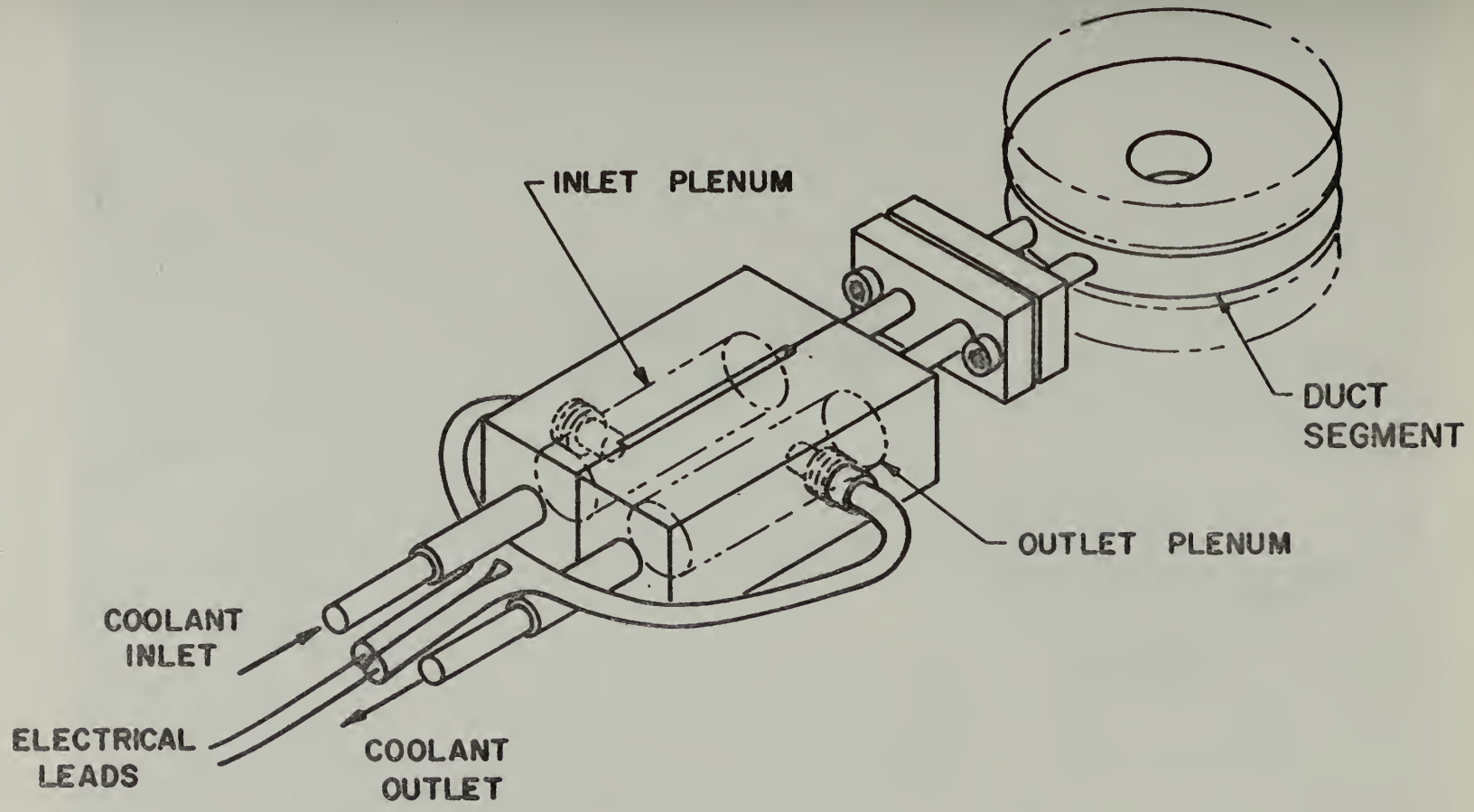

Figure II.5 ΔT-Transducer Assembly

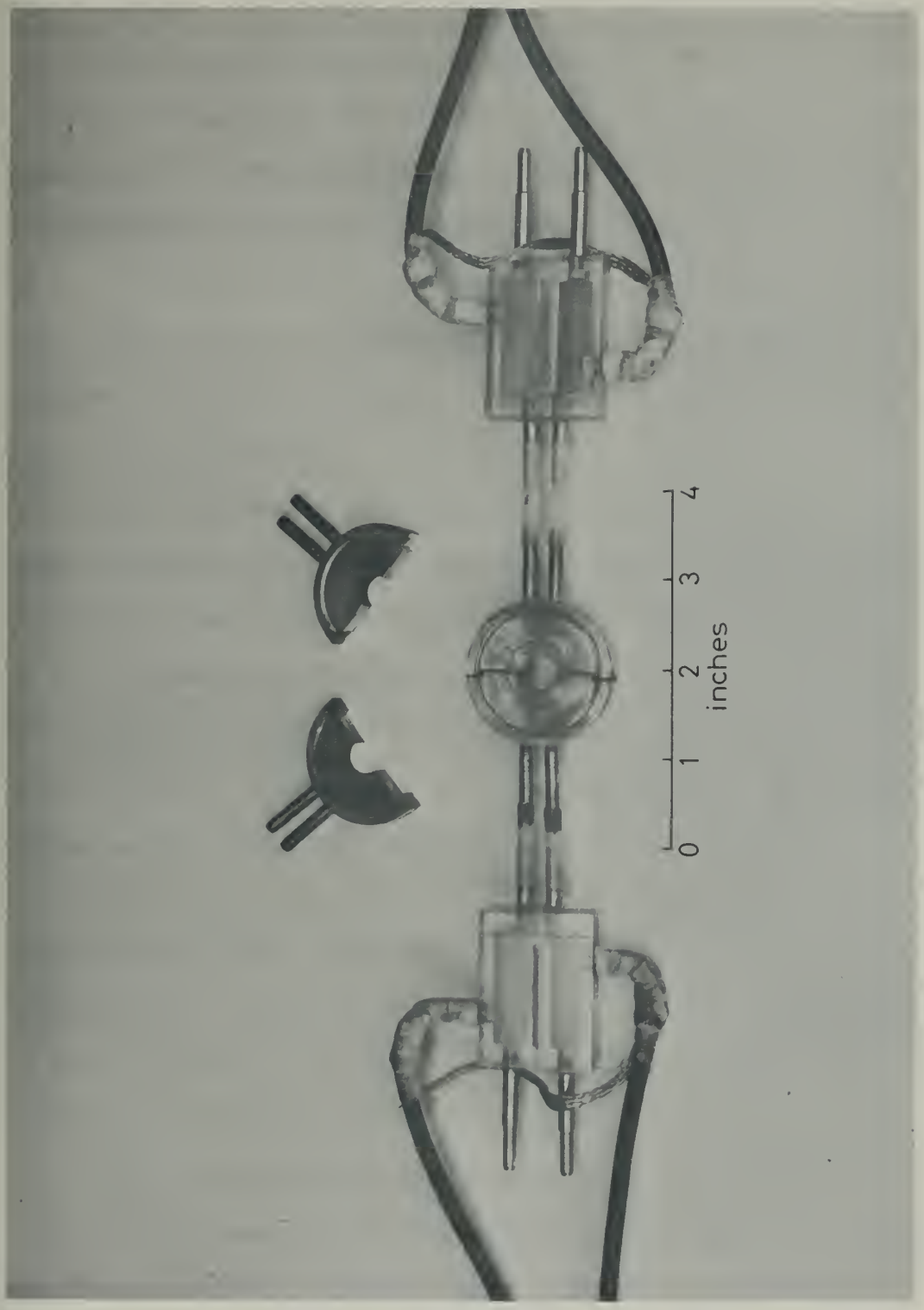

Figure II.6 Radiation Gage

water cooled, and supplied with individual ΔT-transducers. The inside wall of each half segment is coated with either a highly reflecting (aluminum) or highly absorbing (black) surface. The overall dimensions of the assembled gage are precisely the same as those of a standard duct segment. A thorough discussion of the principle of operation, the fabrication, and the associated experimental problems involved in the use of the radiation gage are left to the Appendix.

The operating gas flow rate and the coolant flowrates through the cathode and those duct segments serving as calorimeters are measured with precision accuracy (± 1%) flowmeters (Fischer & Porter model no. 10A0735). The two gas flowmeters have a combined range of from 0.02 to 1.50 lb/min in argon. At the time of each flowmeter reading, the inlet gas temperature and pressure are measured and used to correct the indicated flow rate should they differ from the temperature and pressure of calibration. An additional precision accuracy flowmeter is used to measure the total coolant flow rate to the plasma generator.

With measurement of the arc current (I) and axial voltage distribution (E), the gas inlet temperature (T_{INLET}) and flow rate ($\dot{m}$), and the power losses to the duct segments (PLS) and to the cathode (PLC), the axial

distribution of the gas enthalpy can be determined by performing energy balances at successive axial locations.

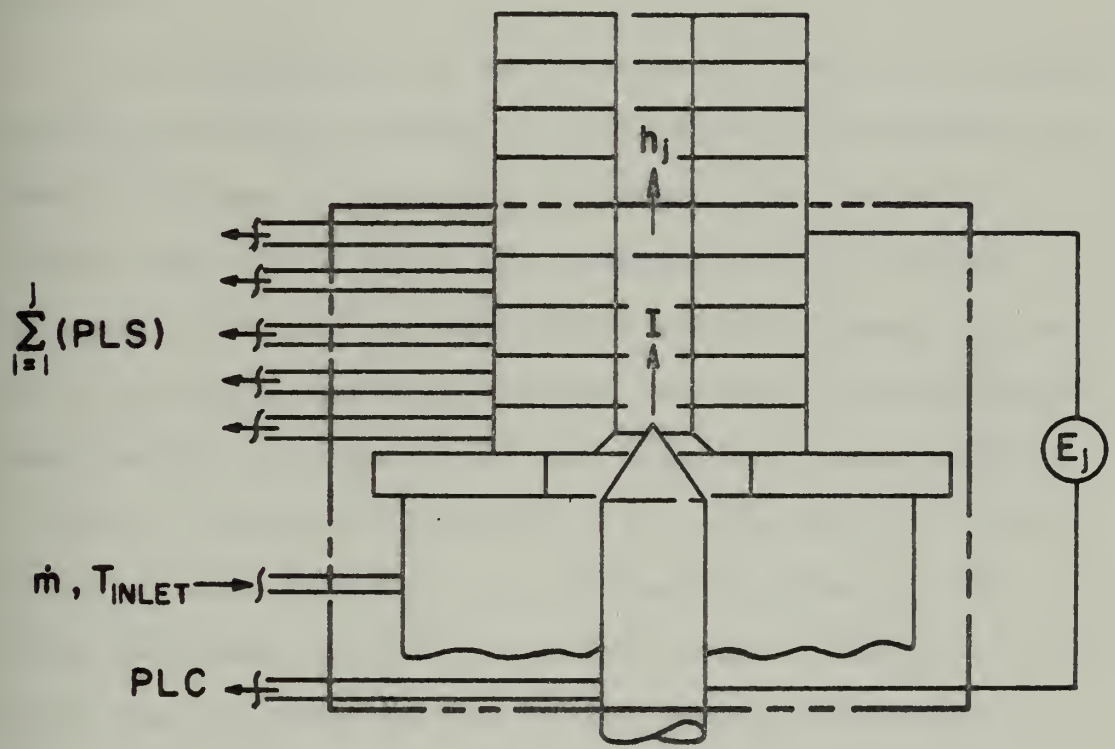

Figure II.7 Energy Balance Diagram

With reference to Figure II.7, the enthalpy of the gas at the exit plane of a segment in the arc heating region is given by

$$h_j = C_p T_{INLET} + \frac{E_j I - \sum_{i=1}^{j} (PLS)_i - PLC}{\dot{m}} . \qquad (II.3)$$

This value is then algebraically averaged with the enthalpy determined by the previous (j-1) energy balance, and the resulting "mixed-mean" enthalpy is assigned to an axial location corresponding to the center of the j^{th} segment.

To experimentally verify the accuracy of the diagnostic procedures employed in this study, an attempt was made to "close off" the energy balance for the entire plasma generator. While the precision of this energy balance is limited by unavoidable ambient losses, it was still possible to obtain closure to within the cumulative experimental uncertainty of the component measurements (± 20%). A more precise check is one based on a local energy balance performed on a segment located in the fully-developed portion of the arc heating region*. In every case, closure of this local energy balance was obtained to within 5% - a value comparable to the total uncertainty of these measurements (±5-10%). The consistent reproducibility of data taken over a two year period provides further confidence in the accuracy of the measurements as well as the consistency of the overall system.

A detailed uncertainty analysis is used for estimating the uncertainties associated with each measured

---

* The nature of this energy balance will be discussed in detail in the following chapter (Section III.3).

variable and for calculating the propagation of these uncertainties into each reported result. The method used in this analysis is the standard approach for single-sample experiments[36]. The uncertainty calculations, as well as the conversion and reduction of raw data, are performed on the computer. The thermo-physical properties required for determining the mean temperature, $T_m=T_m(h_m)$, and the Nusselt number-Ohmic heating parameter correlations (k_m and σ_m) are obtained from DeVoto[37] and Drellishak, Knopp, and Cambel[38] in the case of Ar; Lick and Emmons[39] and DeVoto and Li[40] in the case of He; and Drellishak, Aeschliman, and Cambel[41] and Avco[42] for N_2. The reported uncertainties of these properties are also considered in the aforementioned uncertainty analysis. A more detailed description of the arc facility, diagnostic techniques, and uncertainty analysis is given by Lukens[43].

CHAPTER III EXPERIMENTAL RESULTS

III.1 Range of Measurements

Experimental data were acquired for Ar, N_2, and He arcs over the following ranges of laminar flow operating conditions:

Argon; I = 35 - 240 amp, $\dot{m}$ = 0.03 - 0.11 lb/min, constrictor length = 5 in (20 segments).

Nitrogen; I = 100 - 200 amp, $\dot{m}$ = 0.03 lb/min, constrictor length = 5 in (20 segments).

Helium; I = 50 amp, $\dot{m}$ = 0.07 lb/min, constrictor length = 2.5 in (10 segments).

All measurements were made with a 1.0 diameter copper duct operating at near atmospheric pressure. The assertion of laminar flow is based upon the flow transition studies by Incropera and Leppert[44] and by Runstadler[10] in which the onset of turbulence is reported to occur at a mean Reynolds number (based on properties evaluated at T_m) of 700 to 900. The largest value of the mean Reynolds number encountered in this study is approximately 600 (Argon, I = 35 amp, $\dot{m}$ = 0.11 lb/min). Hence, the above

stated ranges of operating conditions are assumed to be representative of laminar flow.

Rather than presenting a complete tabulation of the data acquired for the inlet region, certain data were selected to demonstrate the effect of varying gas flow rate and arc current on the development characteristics of the arc. All of the acquired data pertaining to the asymptotic region are presented along with related data from other investigators. The interpretation of the experimental results as well as comparisons with related theories will be the subject of Chapter IV.

III.2 Electrical Characteristics

Prior to presenting the experimental data for the arc-column (electrical) characteristics, a discussion is in order concerning the method employed in the acquisition of this data.

A method frequently used in the measurement of arc-column characteristics involves use of the duct segments as "floating" potential probes[10,12,15,32]. It is commonly recognized, however, that a floating duct wall will assume a potential which is negative with respect to the plasma core by an amount equivalent to the plasma sheath potential*. Accordingly, on the assumption that

---

* Further treatment on the formulation and characteristics of plasma sheaths is given in references [30] and [45].

the sheath potential is appreciable, some investigators have questioned the suitability of using a floating duct wall to measure plasma potentials.

In reference to their cascade arc potential measurements, this question has been raised most strongly by Pfender, et al.[6,7]. In performing their measurements, they allowed a current (I_a) to be drawn from the duct wall while they simultaneously monitored the potential of this wall with respect to the cathode. These measurements indicated that the recorded wall potential was strongly influenced by the magnitude of the current drawn. In particular, they observed that the voltage increases by 40 to 100% over the floating wall ($I_a = 0$) potential when a current of up to 50 ma is drawn. Above 50 ma, the segment potentials were observed to be independent of the current drawn. With regard to this observation, they argued that, for $I_a > 50$ ma, the charge separation which otherwise would exists in the plasma sheath region is exactly cancelled and, consequently, the duct wall is at the potential of the plasma column. They therefore concluded that floating wall potential measurements do not provide a suitable indication of the actual plasma potential, but that accurate measurements of this parameter can be made by recording the wall potential while a current in excess of 50 ma is drawn from the wall.

In contrast, Emmons[12,13] indicates that the sheath potentials for an argon-copper duct combination are approximately 1 to 2 volts, for which case the floating wall potentials are suitably close to those in the arc column. In support of this contention is the experimental technique used by Maecker[15] wherein every attempt was made to eliminate impressed wall currents (I_a) while performing plasma potential measurements*. Schreiber[46], on the other hand, has measured significant voltage increases with current drawn, but he attributes these increases to voltage drops across the relatively cool gas boundary layers. Additional support for Schreiber's deduction can be inferred from the measurements made by researchers at Dartmouth[32,33]. While the Dartmouth data were used primarily in support of anode studies, the arc configuration and external circuitry used for these measurements are similar to those employed in this study (Figure II.4) and to those used by Pfender, et al.[7].

In an attempt to resolve these inconsistencies, the variation in the duct wall potential with current drawn was measured at various axial locations and arc currents. As shown in Figure III.1, these measurements indicate that

---

* Maecker contends that the measured wall potential difference between two segments will be in error by an amount proportional to the impressed current, I_a.

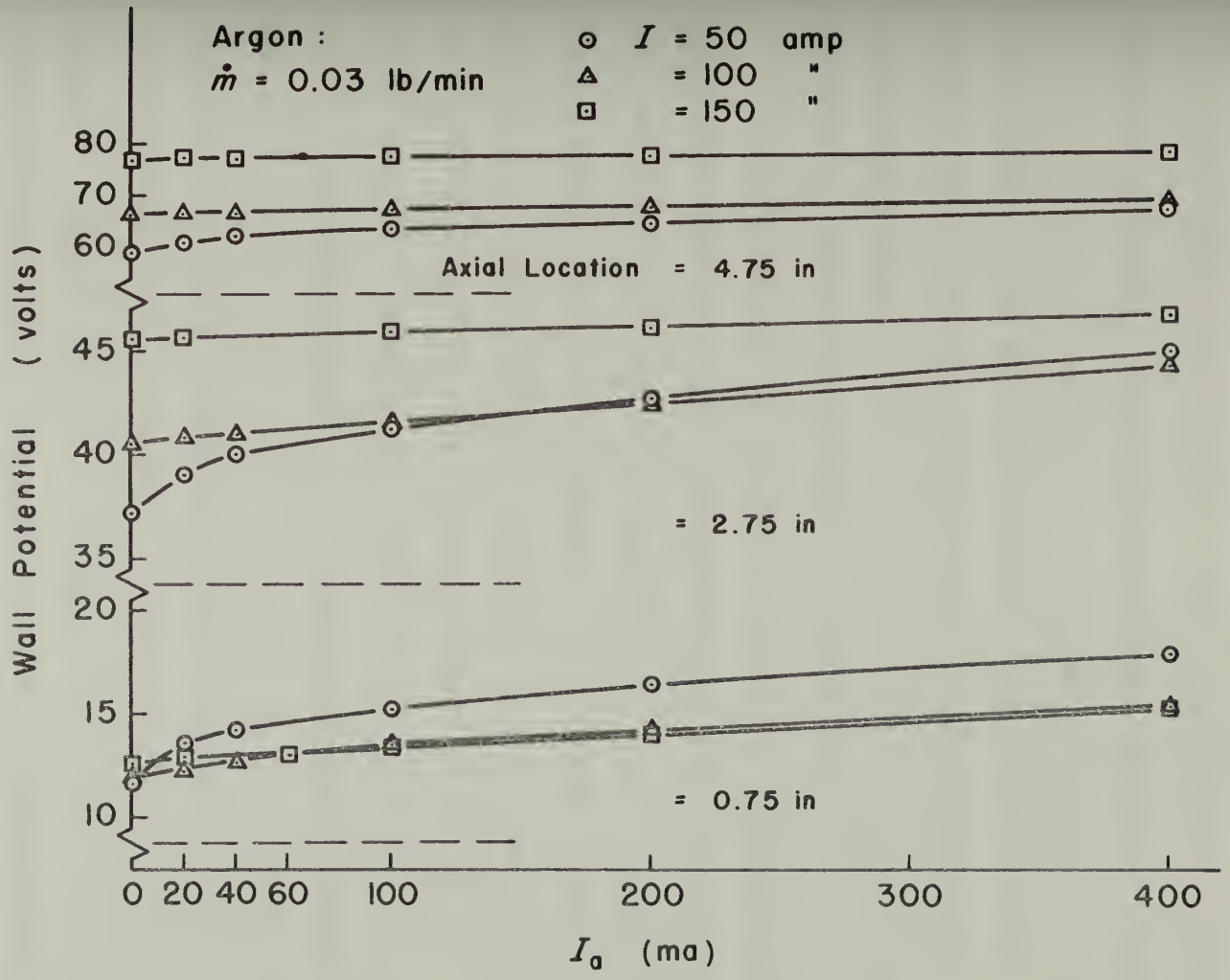

Figure III.1 Dependence of Wall Potential on Current Drawn, Arc Current, and Axial Location

the percentage increase in wall potential with increasing I_a diminishes both with increasing axial distance and with increasing arc current. They also indicate that the wall potential increases continuously with increasing I_a over the entire range of I_a values investigated. In this respect, the distributions of Figure III.1 are qualitatively similar to the potential distributions recorded by Maecker[15] and to the lower current ranges of anode conduction reported by Runstadler[33].

Simultaneous calorimetric and wall potential measurements indicate that the total wall heat flux to a duct segment does not vary appreciably (< 3%) over the entire range of I_a. In addition, the value of the asymptotic electric field intensity ($E_{x,a}$) was observed to be independent of the current drawn. This fact is discussed by Emmons and Land[11] and by McKee, et al.[32] and is strongly supported by the experimental measurements of Morris, et al.[14], wherein the voltage gradient was measured using three independent methods. With the first method, the value of $E_{x,a}$ was computed from the asymptotic energy balance equation (this equation is discussed later in this chapter) along with calorimetric measurements of the power losses to the duct segments. The second method, which is similar to that employed by Maecker, utilizes two of the duct segments as potential

probes. Unlike Maecker's method, however, a small current was supplied to the arc through these probes (in an attempt to cancel the voltage drop across the "contact resistance" between the probes and the arc column) while the potential difference between the two duct segments was measured. This potential drop was then divided by the distance between the two probe segments to give the value of $E_{x,a}$. The third method used by Morris, et al. involved a cathode withdrawal experiment wherein the total arc current was held constant while the total (cathode to anode) voltage drop was recorded as a function of the total (cathode to anode) duct length. These three methods, when applied to the central region of a hydrogen arc, resulted in values of the electric field intensity which agreed to within approximately 10% - a value comparable to the combined uncertainties of these measurements.

The agreement demonstrated by these experiments is presumably a result of the conditions which characterize the fully-developed region. That is, regardless of the magnitude of possible radial electric field components, the voltage difference between any two axial points in the fully-developed region is invariant as long as the two points are at the same radial location. If this were not the case, the axial component of the electric field intensity would vary with axial location and the flow

would no longer be asymptotic. The independence of $E_{x,a}$ with I_a was tested under the most severe condition (I = 50 amps, I_a = 400 ma) of this investigation and, as shown in Figure III.2, the slopes of the linear portions of the wall potential distributions ($E_{x,a}$) are the same for I_a = 0 and I_a = 400 ma. It is further noted that the electric field intensity distribution on either side of a segment from which current is being drawn is unaffected by the wall potential variations of that segment.

Although it is concluded that the current drawn from a duct segment (up to I_a = 400 ma) does not appreciably effect the total wall heat flux or $E_{x,a}$, the increase in wall potential with increasing I_a will nonetheless have a direct effect on the energy balance measurements used to determine the mean enthalpy of the gas, particularly at the lower arc currents. As indicated in Figure III.3, the mean enthalpy of a 50 amp, argon plasma is considerably greater when computed using wall potentials measured with I_a = 400 ma than it is when computed with floating wall potentials. While the relative accuracy of these two distributions could best be determined by comparison with experimental enthalpy profile data, such data are not available. However, a comparison is made with the non-equilibrium numerical solution by Clark[25]. This solution, as applied to the asymptotic region of an

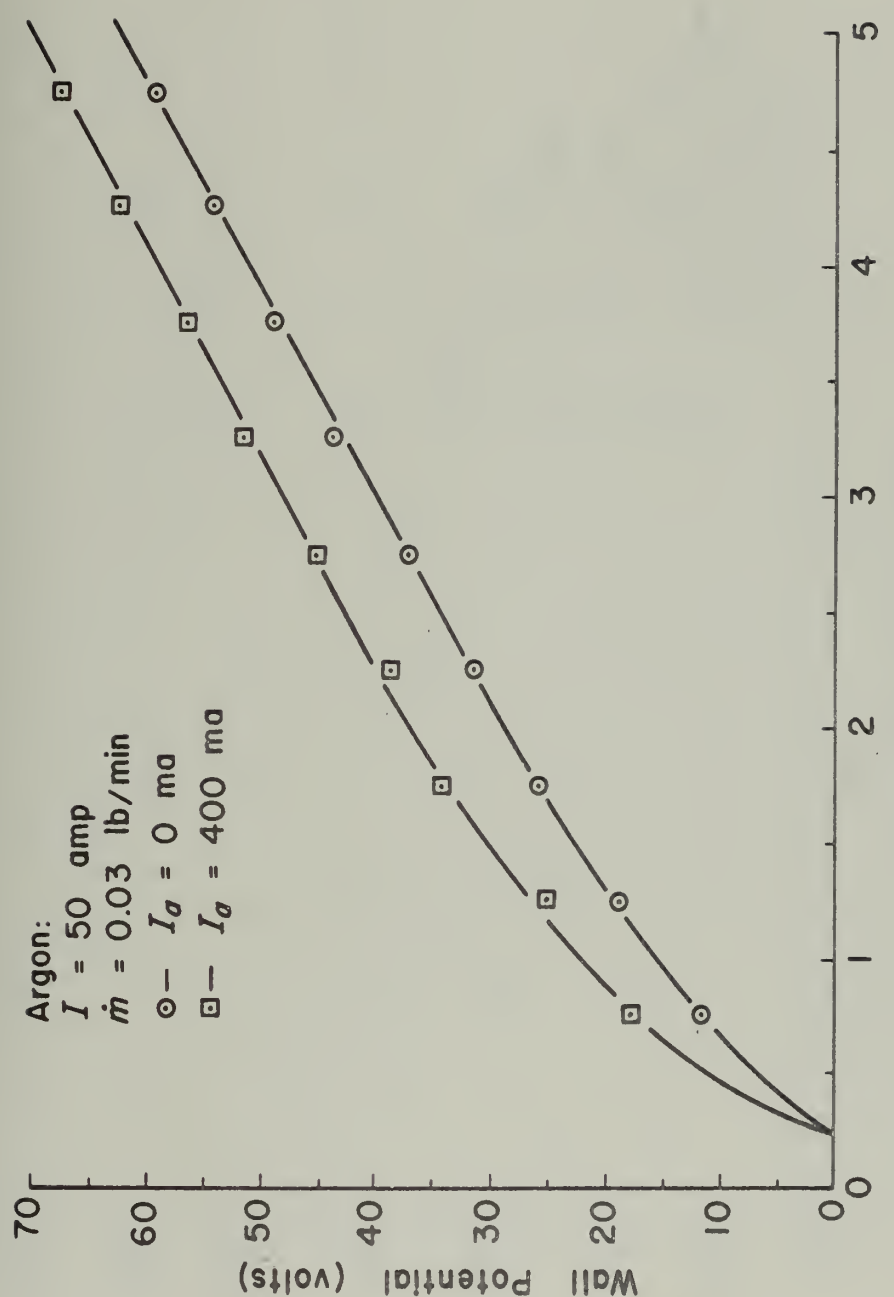

Figure III.2 Axial Distribution of Wall Potential with Current Drawn

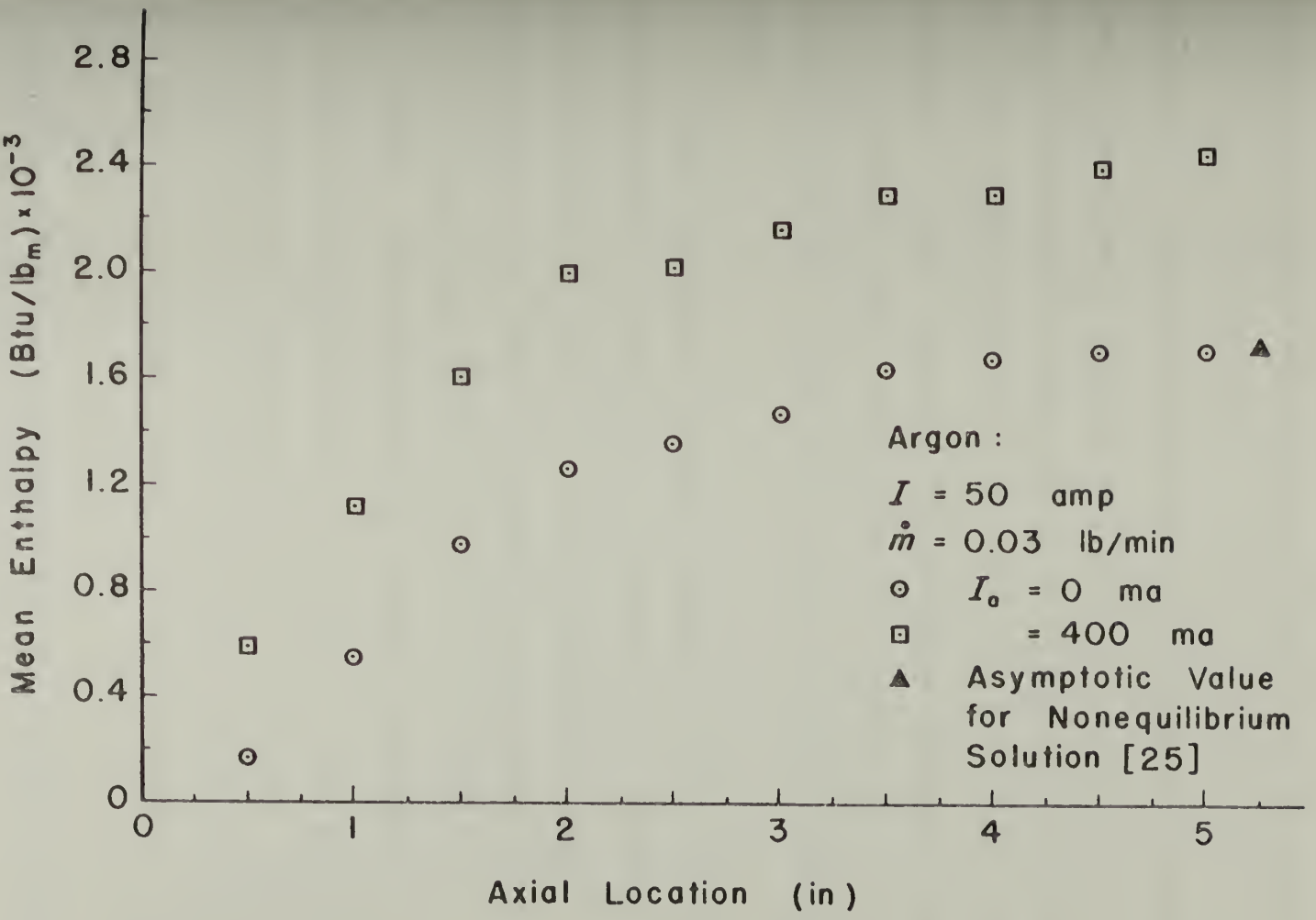

Figure III.3 Axial Distribution of Mixed-Mean Enthalpy with Current Drawn

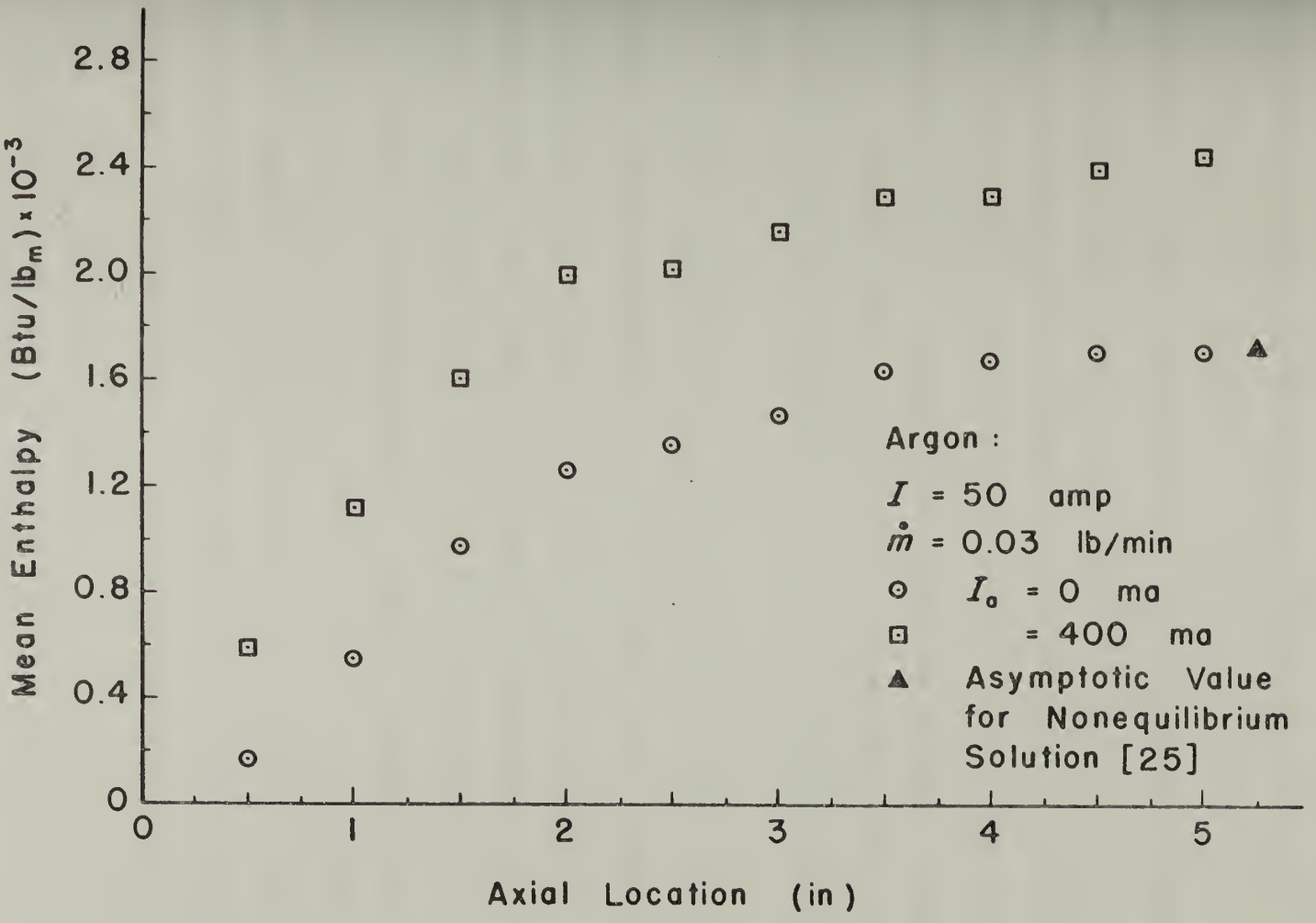

Figure III.3 Axial Distribution of Mixed-Mean Enthalpy with Current Drawn

atmospheric argon plasma in a 1.0 cm diameter duct, predicts electric field intensity and total wall heat flux values which agree with measured values to within the experimental uncertainties (< 6%)*. As indicated in Figure III.3, this solution also predicts an asymptotic mean enthalpy which agrees well with the experimental value determined from the use of floating wall potentials. While the conclusions that can be drawn from this comparison are, at best, tenuous, the agreement between theory and experiment shown in Figure III.3 indicates that the floating duct wall serves as the more suitable potential probe.

After modifying the wall boundary conditions to include current drawn from the duct wall, the nonequilibrium solution by Clark[25] (which includes a plasma sheath model) was used to investigate the effect of I_a on the plasma sheath potential. At I = 50 amp and I_a = 400 ma, the nonequilibrium solution predicts a decrease (from its floating wall value) in the plasma sheath potential from 3.60 volts to 1.75 volts. This predicted reduction in sheath potential is considerably less than the increases in wall potential measured under

---

* Comparisons between experiment and the nonequilibrium model are presented in Chapter IV.

the same conditions*.

On the basis of the measured wall potential distributions of Figure III.1, and on the basis of the comparisons with the nonequilibrium solution, it is concluded that the observed increases in wall potential are primarily a result of the wall current (I_a) being conducted across the thin layers of relatively high electrical resistance gas adjacent to the duct walls**. Accordingly, it is felt that the "floating" wall potential provides a more accurate measure of the actual plasma column potential, at least for those conditions where the plasma sheath potential is small in comparison to the wall potential (on the basis of the nonequilibrium solution, the sheath potential, which increases with increasing arc current, attains a maximum value of approximately 5.0 volts at I = 240 amp). Therefore, all of the following data pertaining to the electrical characteristics of the arc-column are based upon floating wall potential measurements.

The axial distribution of the wall potential for an argon arc and its variation with arc current and with

---

* A decrease in the plasma sheath potential results in an increase in the duct wall potential measured with respect to the cathode.

**This process is treated in greater detail by Runstadler[33].

operating gas flow rate are shown in Figures III.4 and III.5, respectively. Aside from the anode fall region, the wall potential varies linearly with axial distance for entry lengths greater than 2.5 inches. The 0.25 in (1 segment width) location of the zero potential intercept is due to the positioning of the cathode within the initial nozzle-shaped segment.

As indicated in Figure III.5, the increase in potential with increasing flow rate is to be expected since, with an increase in the thermal development length (and thus an increase in the overall arc resistance), a larger potential must be applied to maintain a constant arc current. In contrast, if the fully-developed temperature profiles are, in fact, independent of gas flow rate (as they must be in the presence of negligible viscous dissipation), then the asymptotic value of the electric field intensity ($E_{x,a}$) should not vary with gas flow rate. Such is the case for the lower flow rates shown in Figure III.5. The slight variation in $E_{x,a}$ with higher flow rates is attributed to possible departures from axisymmetric flow and nonuniform arc attachment at the anode surface.

The asymptotic values of the electric field intensity for Ar, N_2, and He and their dependence on arc current are plotted in Figure III.6. Included for comparison are the experimental distributions of Runstadler[10]

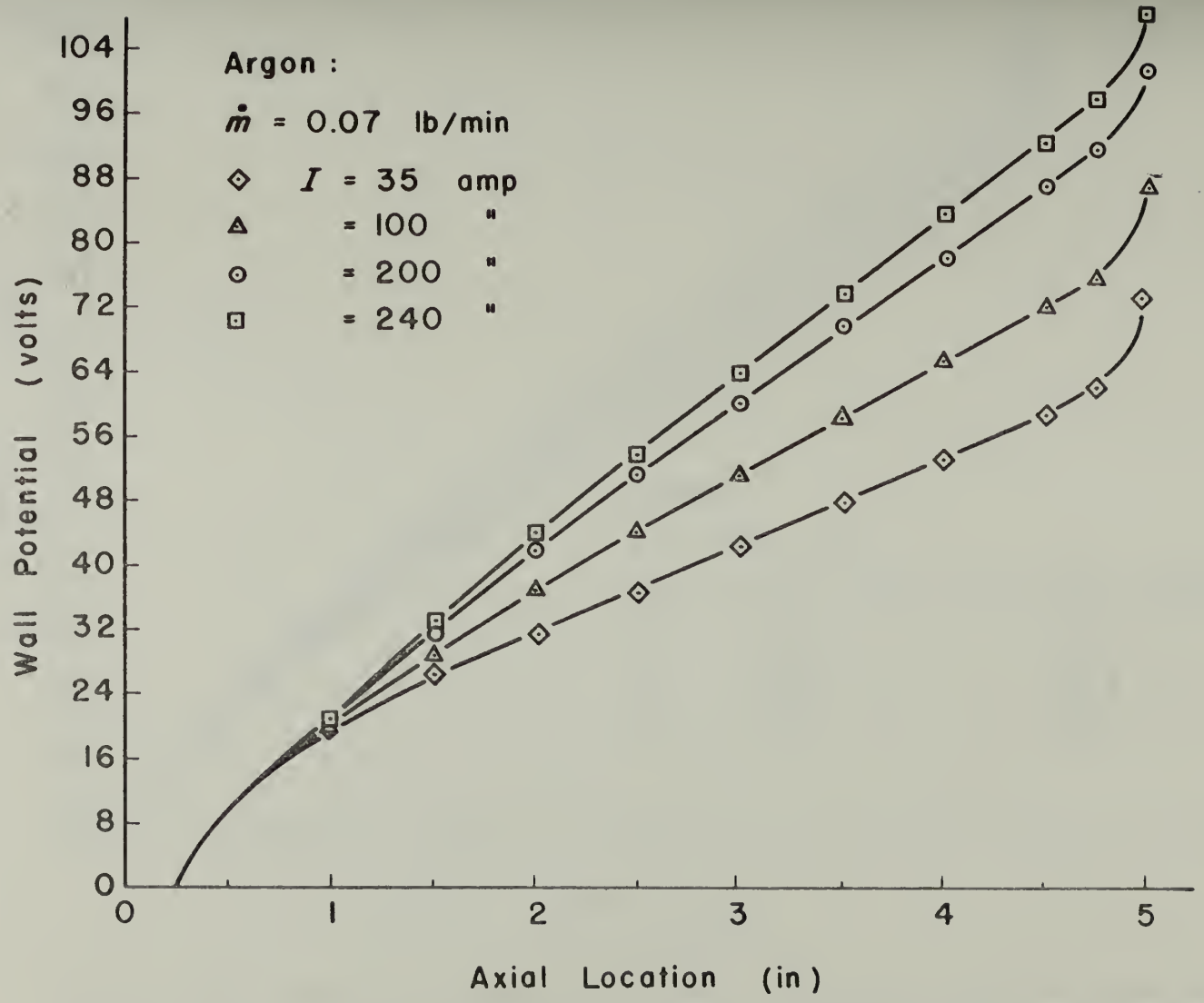

Figure III.4 Axial Distribution of Wall Potential with Arc Current

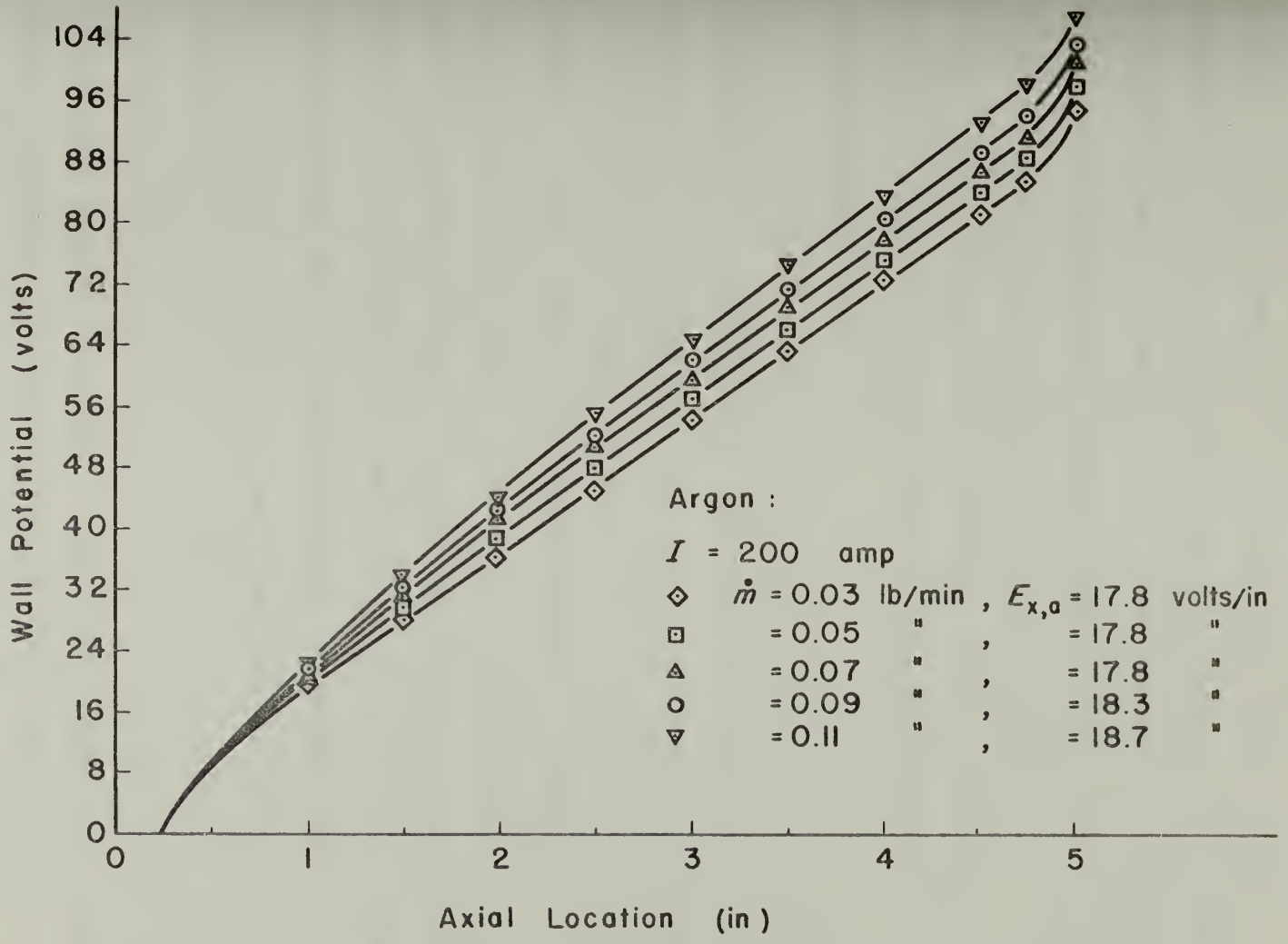

Figure III.5 Axial Distribution of Wall Potential with Gas Flow Rate

and Emmons and Land[11] in the case of Ar, Emmons[13] and McKee, et al.[32] in the case of He, and Emmons[13] for N_2. While Emmons[13] contends that there are no regions (in a tube with L/D = 14) for which his N_2 data are independent of laminar flow rate, asymptotic conditions (as evidenced by constant values of E_x and q in the axial direction) were observed in this study for a $L/D \geq 12.6$. Consequently, Emmons' lowest flow rate data were chosen as being the most representative of fully-developed flow.

Arc-column electrical characteristics are commonly presented in a reduced form wherein the dependence on duct radius (R) is removed by plotting I/R or E_xI as a function of E_xR[11,12,33]. This reduced form is only applicable, however, under those conditions for which both nonequilibrium effects and radiation are negligible. According to the variable tube radius experiments reported by Emmons[13] and Emmons and Land[11] and according to comparisons made in this study between experiment and equilibrium and nonequilibrium numerical solutions (Chapter IV), conditions exist for which radiation and departures from equilibrium have a significant effect on overall arc characteristics. For this reason, the experimental results which were selected for comparison in Figure III.6 pertain only to 1.0 cm diameter ducts.

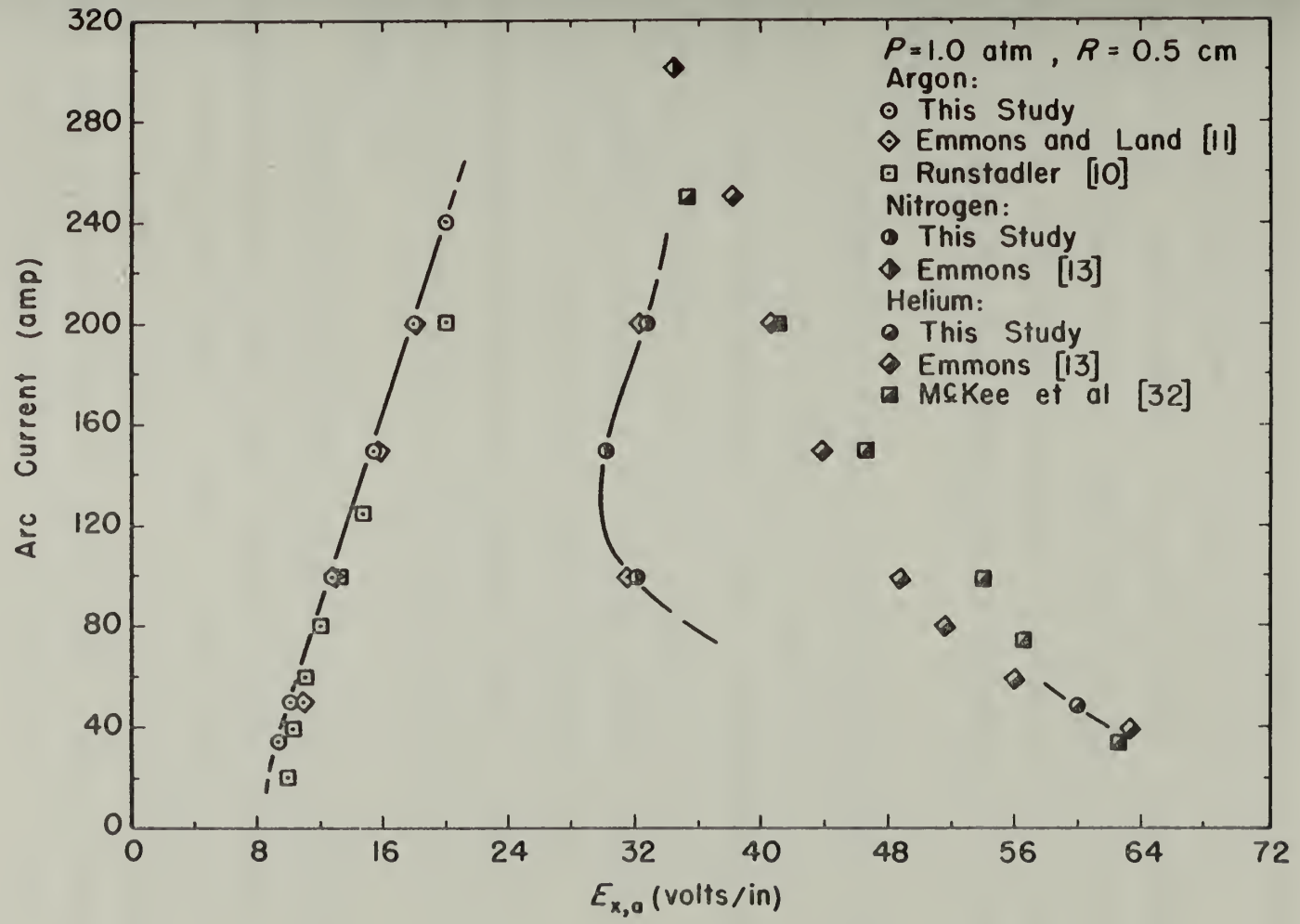

Figure III.6 Comparison of Experimental Asymptotic Arc-Column Characteristics

III.3 Wall Heat Flux

Typical axial distributions of the total wall heat flux (q) for several arc currents and laminar gas flow rates in argon are shown in Figures III.7 and III.8, respectively. As indicated in Figure III.8, q approaches a constant value which is independent of gas flow rate. This behavior provides additional experimental verification in support of the assumption of negligible viscous dissipation.

The asymptotic values of the total wall heat flux (q_a) for Ar, N_2, and He and their dependence on arc current are plotted in Figure III.9. In comparison with the values for argon, the larger values of q_a (and $E_{x,a}$) measured in nitrogen and helium reflect the dissociation (N_2) and relatively high ionization (He) energies which characterize these two gases. Further comparisons between these three gases are deferred to Chapter IV.

Because of the absence of data in the literature, comparison of the total wall heat flux data reported in this study with that of other investigators is not possible; however, confidence in the validity of the q_a data in Figure III.9 may be established from the favorable comparisons of Figure III.6 ($E_{x,a}$ versus I). An energy

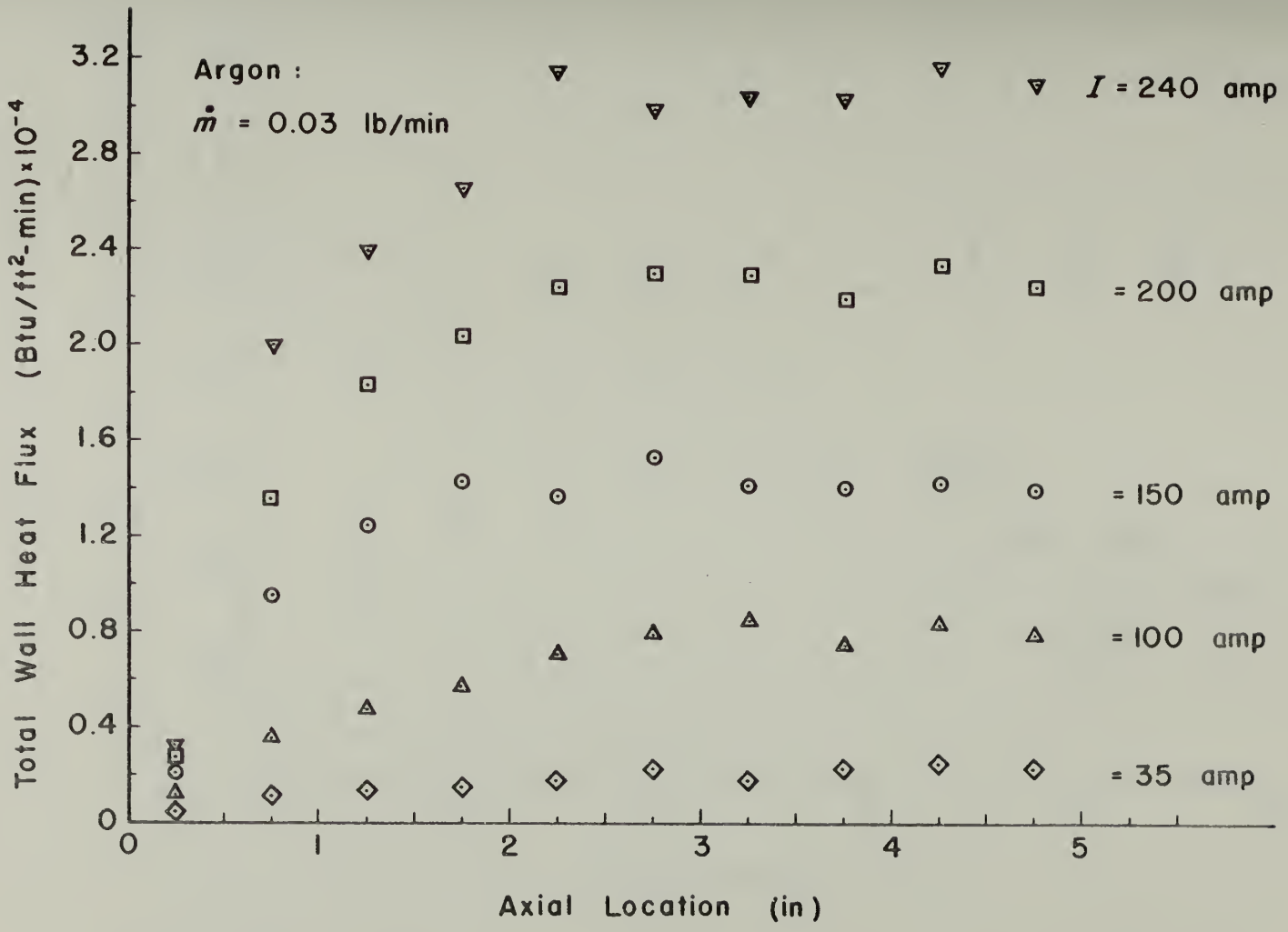

Figure III.7 Axial Distribution of Total Wall Heat Flux with Arc Current

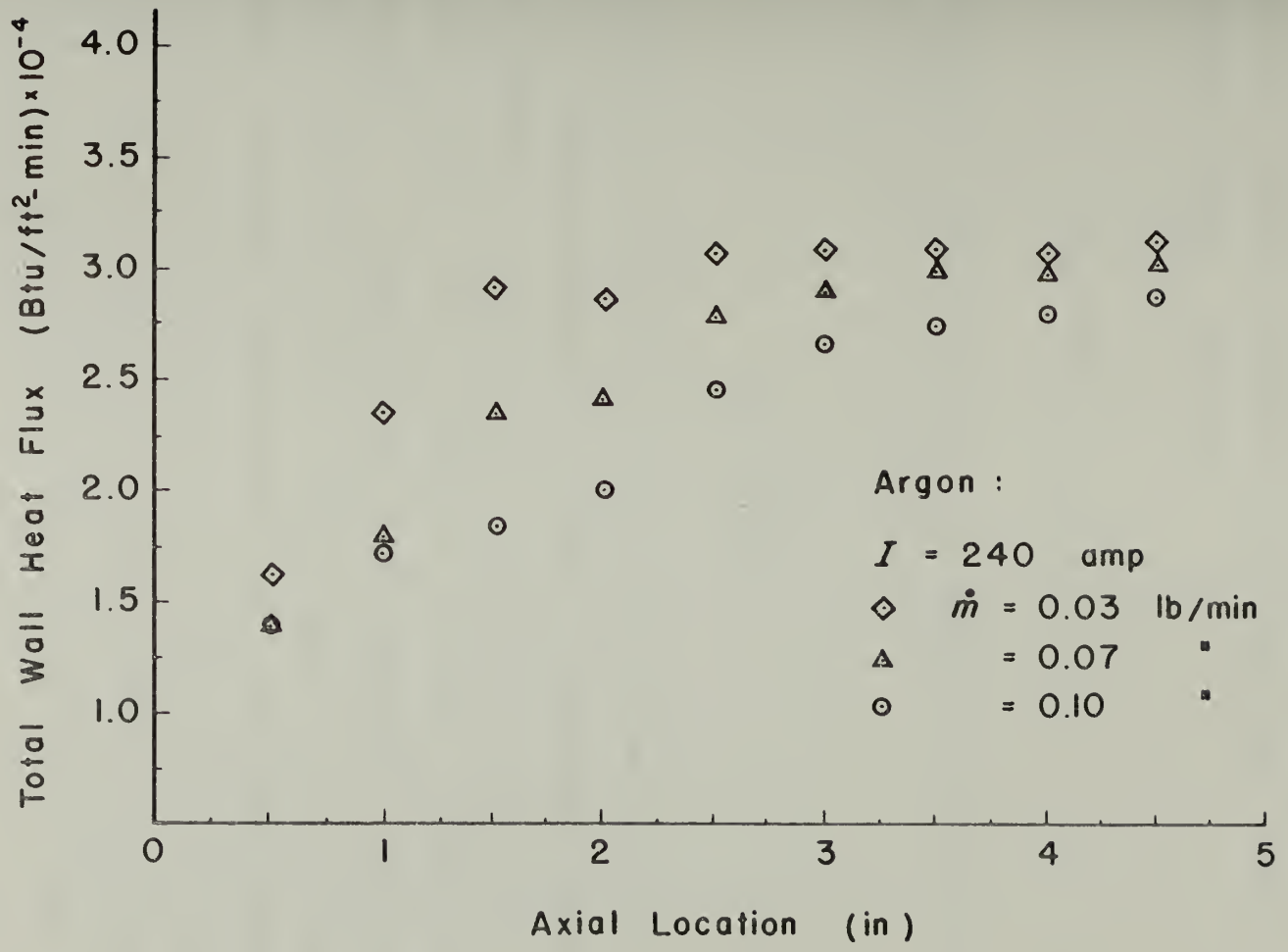

Figure III.8 Axial Distribution of Total Wall Heat Flux with Gas Flow Rate

balance performed on a segment in the asymptotic region dictates that the rate of energy removal through the tube wall must be balanced by the local input rate of electrical energy. That is,

$$q_a \cdot 2\pi R \, \Delta x = E_{x,a} \, \Delta x \cdot I. \qquad \text{(III.1)}$$

According to this expression the asymptotic value of the total wall heat flux is expressed by,

$$q_a = \frac{E_{x,a} I}{2\pi R} \cdot \qquad \text{(III.2)}$$

Therefore, confirmation of the q_a data shown in Figure III.9 is implicit with the favorable comparisons between the asymptotic electric field intensity data for argon shown in Figure III.6. Moreover, the local energy balance performed on a segment in the fully-developed region provides a convenient check on the accuracy of the calormetric and wall potential measurements. As is evident from the q_a and $E_{x,a} I/2\pi R$ distributions for argon shown in Figure III.9, closure of this local energy balance is obtained to within the combined experimental uncertainties of q_a ($\pm$ 6%), $E_{x,a}$ ($\pm$ 3%), and I ($\pm$ 1%).

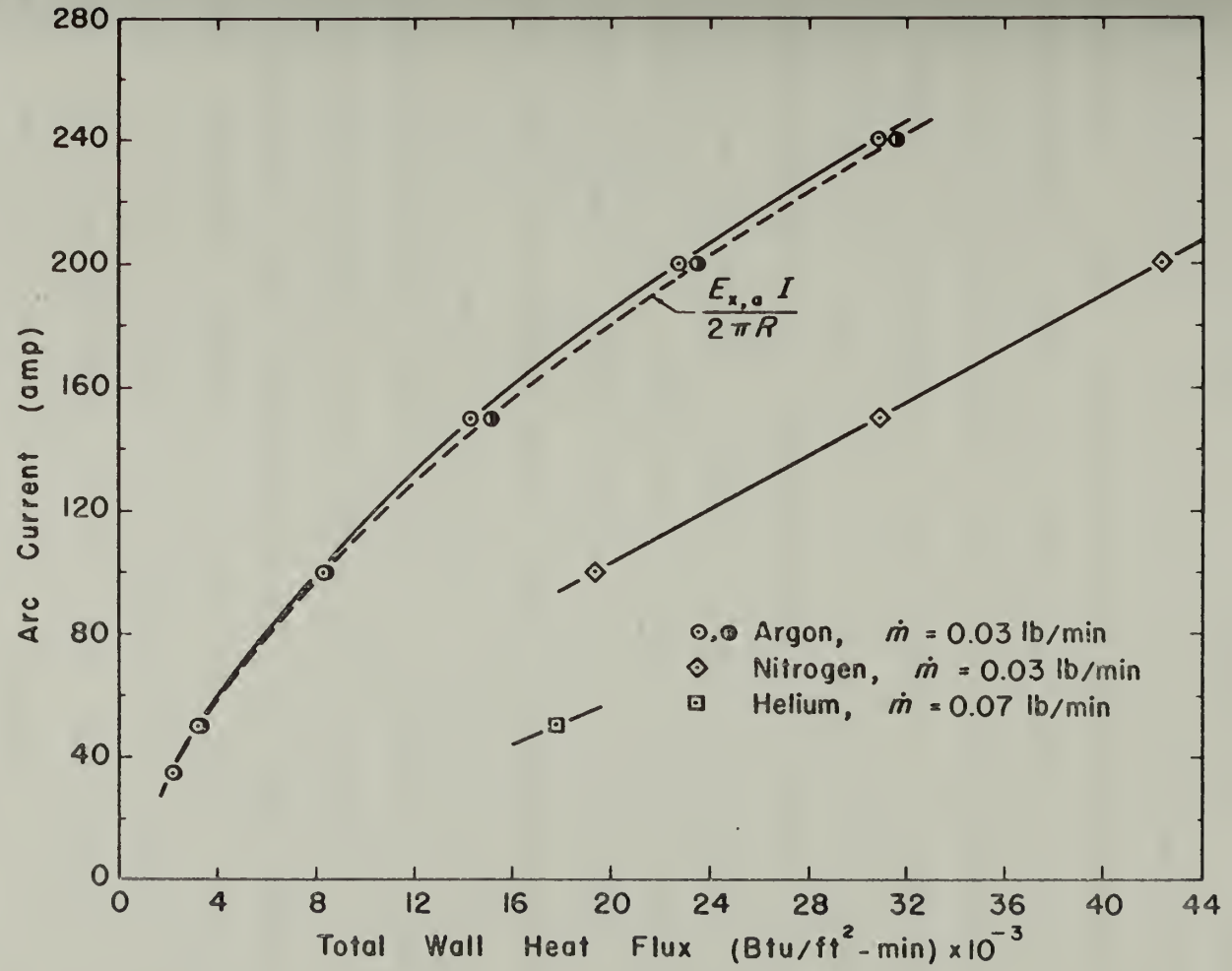

Figure III.9 Variation of the Total Wall Heat Flux with Arc Current in the Asymptotic Region

The percentage contribution to the total wall heat flux due to radiation from a fully-developed argon plasma and its variation with arc current is shown in Figure III.10. Also shown are the experimental data of Barzelay[47] and Emmons[12,13]. The Harvard data are actually somewhat redundant in that the distribution reported by Emmons[13] was obtained by applying a correction factor of 1.5 to the data reported by Barzelay (the total radiation meter used at Harvard is discussed in the Appendix). In computing the electrical conductivity and radiation source strength properties for argon, Emmons determined that the correction factor was necessary in order to obtain the best fit to overall arc data. According to Figure III.10, however, better agreement exists between the radiation data of this study and the original Harvard data reported by Barzelay.

As discussed in Chapter II, the axial distribution of the mixed-mean enthalpy (h_m) is obtained by closing off the energy balance at successive axial locations. The corresponding mean temperatures (T_m) are then obtained from the caloric equation of state [38,39,41]. Figures III.11 and III.12 depict the respective arc current and gas flow rate dependency of the axial distribution of the mean temperature in argon. The convergence of the data in Figure III.12 provides further evidence of the attainment of a fully-developed condition which is independent of operating gas flow rate.

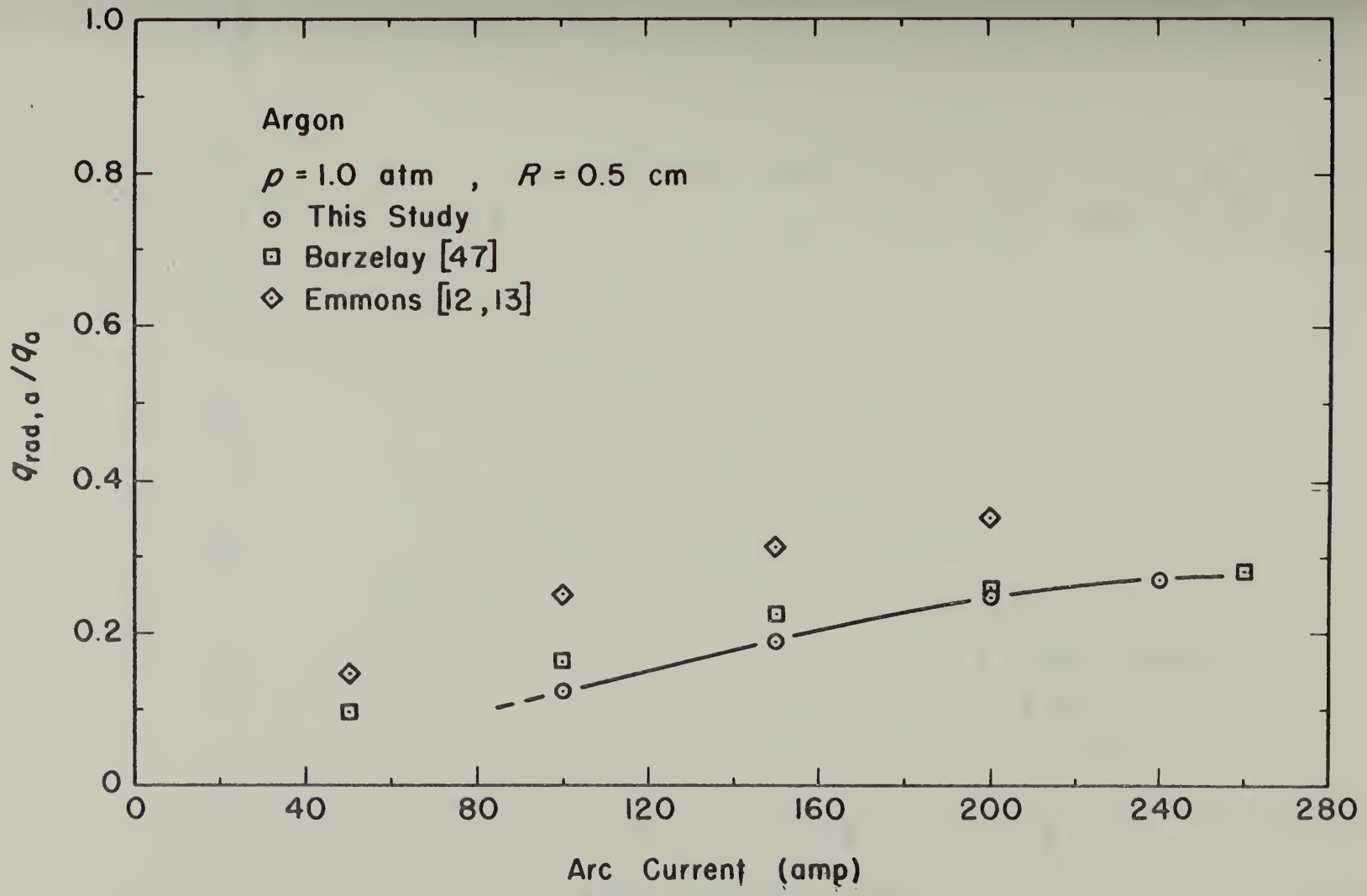

Figure III.10 Variation of the Radiative Wall Heat Flux with Arc Current in the Asymptotic Region of an Argon Plasma

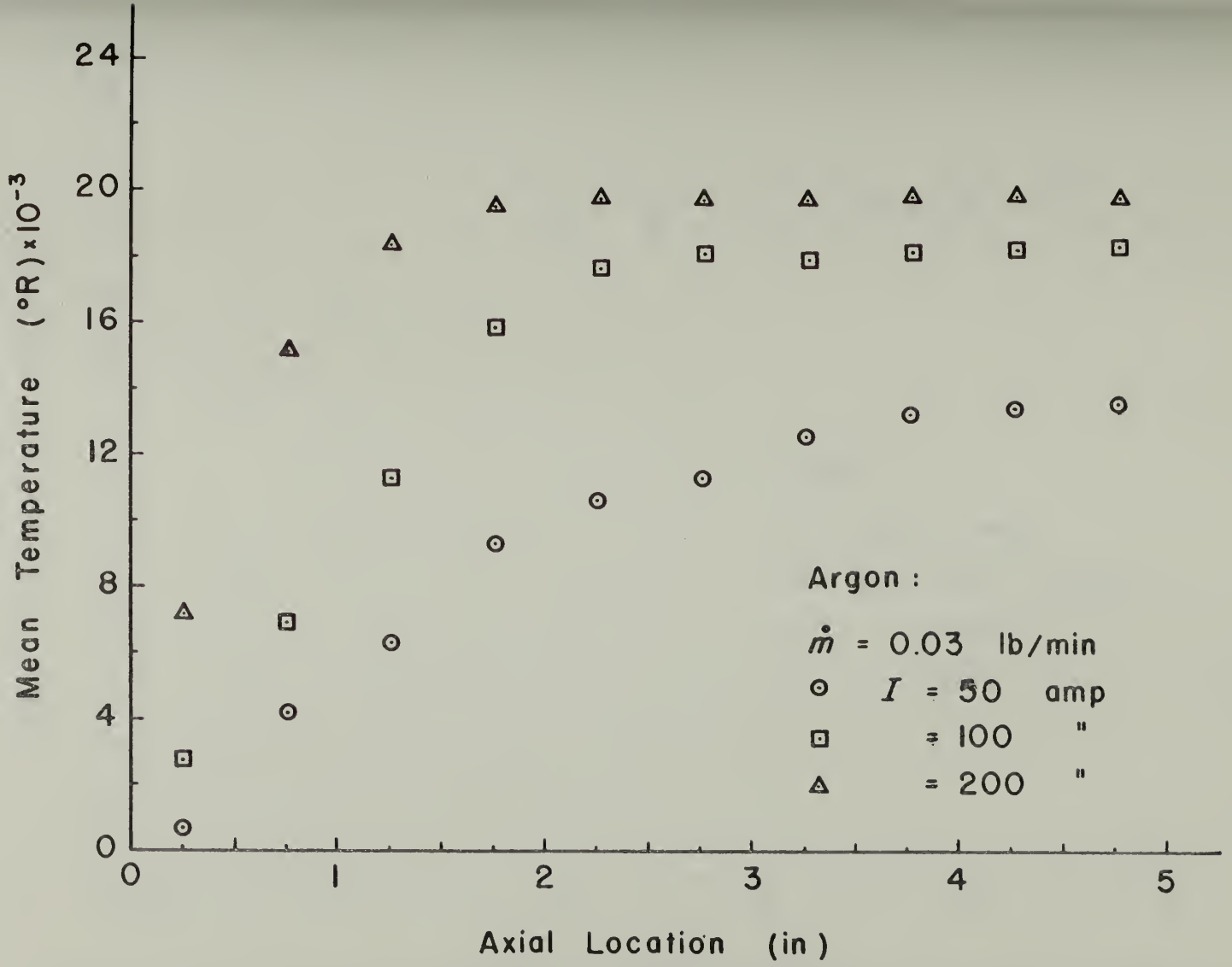

Figure III.11 Axial Distribution of Mean Temperature with Arc Current

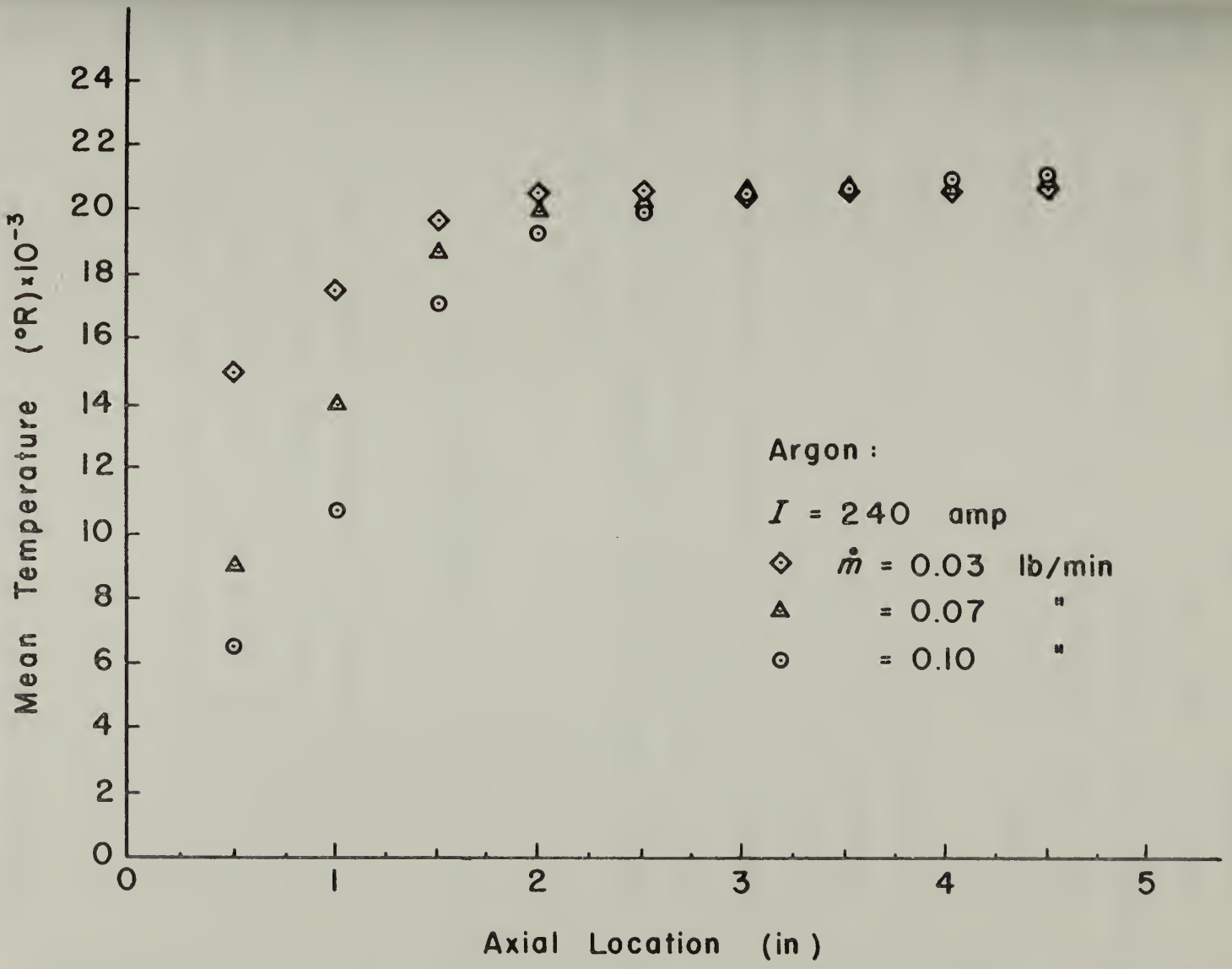

Figure III.12 Axial Distribution of Mean Temperature with Gas Flow Rate

The variations with arc current of the asymptotic mean temperatures in Ar, N_2, and He are shown in Figure III.13. The extraordinarily low value of the mean temperature in helium (nearly an order of magnitude lower than the corresponding value for argon) will be discussed in Chapter IV.

The Nusselt number (Nu = hD/k) is introduced in an attempt to correlate, in terms of appropriate dimensionless parameters, the wall heat transfer in the asymptotic region of the laminar, constricted tube arc. By defining the heat transfer conductance (h) in terms of the total wall heat flux and a temperature potential, the Nusselt number takes the form

$$Nu_m = \frac{2R\, q_a}{k_m (T_{m,a} - T_w)} \qquad \text{(III.3)}$$

where k_m is the thermal conductivity evaluated at $T_{m,a}$ and T_w is the duct wall temperature (assumed constant at 500°K)* Introduction of the local energy balance in the asymptotic region (Equation III.2) into Equation III.3 yields

---

*While this value of T_w was chosen so as to be consistent with the assumed value used in the equilibrium solution by Bower and Incropera [20], it is noted that a considerable variation (say, ±50%) in T_w will have little effect on the difference $(T_{m,a} - T_w)$ since $T_{m,a}$ is of the order of 10^4°K.

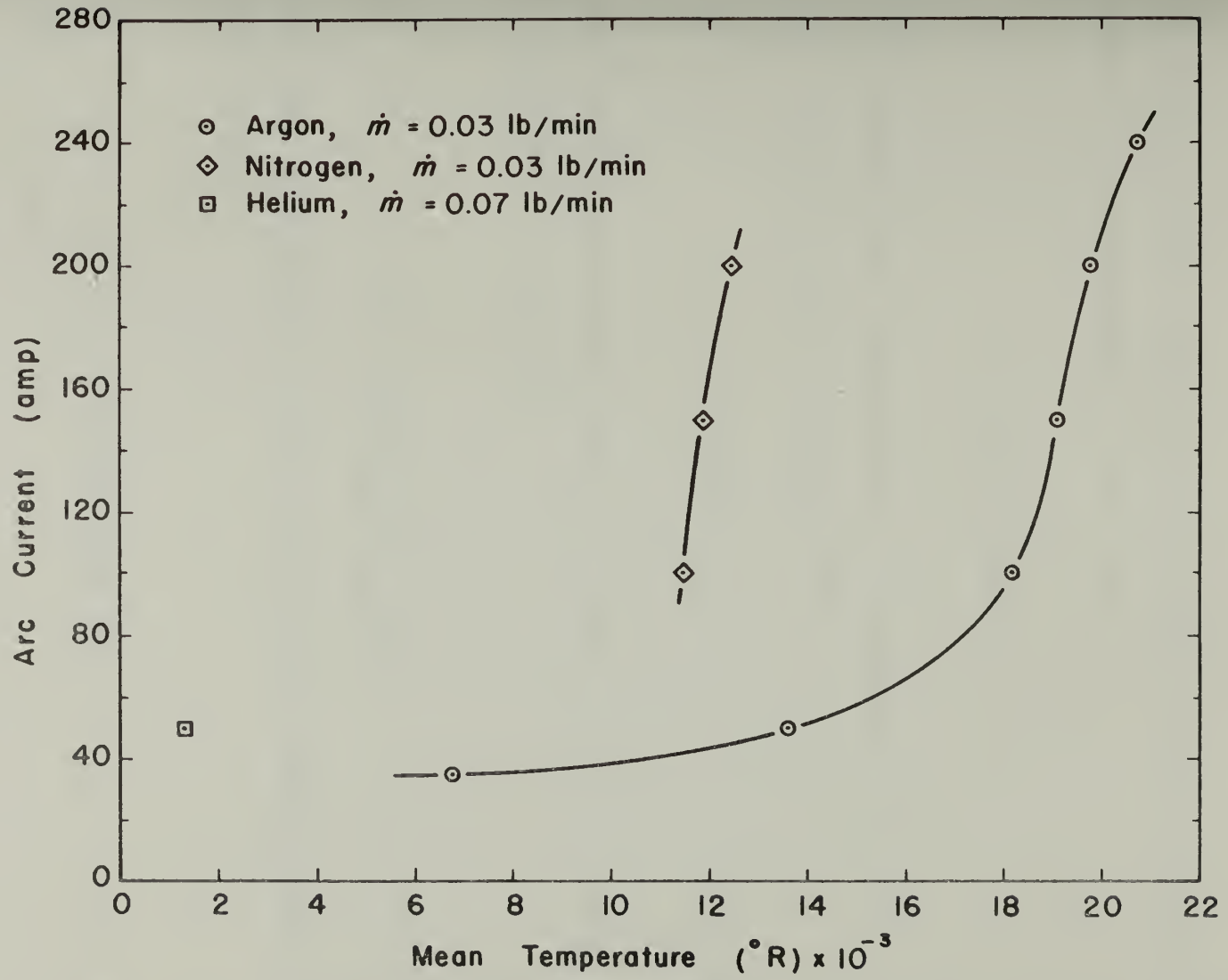

Figure III.13 Variation of the Mean Temperature with Arc Current in the Asymptotic Region

$$Nu_m = \frac{E_{x,a} I}{\pi k_m (T_{m,a} - T_w)} . \qquad \text{(III.4)}$$

The electric field intensity is in turn related to the arc current by an expression of the form

$$I = 2\pi E_{x,a} \int_0^R \sigma r dr .$$

If the electrical conductivity (σ) is assumed to be constant and is evaluated at $T_{m,a}$, then

$$I \simeq \pi R^2 E_{x,a} \sigma_m . \qquad \text{(III.5)}$$

Substituting this relationship into Equation III.4 gives an expression of the form

$$Nu_m = \frac{I^2}{(\pi R)^2 \sigma_m k_m (T_{m,a} - T_w)} . \qquad \text{(III.6)}$$

It is now convenient to introduce an Ohmic heating parameter defined as

$$Oh_m \equiv \frac{R^2 \sigma_m k_m (T_{m,a} - T_w)}{I^2} , \qquad \text{(III.7)}$$

which may then be used to correlate the Nusselt number through the relationship

$$Nu_m = \frac{1}{\pi^2} (Oh_m)^{-1.0} \quad . \qquad \text{(III.8)}$$

This correlation is plotted in Figure III.14 for argon along wth the correlation obtained by Bower and Incropera[20] from numerical considerations. While the numerically predicted correlation compares reasonably well with the experimental data, it consistently overpredicts Nu_m. Better agreement with experiment is gained by multiplying Equation III.8 by a constant. In so doing the experimental data (for argon with $I \gtrsim 100$ amp) is correlated to within 4% of the relationship

$$Nu_m = \frac{1.145}{\pi^2} (Oh_m)^{-1.0} \quad . \qquad \text{(III.9)}$$

Since Equation III.8 is independent of the type of gas, the above correlation should apply equally well for nitrogen and helium. While the experimental values of the Nusselt number for these two gases (as well as for the lower current values in argon) fall within the range of values included in Figure III.14, the corresponding values of Oh_m fall well below ($\sim 10^{-3}$ to 10^{-5}) those appearing in the figure. The cause of these rather marked deviations

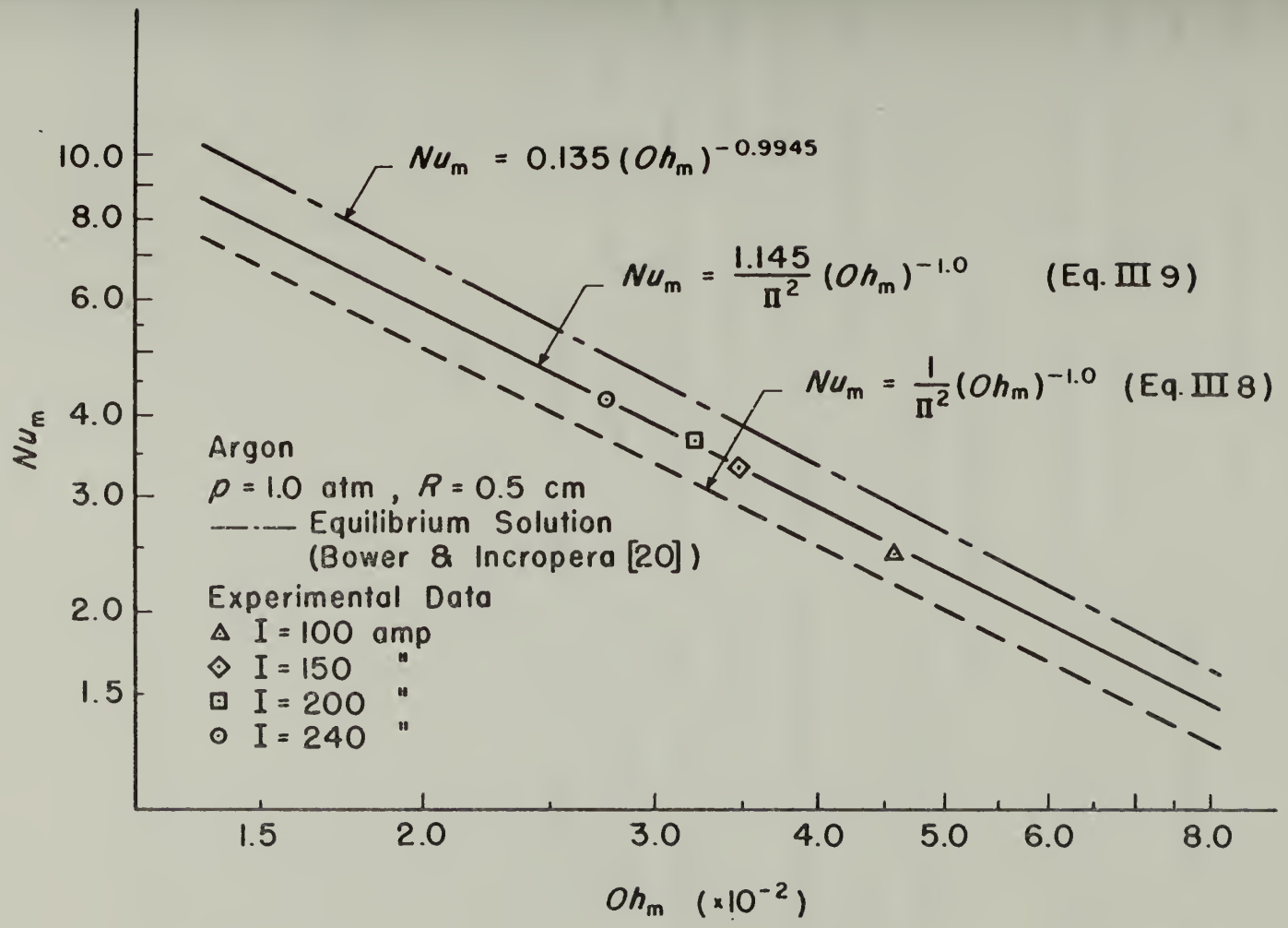

Figure III.14 Comparison of Experimental and Numerical Nusselt Number Correlations in the Asymptotic Region of an Argon Plasma

from Equation III.8 is most likely due to the inaccuracies which result from evaluating k_m and σ_m at the mean temperature and/or the inaccuracies which result from use of these equilibrium properties under conditions which are most likely characterized by significant departures from local thermodynamic equilibrium. The latter point will be the subject of further discussion in the following chapter.

III.4 Anode Heat Flux

Figure III.15 illustrates the dependency of the total anode heat flux on arc current for Ar, N_2, and He. At gas flow rate and arc current combinations for which the anode is preceded by a fully-developed region, the anode heat transfer was observed to vary only slightly ($\lesssim$ 10%) with gas flow rate and to vary linearly with arc current (for I > 100 amp) according to the expression

$$Q_A = 8800 + 155\ I \qquad \text{(III.10)}$$

for argon, and

$$Q_A = -\ 4300 + 367\ I \qquad \text{(III.11)}$$

for nitrogen.

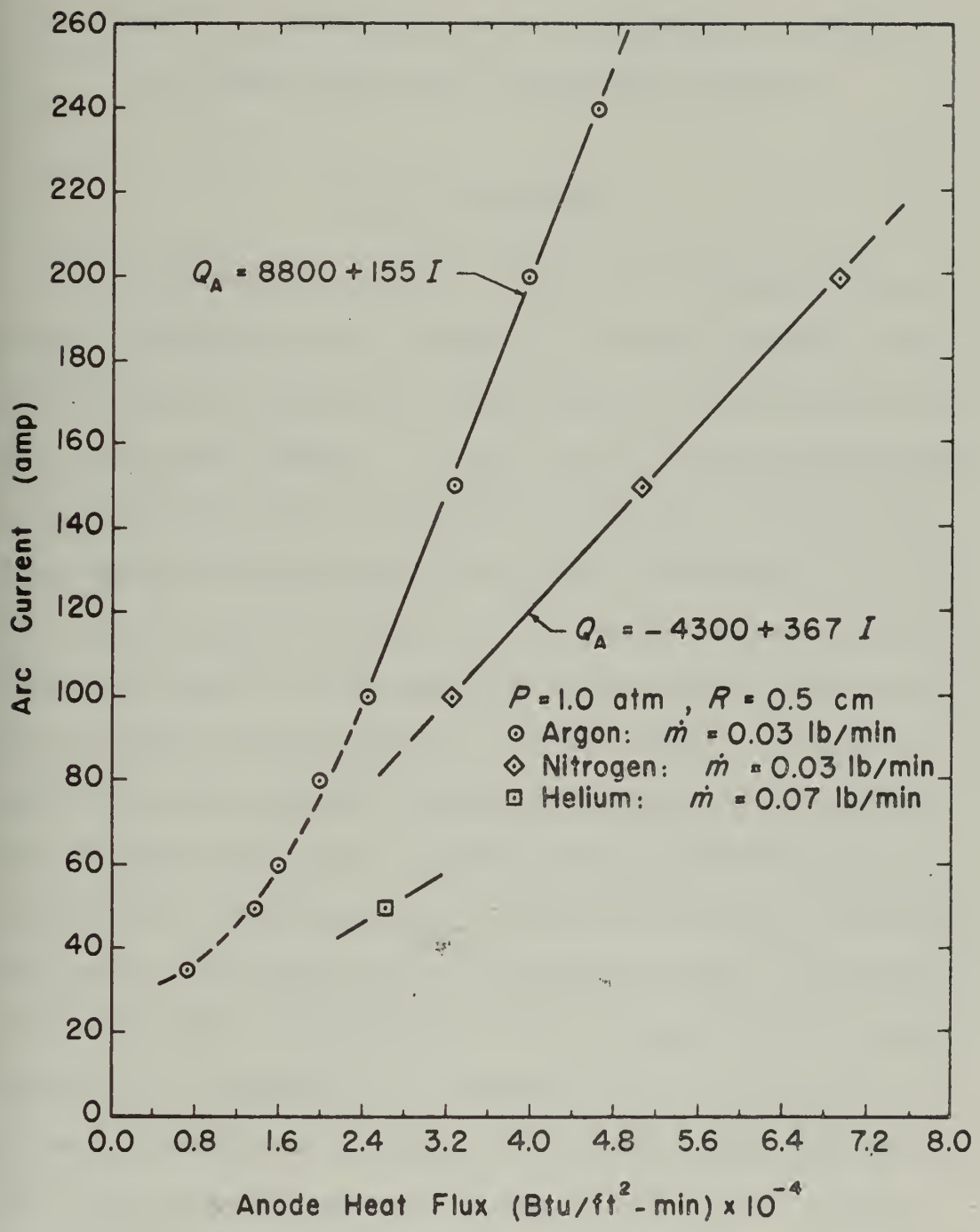

Figure III.15 Variation of Anode Heat Transfer with Arc Current

CHAPTER IV INTERPRETATION OF EXPERIMENTAL RESULTS AND COMPARISON WITH THEORETICAL STUDIES

IV.1 Discussion

The performance of any comparison between experimental and theoretical results, of course, necessitates compatibility between the experimental configuration and the theoretical model. In this study, this compatibility is achieved only for the asymptotic region of the arc. Although considerable data have been acquired for the inlet region of the constrictor, it was determined that measurements made in this region were extremely sensitive to the entrance configuration. In particular, variation of the duct inlet geometry (effected through adjustment of the cathode-nozzle gap) significantly influenced the measured axial distributions of the electric field intensity and total wall heat flux in the inlet region. Similarly, all theoretical considerations for the arc-heating region require the assumption of entrance flow profiles and, as shown by Bower and Incropera[20], predictions for the inlet region depend upon the assumed form of the initial velocity and enthalpy profiles. Accordingly, this sensitivity of experimental and theoretical results to entrance

conditions precludes any meaningful comparison for the inlet region. In contrast, the experiments of this study and the numerical solution[20] indicate that entrance effects have no bearing on either measured or predicted quantities for the asymptotic region and, therefore, a meaningful comparison of results applicable to this region is possible.

This chapter will deal only with comparisons between experiment and theory which apply to the asymptotic (and anode) regions of the constricted tube arc. In particular, comparisons for argon will be made between the experimental results of this study and the analytical solution by Stine and Watson[18], the numerical equilibrium solution by Bower and Incropera[20], and the numerical nonequilibrium solution by Clark[25]. Owing to the scarcity of experimental data acquired in this study for helium, the experimental data of Emmons[13] will be used for comparison with the theoretical results obtained by Bower[56], Pytte and Williams[48], and Pytte and Winsor[24]. For nitrogen, comparisons will be made between the experimental results of this study and the Stine-Watson analytical solution. In making these comparisons, emphasis will be placed upon ascertaining the influence of nonequilibrium effects on the arc parameters. In comparing the anode heat transfer model of Pfender, et al[6,7] with the experimental results of

this study, attention is given to determining the ability of this model to accurately predict the anode heat flux, particularly in light of available empirical correlations.

IV.2 Comparisons For Argon

Although the equilibrium model of Bower and Incropera and the nonequilibrium model of Clark have been adequately discussed previously, more must be said of the Stine-Watson analytical solution before using it in subsequent comparisons. As reported by Jedlicka and Stine[5], the expressions for the electric field intensity and total wall heat flux which result from this closed form solution are given by

$$E_x = \frac{C_3}{d} \left[1-e^{-C_2 L/\dot{m}}\right]^{-1/2} \qquad \text{(IV.1)}$$

and

$$q = C_4 \frac{I}{d^2} \left[1-e^{-C_2 L/\dot{m}}\right]^{1/2} , \qquad \text{(IV.2)}$$

where the constants C_2, C_3, and C_4 are specific functions of the constant pressure gas transport properties, d is the duct diameter, and L is the duct inlet length. When applied to the asymptotic region ($L \to \infty$) of the constricted tube arc, Equations IV.1 and IV.2 reduce to the expressions:

$$E_{x,a} = \frac{C_3}{d} \tag{IV.3}$$

$$q_a = C_4 \frac{I}{d^2} \cdot \tag{IV.4}$$

Basing the above equations upon the tube radius and using the following results for the constants C_3 and C_4 [49]

$$C_3 = \frac{2.4}{Ag^{1/2}} \tag{IV.5}$$

$$C_4 = \frac{0.383}{Ag^{1/2}} , \tag{IV.6}$$

Equations IV.3 and IV.4 take the form

$$E_{x,a} = \frac{2.4}{Ag^{1/2}} \frac{1}{R} \tag{IV.7}$$

and

$$q_a = \frac{0.383}{Ag^{1/2}} \frac{I}{R^2} \cdot \tag{IV.8}$$

Ag (mho/watt) represents the assumed linearized relationship between the electrical conductivity and the heat flux potential ϕ ($\phi \equiv \int k dT$), and the units for the remaining variables are $E_{x,a}$(volts/m), q_a(watts/m^2), I(amp), and

R(m). While the results reported by Stine and Watson[18] are primarily for nitrogen and air, this simplified model has been modified by Bower[17] to include the appropriate linearized property relationships for argon. By applying the value of Ag reported by Bower, the simplified Stine-Watson expressions (for argon with R = 0.5 cm) are then given by

$$E_{x,a} = 9.55 \text{ volts/in} \qquad \text{(IV.9)}$$

and

$$q_a \text{ (Btu/ft}^2\text{-min)} = 63.4 \text{ I(amp)} \; . \qquad \text{(IV.10)}$$

The asymptotic values of the electric field intensity ($E_{x,a}$), total wall heat flux (q_a), fraction of radiative to total wall heat flux ($q_{rad,a}/q_a$), mixed-mean enthalpy ($h_{m,a}$), and mean temperature ($T_{m,a}$), as computed from the equilibrium[20] and nonequilibrium[25] models, are listed in Table IV.1 along with the corresponding experimental results for an argon arc. The values from Table IV.1, along with results obtained from Equations IV.9 and IV.10 for the Stine-Watson model, were used to generate the plots shown in Figures IV.1 through IV.5.

The large disparities (in both the magnitude and the functional dependence on arc current) between the

Table 7.11. A Comparison Between Experimental Results and Equilibrium and Nonequilibrium Theoretical Predictions for the Asymptotic Region in Argon (p = 1.0 atm, R = 0.5 cm, and T_w = 500°K).

I (amp)	Source*	$E_{x,a}$ (volts/in)	q_a (Btu/ft^2 - min)	$\frac{q_{rad,a}}{q_a} \times 100$	$h_{m,a}$ (Btu/lbm)	$T_{m,a}$ (°R)
35	Experiment	9.3	2,170	--	840	6,790
	Equil. Sol'n.[20]	11.04	2,562	8.35	1,631	13,048
	Nonequil. Sol'n.[25]	9.29	2,195	1.14	1,470	--
50	Experiment	10.1	3,110	--	1,700	13,600
	Equil. Sol'n.	11.05	3,663	13.5	1,941	15,145
	Nonequil. Sol'n.	9.98	3,315	2.87	1,735	--
100	Experiment	12.6	8,270	12.3	2,720	18,200
	Equil. Sol'n.	12.57	8,332	27.6	2,946	18,706
	Nonequil. Sol'n.	12.81	8,480	12.4	2,680	--
150	Experiment	15.3	14,300	19.0	3,160	19,100
	Equil. Sol'n.	14.37	14,290	37.4	3,930	20,274
	Nonequil. Sol'n.	15.73	15,600	19.2	--	--
200	Experiment	17.8	22,800	24.7	3,550	19,800
	Equil. Sol'n.	16.20	21,460	44.0	4,987	21,445
	Nonequil. Sol'n.	18.43	24,400	23.8	--	--

* The nonequilibrium predictions[25] are for a noncatalytic wall.

Table IV.1. (Cont'd)

I (amp)	Source*	$E_{x,a}$ (volts/in)	q_a (Btu/ft^2 -min)	$\frac{q_{rad,a}}{q_a} \times 100$	$h_{m,a}$ (Btu/lbm)	$T_{m,a}$ (°R)
240	Experiment	19.9	30,900	26.8	4,340	20,800
	Equil. Sol'n.	17.45	27,760	47.7	5,995	22,337
	Nonequil. Sol'n.	20.45	32,450	26.0	--	--

* The nonequilibrium predictions[25] are for a noncatalytic wall.

$E_{x,a}$ (Figure IV.1) and q_a (Figure IV.2) distributions computed from the simplified Stine-Watson model and those obtained experimentally are thought to be the result of two oversimplifications inherent in the model. In particular, the use of linearized property relationships and the assumption of negligible radiation losses, particularly at the higher arc currents, are thought to be the primary cause of these disparities.

The comparison between the numerical solution by Bower and Incropera and the experimental results indicate that the equilibrium theory agrees favorably with experiment in the 100 amp range, while it overpredicts and underpredicts the experimental data for both $E_{x,a}$ and q_a at lower and higher arc currents, respectively. A plausible explanation for the overprediction at the lower arc currents can be obtained by considering the following expression for Ohm's law

$$E_x = \frac{I}{2\pi \int_0^R \sigma r dr} \quad . \tag{IV.11}$$

If the low current arc is characterized by significant departures from thermochemical equilibrium, the electrical conductivity used in the equilibrium solution will be less than the actual value of σ in those regions where nonequilibrium conditions prevail. Consequently, the theoretical

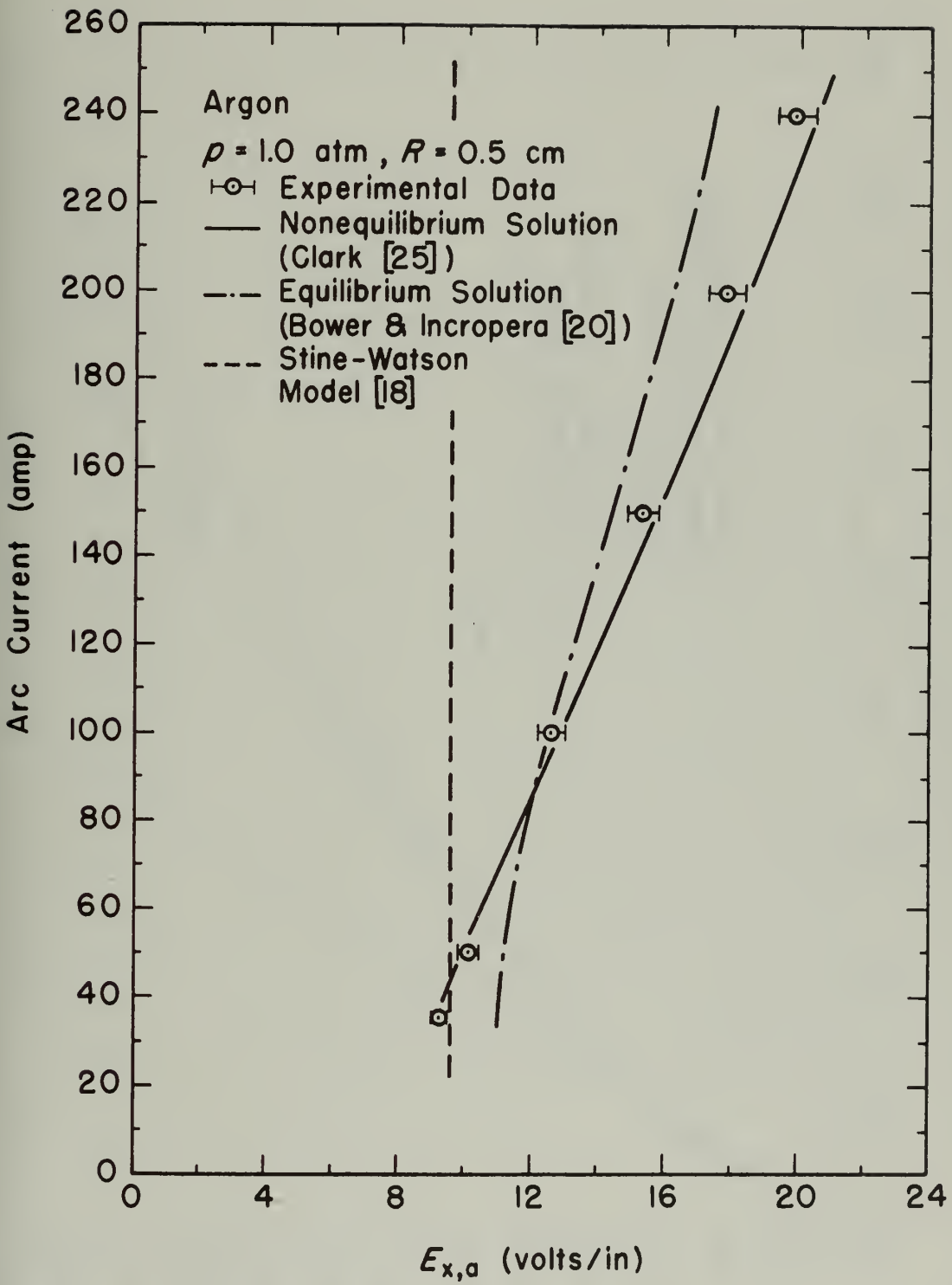

Figure IV.1 Comparison Between Experiment and Theory for the Asymptotic Electric Field Intensity in Argon

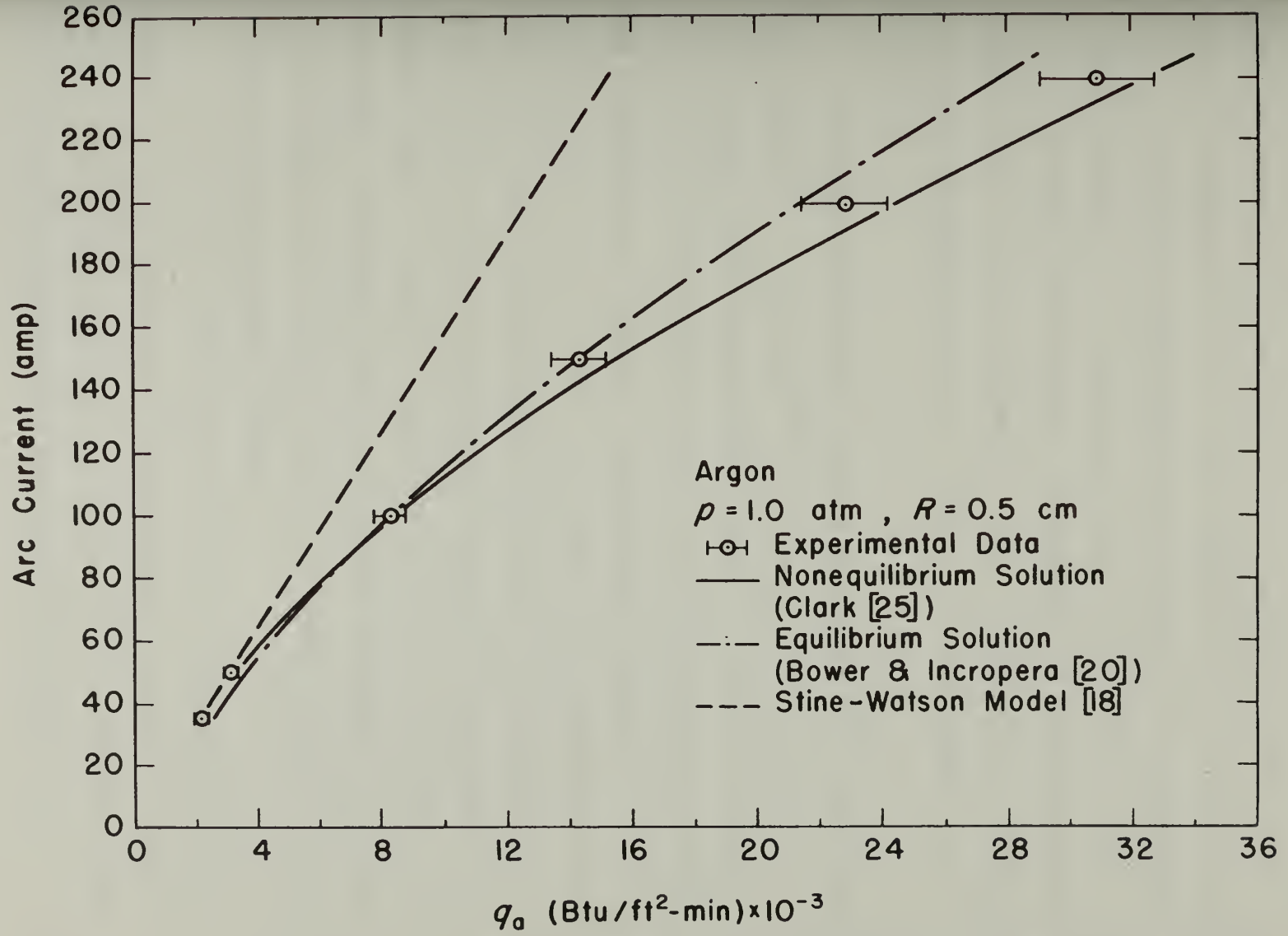

Figure IV.2 Comparison Between Experiment and Theory for the Asymptotic Total Wall Heat Flux in Argon

evaluation of the integral of the electrical conductivity over the tube cross-section will be reduced, which, according to Equation IV.11, will result in an overprediction of $E_{x,a}$, increased Joule heating, and thus an accompanying overprediciton of the total wall heat flux. While this nonequilibrium effect suitably explains the lower current comparisons, it does not explain why the equilibrium theory apparently underpredicts $E_{x,a}$ and q_a at the higher arc currents.

Recent theoretical studies by Kruger[50], Incropera and Viegas[23], and Clark[25] and recent experimental spectroscopic data reported by Bott[21] and by Incropera and Giannaris[22] indicate that arc nonequilibrium effects are most severe at low arc currents and diminish with increasing arc current. On this basis, the experimental results and equilibrium predictions which are compared in Figures IV.1 and IV.2 should converge with increasing arc current when, in fact, they diverge for $I > 100$ amp. Accordingly, the equilibrium underpredictions for $E_{x,a}$ and q_a at higher arc currents would not appear to be a result of wall-induced nonequilibrium.

A plausible explanation for the high current disparity is the inability of the equilibrium model to properly account for conduction effects at the elevated temperatures associated with high current operation. In

particular, it is possible that the equilibrium model is underpredicting the energy transfer to the tube wall due to conduction. This contention is supported by the comparisons for the fraction of radiative to total wall heat flux shown in Figure IV.3, as well as by the mean enthalpy and mean temperature comparisons of Table IV.1. Specifically, it is noted from Figure IV.3 that, while excellent agreement exists between experiment and the nonequilibrium predictions for $q_{rad,a}/q_a$, the equilibrium prediction, for $I > 100$ amp, is nearly double the nonequilibrium and experimental distributions. In comparing the equilibrium and nonequilibrium predictions for $q_{rad,a}/q_a$, it may be argued that the observed differences are possibly a result of a dissimilarity in the radiation source density terms used in the two solutions. This is not the case, however, for it has been shown by Clark[25] that, in the limit of equilibrium, the radiation model employed in the nonequilibrium solution agrees favorably with the radiation source density used by Bower and Incropera. Moreover, both of these plasma radiation models are consistent with the assumed wavelength distribution of the radiation incident upon the surfaces of the radiation gage (see the Appendix). The overprediciton of $q_{rad,a}/q_a$ is therefore most likely due to the higher temperature levels which characterize the equilibrium solution. This fact is

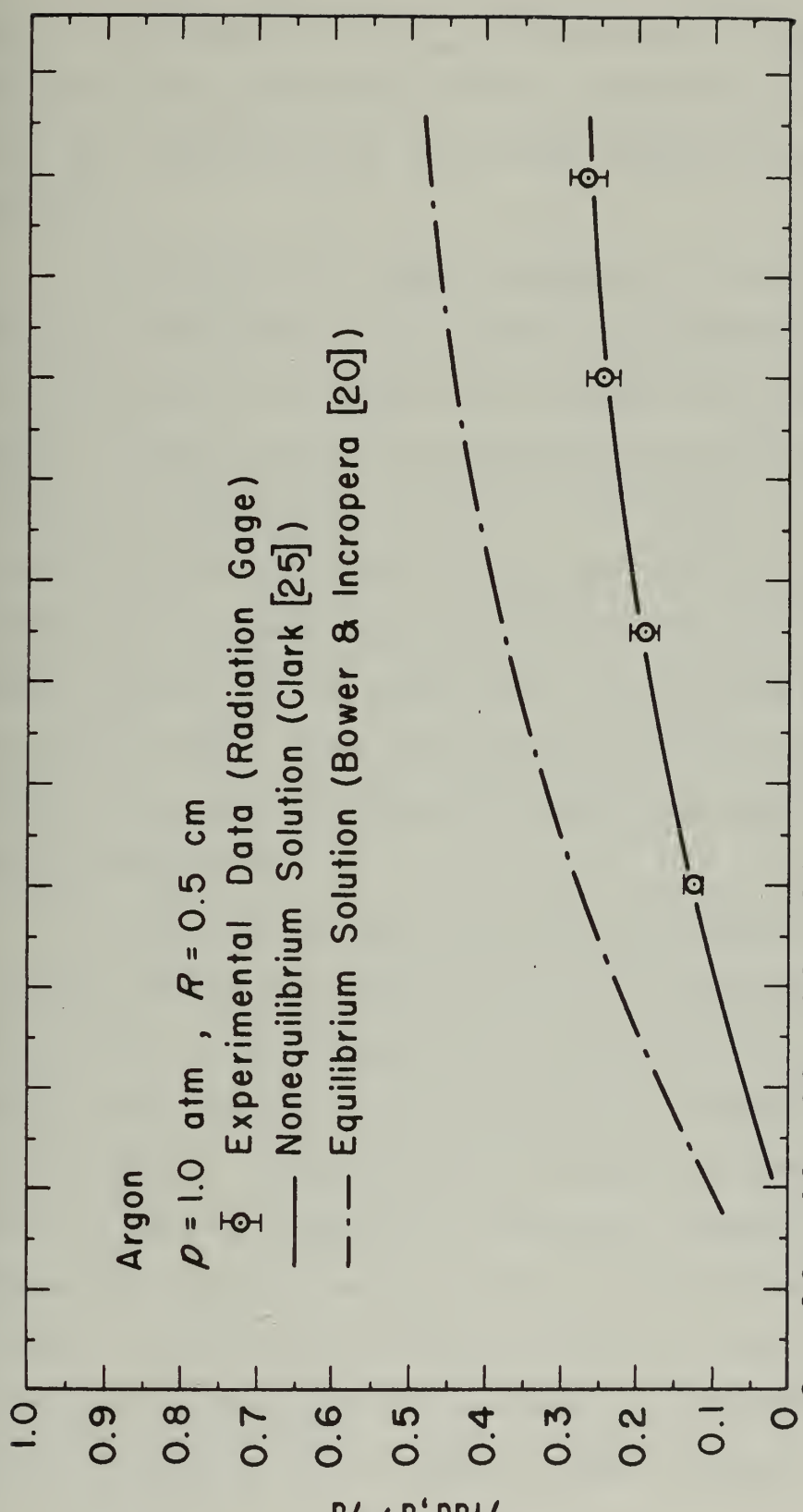

Figure IV.3 Comparison Between Experiment and Theory for the Fraction of Radiative to Total Wall Heat Flux for the Asymptotic Region in Argon

further evidenced by the $T_{m,a}$ comparisons of Table IV.1 as well as by the comparisons between equilibrium, nonequilibrium, and experimentally determined temperature profiles[25].

On the basis of these arguments, it is concluded that, for the higher (I > 100 amp) arc currents in argon, the reduction of the equilibrium temperature profiles needed to bring about a corresponding reduction in the electrical conductivity and thus an increase in $E_{x,a}$ and q_a (along with a decrease in $q_{rad,a}/q_a$ and $T_{m,a}$) could be achieved if the equilibrium model were to provide for greater energy loss by conduction. In an effort to confirm this premise, some attention was given to the thermal conductivity model of DeVoto[37] which was employed in the equilibrium solution.

In addition to the conventional translational mode of energy conduction, there will be a transport of chemical energy (in the form of the energy of recombination) through the ordinary (or concentration) diffusion of electron-ion pairs towards the outer regions of the arc. While the global conservation equations employed in the equilibrium model do not explicitly account for ordinary diffusion, an attempt is made to implicitly account for the resulting transport of ionization (or recombination) energy through use of a reactive thermal conductivity

(λ_R). From the work of DeVoto[37], λ_R is defined by the heat flux vector expression

$$\bar{q} \equiv -k'\nabla T - \lambda_R \nabla T \ , \qquad \text{(IV.12)}$$

where k' is the translational thermal conductivity. This expression evolves from the more general form of the heat flux vector equation by replacing the diffusion contribution to $\bar{q}$ by the term $-\lambda_R \nabla T$, wherein it is assumed that the gradient of concentration can be replaced by a temperature gradient through the equilibrium law of mass action*. The point to be made here is that the critical assumption inherent in DeVoto's formulation of the reactive thermal conductivity is that of local chemical equilibrium. More specifically, it is assumed that, in the case of a chemically reacting mixture, all forward and reverse reaction rates are sufficiently fast to preclude any effect on the local composition due to ordinary diffusion. Otherwise, use of the equilibrium law of mass action to relate concentration and temperature gradients could not be justified. Conversely, in a constricted tube plasma which is characterized by strong concentration gradients, it is certainly

---

*This derivation is treated in detail by Butler and Brokaw[51] and by Fay[52].

possible that the local atomic composition will be significantly influenced by ordinary diffusion[25], in which case the assumption of local chemical equilibrium is invalid. It is therefore suggested that the high current disparity between experimental and equilibrium theoretical results is due, in part, to a chemical nonequilibrium effect on the reactive thermal conductivity.

In connection with the above discussion, it is important to note that this observation is seemingly inconsistent with previous considerations which indicated that the departure from thermochemical equilibrium is less severe at higher arc currents. However, in comparing DeVoto's calculations for the translational and reactive thermal conductivities[37], it is noted that the percentage contribution to the effective thermal conductivity ($k_{EFF} = k' + \lambda_R$) due to λ_R increases from zero at T = 6,000°K to approximately 50% at T = 14,000°K. Accordingly, any errors which may be introduced as a result of using DeVoto's formulation for λ_R would become increasingly more significant at higher arc temperatures. In this respect, it is suggested that the failure of the equilibrium solution to provide for sufficient energy loss by conduction at the higher arc currents (I > 100 amp) is due to both its inability to allow for sufficient transport of ionization energy to the tube walls and its inability to explicitly account for the effects of

diffusion on the local gas composition. In particular, it is suggested that the thermal conductivity values (specifically, λ_R) employed in the equilibrium solution should be higher in order to bring the equilibrium theory predictions into better agreement with both the experimental observations and the nonequilibrium predictions. This contention is supported by the statements of Maecker[15] and by the comparisons reported by Morris, et al.[14]. These indicate a significant increase (by as much as a factor of two) in experimentally determined values of thermal conductivity over the corresponding predictions by DeVoto for temperatures greater than 10,000°K.

While attempts have been made to interpret Figures IV.1 through IV.3 on the basis of nonequilibrium effects and thermal conductivity considerations, final judgement on the adequacy of the equilibrium model cannot be made until the combined experimental and theoretical uncertainties are considered. In an attempt to determine the range of uncertainties associated with the equilibrium solution, a parametric study was conducted[53] wherein the properties (σ, k_{EFF}, and P_R) were selectively varied over their respective limits of estimated accuracy (σ, ± 15%; k_{EFF}, ± 10%; and P_R, ± 15%)*. It was determined

---

*The theoretical uncertainties for σ and k_{EFF} were set by DeVoto (private communication with Kingsbury[60]) while the uncertainty in P_R was arbitrarily selected[53].

from this study that the upper uncertainty limit for $E_{x,a}$ and q_a resulted from decreasing σ by 15%, increasing k_{EFF} by 10%, and increasing P_R by 15%, while the lower limit resulted from increasing σ by 15%, decreasing k_{EFF} by 10%, and decreasing P_R by 15%. The corresponding uncertainty bands for the equilibrium predictions are shown in Figures IV.4 and IV.5 along with the experimental data and the related experimental uncertainities, $E_{x,a}$ (±3%) and q_a(±6%). On the basis of the overlap between the theoretical and experimental uncertainty bands, and in view of the previous discussion concerning the use of DeVoto's formulation for the thermal conductivity, it is concluded that, to within the existing knowledge of plasma transport and radiation properties, single-fluid models are suitable for predicting asymptotic values for the electric field intensity and total wall heat flux, at least for the range of conditions in argon considered in this study. Conversely, the equilibrium model is not suitable for predicting $q_{rad,a}/q_a$ over the entire range of conditions investigated, nor is it adequate for predicting $h_{m,a}$ and $T_{m,a}$ at the lower (< 50 amp) and higher (> 150 amp) arc current conditions. In addition, it is felt that the equilibrium model would not be suitable for predicting $E_{x,a}$ and q_a if the above comparisons were extended to include conditions of lower and higher arc currents. In this respect,

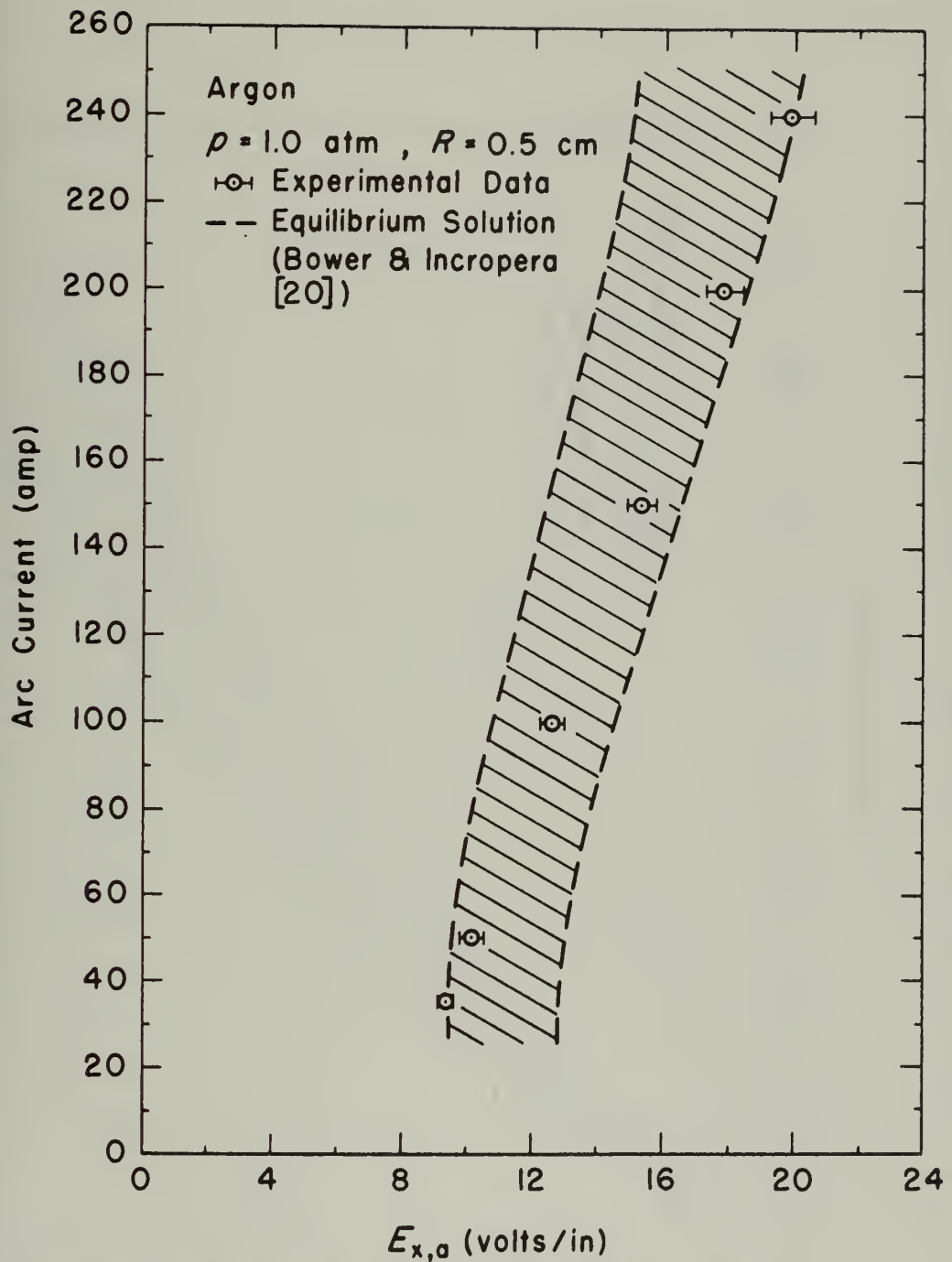

Figure IV.4 Comparison Between the Combined Experimental and Theoretical Uncertainties for the Asymptotic Electric Field Intensity in Argon

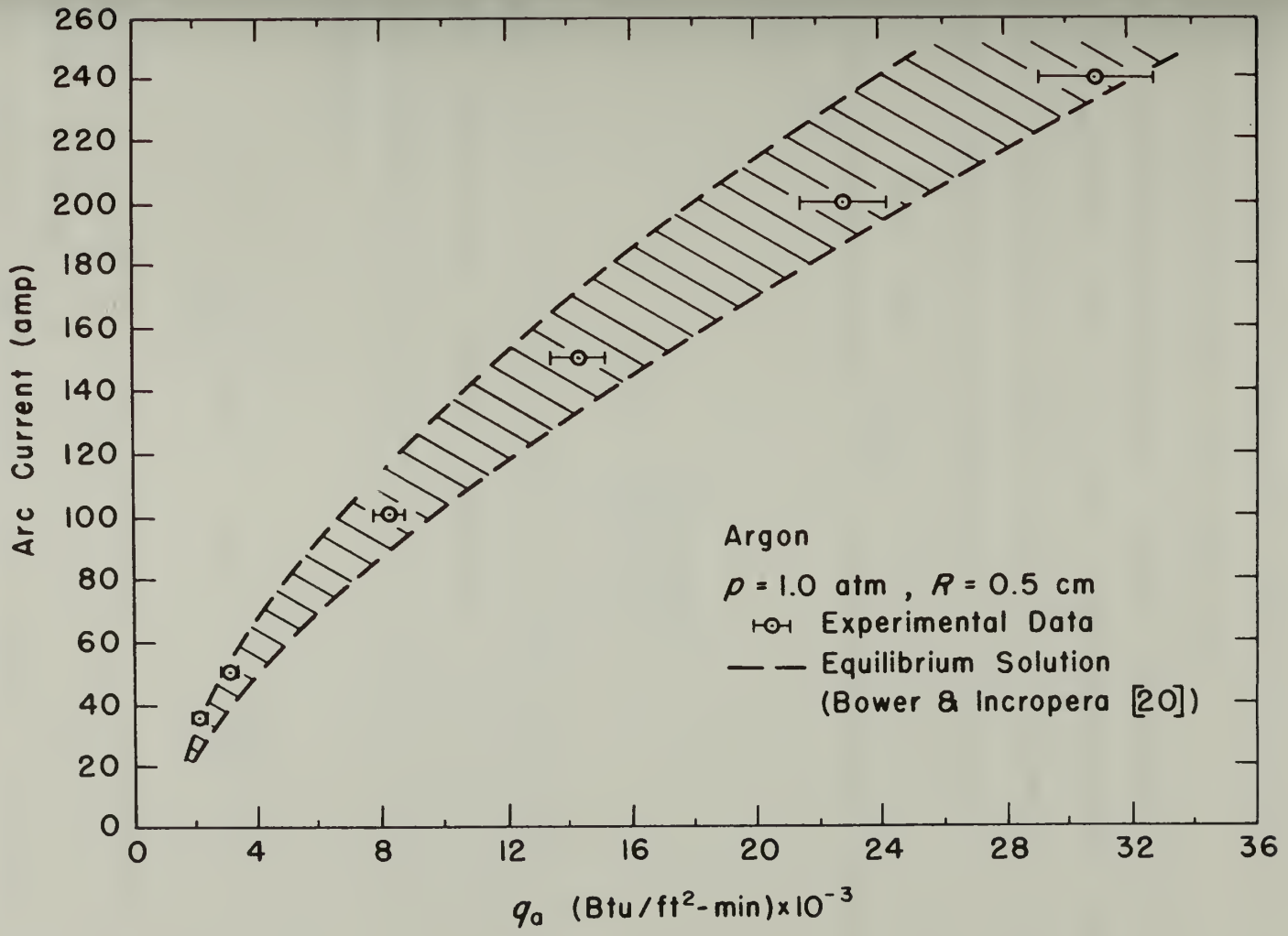

Figure IV.5 Comparison Between the Combined Experimental and Theoretical Uncertainties for the Asymptotic Total Wall Heat Flux in Argon

it is concluded that a more rigorous theoretical treatment, such as the nonequilibrium solution by Clark[25], would be required to accurately model the asymptotic region of the constricted tube argon arc.

Before concluding this section on comparisons for the asymptotic region in argon, some explanation is in order concerning the lack of agreement between the experimental value and the nonequilibrium prediction for $h_{m,a}$ at I = 35 amp (Table IV.1). Calculation of $h_{m,a}$ in the nonequilibrium solution[25] is effected through the expression[54]

$$h_{m,a} \equiv \frac{\int_o^R \rho u h r dr}{\int_o^R \rho u r dr} , \qquad \text{(IV.13)}$$

where $\rho(r)$ is the local density of the plasma and $u(r)$ is the global axial velocity component. The radial enthalpy distribution, $h(r)$, required for the above calculation is given by

$$h(r) = \frac{5}{2}\frac{k}{M_A}[\alpha T_e(r) + T_h(r)] + \frac{I_{ion}}{M_A}\alpha(r) , \qquad \text{(IV.14)}$$

where the first two terms represent the contributions due to the electrons and heavy particles, respectively, and the remaining term represents the chemical enthalpy of recombination (the specific variables are defined in the

nomenclature). In formulating Equation IV.14, the additional enthalpy contributions due to internal electronic excitation and radiation source density effects were assumed negligible. The governing equations for the asymptotic region are obtained from the general set of conservation equations by setting all axial derivatives (with the exception of the pressure gradient, dp/dx) equal to zero[25]. This manipulation, along with the assumptions of negligible viscous dissipation and pressure work, results in a decoupling of the hydrodynamic and thermal flow fields. Consequently, the velocity profiles required in the above definition for $h_{m,a}$ can only be obtained by solving the following asymptotic axial momentum equation

$$\frac{1}{r}\frac{\partial}{\partial r}\left[\mu r \frac{\partial u}{\partial r}\right] - \frac{dp}{dx} = 0 \ . \qquad \text{(IV.15)}$$

It is the uncertainty associated with the determination of dp/dx in Equation IV.15 that renders the nonequilibrium solution unable to accurately predict u(r) and thus $h_{m,a}$ at arc currents less than 50 amp. For the same reason, nonequilibrium predictions for $h_{m,a}$ at currents greater than 100 amp are unrealistic - the agreement in the 50 to 100 amp range is thought to be fortuitous.

IV.3 Comparisons for Helium and Nitrogen

Asymptotic values for helium of the electric field intensity, total wall heat flux, mean enthalpy, and mean temperature computed from the equilibrium model by Bower[55] are listed in Table IV.2. Also listed in this table are the experimental data for helium reported by McKee, et al.[32] and Emmons[13], as well as the 50 ampere data of this study. The data from Table IV.2 were used for the plots of Figures IV.6 and IV.7, wherein it is noted that the experimental q_a values (with the exception of the single q_a value measured calorimetrically in this study) were obtained from the asymptotic energy balance equation (Equation III.2) and the experimental $E_{x,a}$ data.

In comparing the equilibrium theory predictions with the experimental results, it is readily apparent that, unlike the previous comparisons for argon, the single-fluid model is totally deficient in its attempt to accurately describe the overall energetics of the helium arc. The reason for this deficiency is believed to be a result of the severe nonequilibrium conditions which are known to exist in low current ($I < 400$ amp), atmospheric helium arcs.

The pronounced departure of helium arc plasmas from conditions of local thermodynamic eqiulibrium has been observed and discussed by others, among the first of

Table IV.2. A Comparison Between Experimental Results and Equilibrium Theoretical Predictions for the Asymptotic Region in Helium (p = 1.0 atm, R = 0.5 cm, and T_w = 500°K).

I (amp)	Source	$E_{x,a}$ ($\frac{volts}{in}$)	q_a* (Btu/ft^2 - min)	$h_{m,a}$ (Btu/lbm)	$T_{m,a}$ (°R)
35	Experiment[32]	62.4	14,500	--	--
	Equil. Sol'n.[55]	42.4	9,850	17,120	13,800
50	Experiment	60.0	17,800	1,680	1,350
	Experiment[13]	59.1	19,600	--	--
	Equil. Sol'n.[55]	36.1	12,000	19,400	15,700
100	Experiment[13]	48.6	32,200	--	--
	Equil. Sol'n.[55]	28.9	19,200	24,300	19,500
150	Experiment[13]	43.8	43,500	--	--
	Equil. Sol'n.[55]	25.7	25,800	31,700	24,600
200	Experiment[13]	40.4	53,500	--	--
250	Experiment[13]	38.1	63,100	--	--

* Total wall heat flux values for References [32] and [13] were computed from their reported $E_{x,a}$ data ($q_a = \frac{E_{x,a} I}{2\pi R}$).

which were investigators at Harvard[12,13,50,56]. These studies were primarily concerned with determination of the plasma transport properties, σ and k, through use of the so-called inversion method. As discussed by Emmons and Land[12], this method, when formulated under the assumptions of local thermodynamic eqiulibrium and negligible radiative losses, dictates that the reduced arc-column characteristics ($E_{x,a}I$ versus $E_{x,a}R$) should be related by a universal curve independent of tube radius. However, in performing electric field intensity measurements on helium arcs of varying tube radius, Emmons[13] determined that the parameters $E_{x,a}I$ and $E_{x,a}R$ were not uniquely related. Since the assumption of negligible radiation is apparently valid for low current ($I < 400$ amp), atmospheric helium arcs[57], Emmons concluded that helium arcs must be characterized by a significant departure from conditions of local thermodynamic equilibrium.

Further evidence of severe nonequilibrium conditions in helium arcs is provided by Kruger[50], Bott[56], and Aleksandrov, et al.[58]. Specifically, these investigators concluded that the free electrons and upper excited atomic states, while in equilibrium with one another, are not in equilibrium with the lower excited ($n < 3$) and ground states. In addition, Kruger notes that, in the outer regions of the arc, the electron number densities

may be several orders of magnitude higher than would be predicted if the local composition were determined from the assumption of Saha equilibrium. The existence of significant departures from equilibrium can also be inferred from the helium data acquired in this study. As indicated in Table IV.2, energy balance measurements performed on the helium arc dictate an asymptotic mean temperature of 1350°R (or 750°K) and yet, even at such a comparatively low value of $T_{m,a}$, there is sufficient ionization to produce a luminescent arc which is capable of sustaining a current of 50 amperes. This observation suggests the existence of a severe thermochemical nonequilibrium condition in the helium arc. Similar observations were made by Aleksandrov, et al.[58] whose spectroscopically determined electron temperatures were nearly 1.5 orders of magnitude greater than their mean temperatures based upon energy balance measurements.

On the basis of these findings, the comparisons between experiment and the equilibrium theory of Bower[55] (Figures IV.6 and IV.7) are virtually meaningless. That is, since the plasma tube flow situation which the single-fluid model is attempting to describe bears little resemblance to the severe nonequilibrium state which actually exists, a systematic discussion of the differences

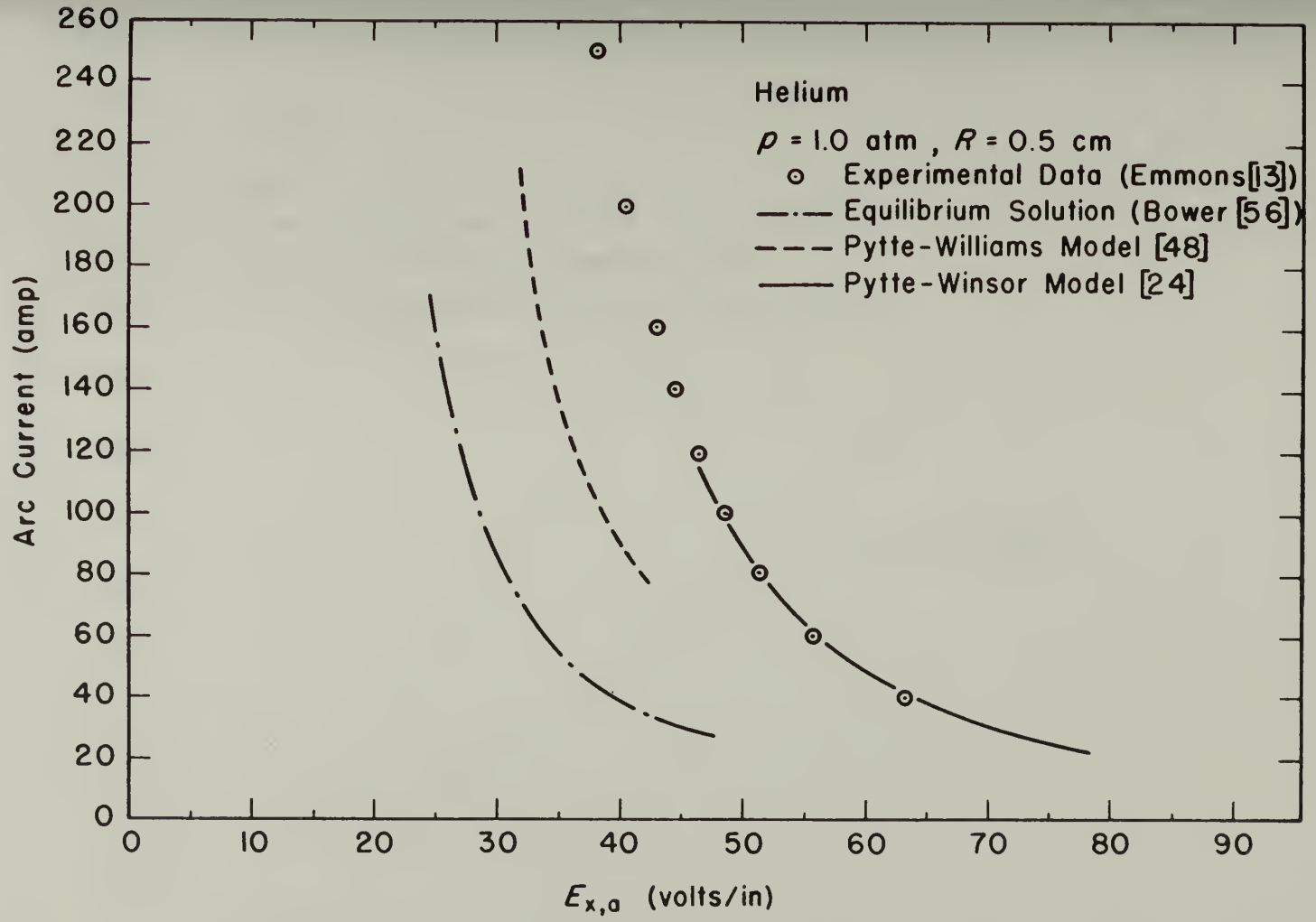

Figure IV.6 Comparison Between Experiment and Theory for the Asymptotic Electric Field Intensity in Helium

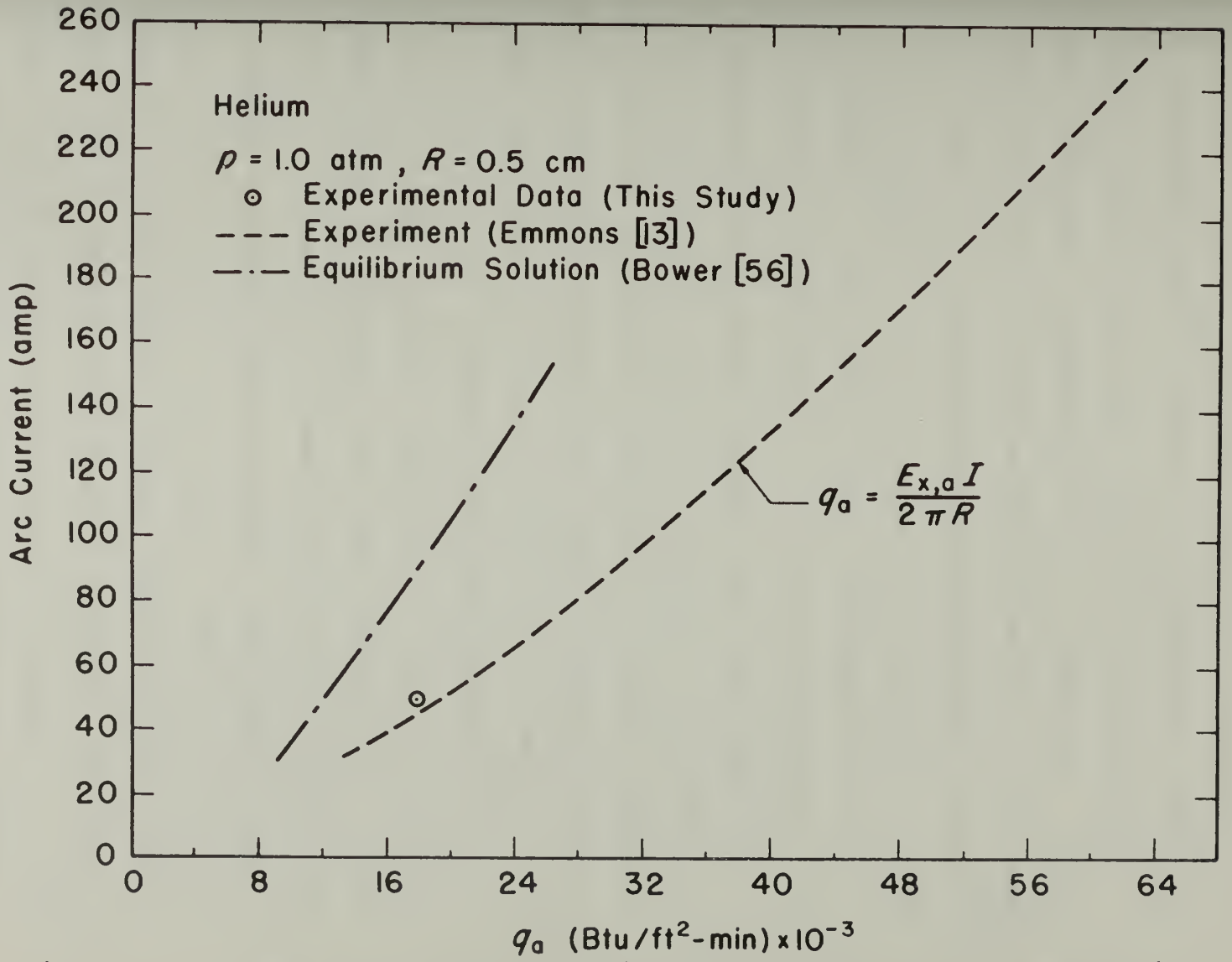

Figure IV.7 Comparison Between Experiment and Theory for the Asymptotic Total Wall Heat Flux in Helium

is not possible. As indicated in Figure IV.6, the prediction of the arc-column characteristics in helium by Pytte and Williams[48] offers some improvement over the numerical solution by Bower; however, this theoretical model continues to underpredict $E_{x,a}$ by some 20%. This underprediction by the Pytte-Williams model is most likely due to the use of equilibrium calculations for σ and k[39] as well as to use of the Elenbaas-Heller equation. Pytte and Winsor[24] have given greater consideration to nonequilibrium in atmospheric helium arcs by proposing a two-temperature theory which is based upon the asymptotic moment equations of continuity, momentum, and energy as derived from an electron transport (Boltzmann) equation. While this model accounts for thermal nonequilibrium between the electrons and heavy particles, it suffers from use of equilibrium thermal conductivity values[39] and use of the Saha equation (evaluated at the local electron temperature) to determine the local composition. In observing the excellent agreement which exists between the Pytte-Winsor predictions and Emmons' experimental data for $E_{x,a}$ (Figure IV.6), it would appear that use of the Saha equation and eqiulibrium thermal conductivities is justified. This agreement is misleading, however, for Pytte and Winsor adjusted their electrical conductivity, σ, in order to obtain the best fit to Emmons' experimental reduced

arc-column data for p = 1.0 atm and R = 0.5 cm. In applying the resulting value of σ to calculations for tube radii other than R = 0.5 cm, the Pytte-Winsor model does predict the trends indicated by the experimentally determined shifts in the $E_{x,a}R$ versus $E_{x,a}I$ curves; however, it fails to predict the magnitude of these shifts[24]. It is believed that this deficiency results from the failure of the Pytte-Winsor model to properly account for chemical nonequilibrium. Accordingly, the need remains for a rigorous, theoretical, multifluid model which treats the thermochemical nonequilibrium flow of helium in the inlet and asymptotic regions of the constricted tube arc.

Similarly, the author knows of no multifluid analyses in the literature from which predicitons of the global parameters, E_x and q can be made for the inlet and asymptotic regions of nitrogen arcs. Consequently, the following comparisons for nitrogen are limited to the single-fluid analytical model by Stine and Watson[18]. As was the case for argon, the generalized Stine-Watson expressions for $E_{x,a}$ and q_a (Equations IV.7 and IV.8) must be adapted to the particular gas and tube radius being considered. For this purpose, the values of $E_{x,a}$ and R for nitrogen reported by Shepard and Watson[3] were used with Equation IV.7 to determine Ag. This value was

then used to give the following simplified expressions for the Stine-Watson model, as applied to the asymptotic region of a nitrogen arc with R = 0.5 cm.

$$E_{x,a} = 26.4 \text{ volts/in} \qquad \text{(IV.16)}$$

$$q_a = 175.5\ I \qquad \text{(IV.17)}$$

These relationships, along with the experimental data from Figures III.6 and III.9, were used for the comparisons of Figures IV.8 and IV.9. Relative to previous comparisons for argon, application of the Stine-Watson model to nitrogen provides better agreement with experiment. While the temperature dependence of the radiation source densities (P_R) for argon and nitrogen are nearly the same[59], the mean temperatures in nitrogen are some 50% lower than the corresponding values of $T_{m,a}$ in argon (Figure III.13). Therefore, the percentage contribution to the total wall heat flux due to radiation from a nitrogen arc plasma would be considerably less than the corresponding contribution for an argon plasma of the same arc current. As such, the negligible radiation assumption implicit in the Stine-Watson model is less severe for nitrogen; nevertheless, as shown in Figures IV.8 and IV.9, this assumption continues to render this model inaccurate at higher arc currents.

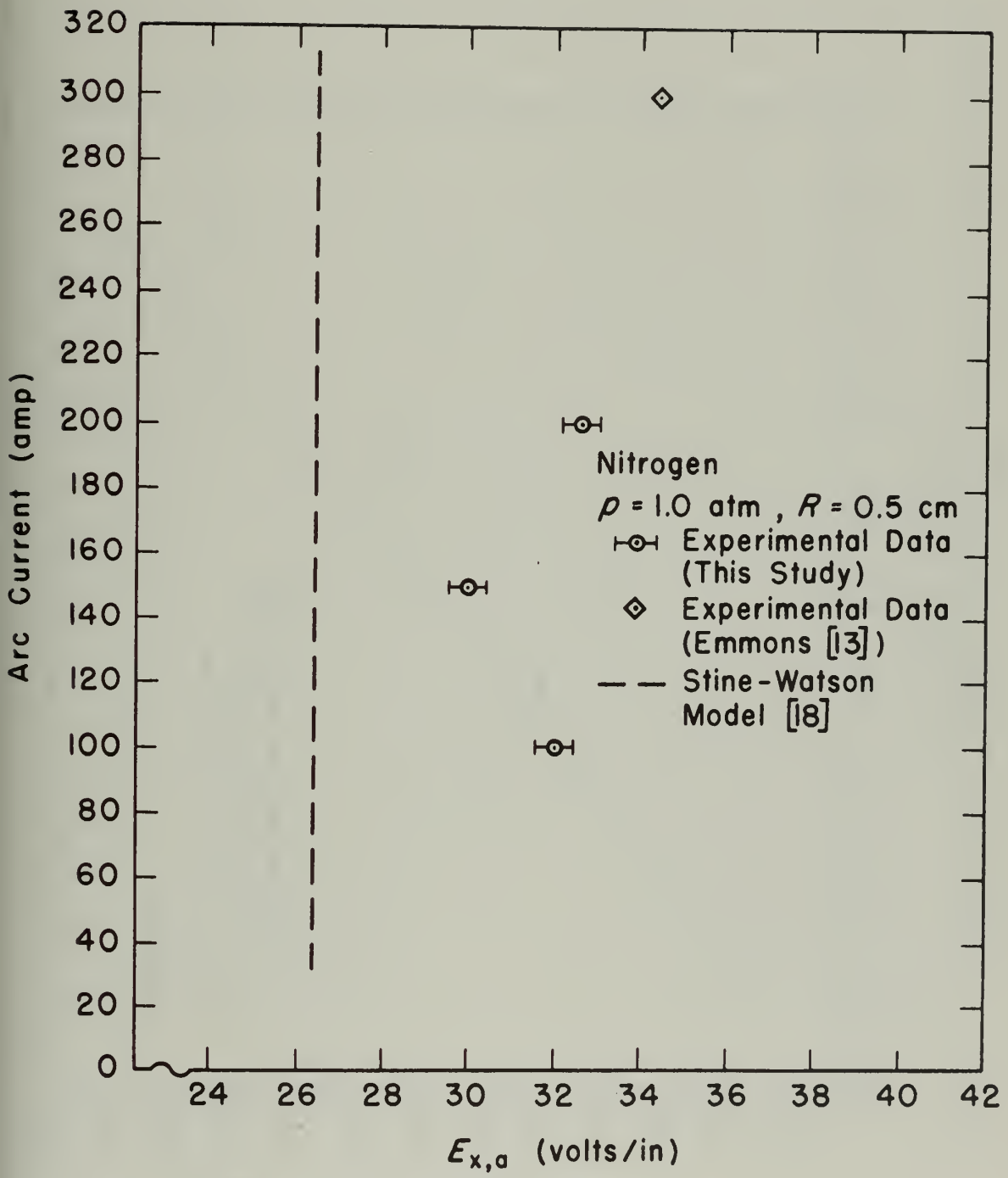

Figure IV.8 Comparison Between Experiment and Theory for the Asymptotic Electric Field Intensity in Nitrogen

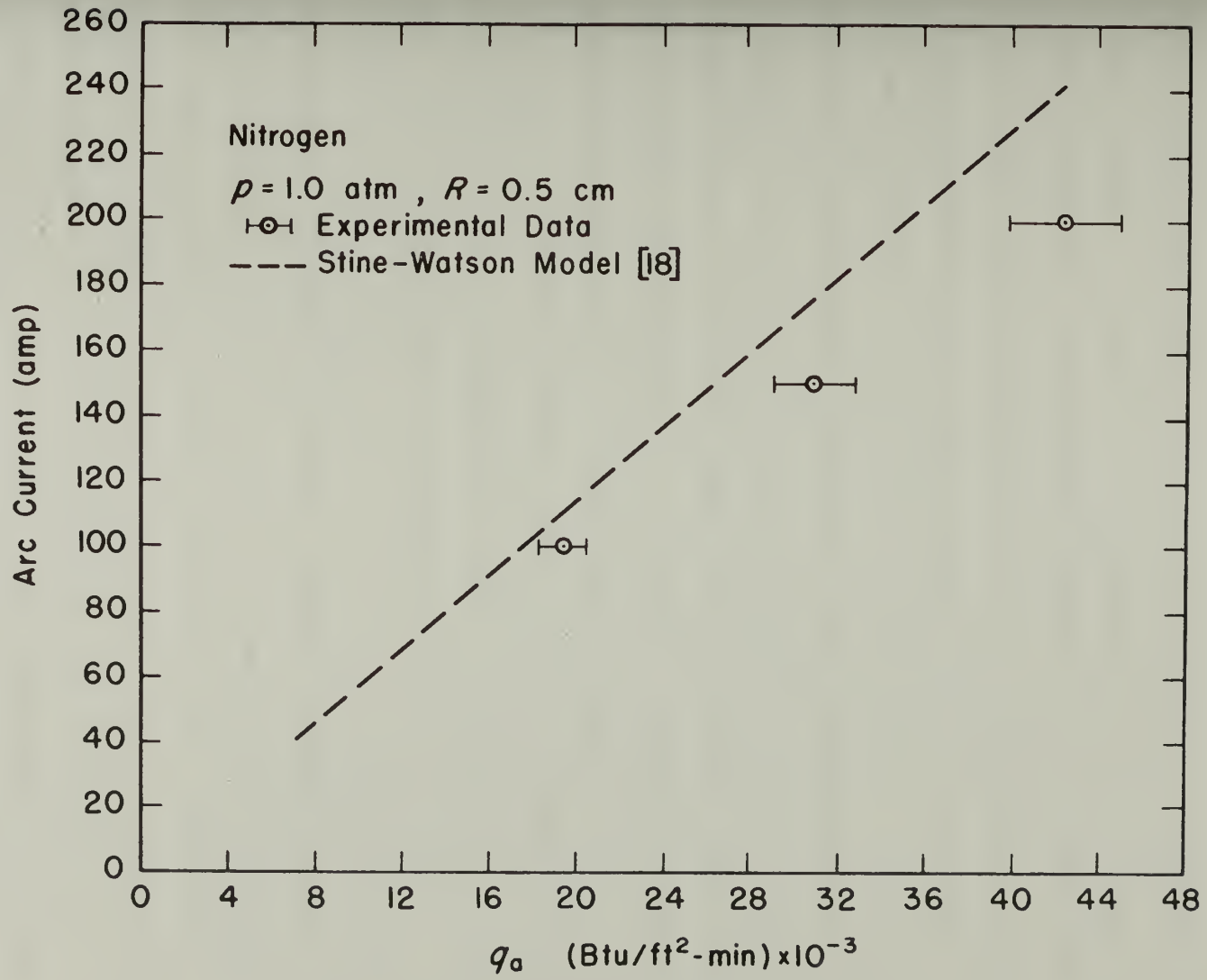

Figure IV.9 Comparison Between Experiment and Theory for the Asymptotic Total Wall Heat Flux in Nitrogen

In making further comparisons between the three gases, it is noted from Figure III.6 that, for a given arc current, successively higher voltages are required to sustain arc operation in going from argon to nitrogen to helium plasmas. Moreover, the increased values of $E_{x,a}$, which reflect the dissociation energy of N_2 and the relatively high ionization potential of He, necessarily result in the proportionately higher values of q_a for nitrogen and helium which are indicated in Figure III.9. On the basis of the increased values of total wall heat flux for nitrogen and helium, it might be expected that the mean temperatures of these two gases would be higher than the corresponding values of $T_{m,a}$ for argon. However, this is clearly not the case. As indicated in Figure III.13, the $T_{m,a}$ values for nitrogen and helium are considerably lower than the $T_{m,a}$ values for argon. In fact, at I = 50 amp, the experimentally determined value of $T_{m,a}$ for helium is more than an order of magnitude lower than the corresponding value for argon, and yet the calorimetrically measured value of q_a for He exceeds the corresponding value for Ar by a factor of nearly six. While this behavior is seemingly anomalous to the rules of convection heat transfer, it is recognized that any attempt at explanation on the basis of the global measurements of this study would be fatuous. While a partial explanation for

the increased wall heat transfer for the helium arc over that for argon can be inferred from the characteristically higher values of thermal conductivity for He (e.g., at $T = 5{,}000°K$, $k_{He} \simeq 9\ k_{Ar}$ [37,40]), a complete explanation cannot be gained without consideration of the microscopic transport phenomena which characterize these gases.

The order-of-magnitude difference between the mean temperatures in argon and helium can be explained on the basis of the relative specific heats for these two gases. That is, while the experimentally determined mean enthalpies for He and Ar are nearly equal (Tables IV.1 and IV.2), the specific heat for helium is nearly an order of magnitude higher than the corresponding value for argon. When evaluated at the experimentally determined values of $h_{m,a}$ for argon and helium (Tables IV.1 and IV.2), the ratio of the constant pressure specific heats (He to Ar) is 9.1 [38,39].

IV.4 Comparisons for the Anode Region

Before comparing experimental and theoretical anode heat transfer results, it is necessary to discuss the theoretical model and its relevance to measured quantities. Since the major portion of the experimental data acquired in this study is for argon, the following discussion and comparisons will deal only with this gas.

An anode heat transfer model which is frequently found in the literature[6,7,26-30] is one based upon an energy balance over the surface of the anode.

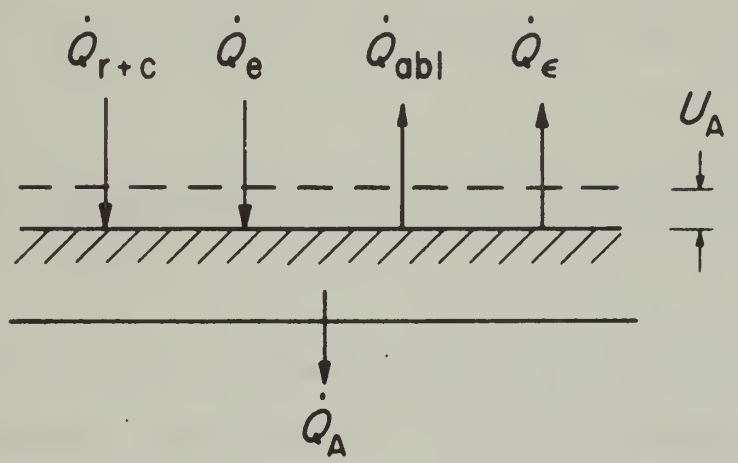

Figure IV.10 Anode Heat Balance Model

With reference to Figure IV.10, this balance is of the form

$$\dot{Q}_A = \dot{Q}_{r+c} + \dot{Q}_e - \dot{Q}_{abl} - \dot{Q}_\varepsilon \ , \qquad \text{(IV.18)}$$

where

$\dot{Q}_A$ = rate of energy loss to the anode cooling water,

$\dot{Q}_{r+c}$ = rate of energy transfer to the anode surface by convection and radiation from the plasma column,

$\dot{Q}_e$ = rate of energy transfer to the anode surface by electrons,

$\dot{Q}_{abl}$ = rate of energy transfer from the anode surface due to ablation of the anode material, and

$\dot{Q}_\varepsilon$ = radiation emissive power of the anode surface.

On the basis of observed negligible degradation of the anode surface after some 60 hours of operation and from calculations for a black surface emitting at the melting temperature of copper, the last two terms in Equation IV.18 are known to be insignificant compared to calorimetrically measured values of $\dot{Q}_A$ and can therefore be neglected. In addition, the energy transferred to the anode surface by the electrons is commonly obtained from the expression[6]

$$\dot{Q}_e = I[\xi\ (\frac{1}{e}\frac{5}{2}kT_e + U_A) + \phi_A], \qquad \text{(IV.19)}$$

where

$\frac{I}{e}\frac{5}{2}kT_e$ = thermal energy of the electrons as they enter the region of "anode fall",

IU_A = additional energy acquired by the electrons due to acceleration through the anode fall region,

$I\phi_A$ = "condensation" energy of the electrons penetrating the anode surface (ϕ_A = work function of the anode material), and

ξ = fraction of energy retained by the electrons after collisions with heavy particles within the anode fall region.

In addition to assuming negligible $\dot{Q}_{abl}$ and $\dot{Q}_{\varepsilon}$, Pfender, et al.[6,7], in working with Equations IV.18 and IV.19 assume a value of unity for ξ and assume that U_A may be represented by the difference between the anode potential (measured with respect to the cathode) and the potential obtained by linearly extrapolating the fully-developed potential gradient ($E_{x,a}$) to the location of the anode (see Figure IV.11). In using these assumptions with selected values of T_e = 10,000°K and ϕ_A = 3.7 volts, Equations IV.18 and IV.19 reduce to

$$\dot{Q}_A = \dot{Q}_{r+c} + I\ (5.85 + U_A). \qquad \text{(IV.20)}$$

If the anode is preceded by a thermally fully-developed region and if the mean enthalpy of the plasma at the anode remains close to $h_{m,a}$, Pfender, et al. argue that $\dot{Q}_{r+c}$ becomes the asymptotic value of the total wall heat flux (q_a). Accordingly, Equation IV.20 takes the form

$$Q_A = q_a + 26.6\ I\ (5.85 + U_A), \qquad \text{(IV.21)}$$

where the constant 26.6 accounts for the area of the anode surface (Q_A and q_a have units of [Btu/ft^2-min]) and the appropriate conversion factor ($0.0569\ \frac{\text{Btu}}{\text{watt-min}}$).

Using the experimental data of this study for q_a and U_A, a comparison is made between the values of Q_A calculated from Equation IV.21 and the measured values of this study (Figure III.15). The results of this comparison are shown in Table IV.3, wherein it is noted that the theoretical model overpredicts the corresponding experimental values by a factor of approximately two. It is felt that a portion of this rather gross overprediction is due to errors associated with assuming that $\xi = 1.0$ and assuming that U_A can be determined by the aforementioned linear extrapolation procedure. These errors are made evident by the anode energy balance measurements of this study which reveal a significant increase ($\sim$ 30% above

Table IV.3. A Comparison Between Experimental Data and Theoretical Predictions for the Total Anode Heat Flux (Argon: p = 1.0 atm, R = 0.5 cm, and $\dot{m}$ = 0.03 lb/min).

I(amp)	Experimental Data (this study)		Q_A (Btu/ft^2-min)	
	q_a (Btu/ft^2-min)	U_A (volts)	Calorimetric Measurements (this study)	Theory (Eq. IV.21)
35	2,170	10.2	7,220	17,120
100	8,270	8.2	24,250	45,670
150	14,300	5.6	32,700	59,950
200	22,800	5.1	39,600	81,100
240	30,900	4.9	46,000	99,500

the value of $h_{m,a}$) in the enthalpy of the gas as it passes through the anode region. In order to obtain such an increase in enthalpy, there must occur a significant transfer of electrical energy to the gas in excess of that required to maintain the asymptotic conditions ($h_{m,a}$ and thus q_a). The electrons, therefore, will in fact lose a portion of their energy (IU_A) to the heavy particles in the fall region and, consequently, ξ will be considerably less than unity. The failure of the theoretical model (Equation IV.21), when applied to the anode configuration of the constricted tube arc, to account for this additional transfer of electrical energy is perhaps best understood by considering a typical anode region potential distribution. With reference to Figure IV.11, the theoretical model assumes that, of the total anode potential rise, E_A, the portion, E_A-U_A, is required to maintain the asymptotic value of $h_{m,a}$ and the remaining portion, U_A, results in energy transfer, via the electrons, to the anode surface (i.e., IU_A). In contrast, the experimental results indicate that, in addition to that portion of the total anode potential rise required to maintain $h_{m,a}$, a portion of E_A is also needed to sustain the increase in the enthalpy of the gas, Δh_A, as it passes through the anode region. Consequently, a fraction of the energy acquired

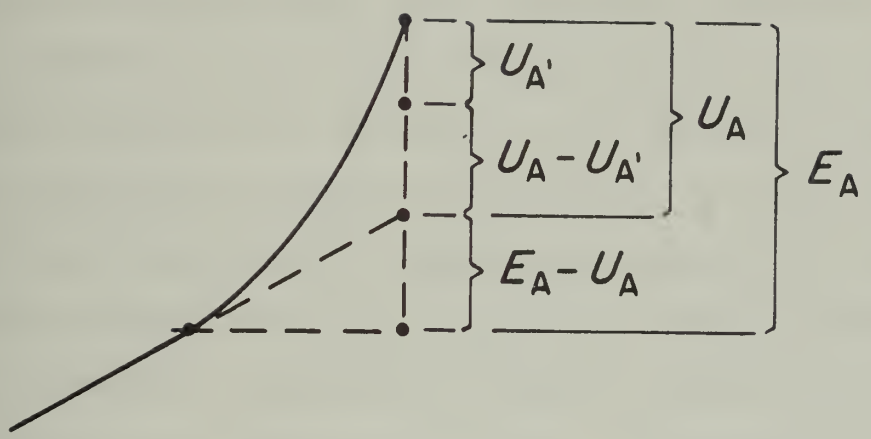

Figure IV.11 Partitioning of Total Anode Fall Potential

by the electrons (IU_A) is in fact transferred to the gas through electron-heavy particle collisions and cannot contribute directly to the total anode heat transfer. Hence, it is concluded that the overpredictions for Q_A which result from the anode heat balance model are at least partially due to the combination of assuming that ξ is unity and that the anode fall potential is given by the linear extrapolation procedure.

To further consider these assumptions as the major sources of error in Equation IV.21, the data of this study

were used to determine both the potential drop required to sustain the gas enthalpy rise Δh_A and the potential drop, to be designated $U_{A'}$, which results in the transfer of electron energy directly to the anode surface ($IU_{A'}$). In this connection and with reference to Figure IV.11, it is assumed that the total anode potential rise, E_A, can be subdivided into the fraction of this potential required to sustain the asymptotic conditions, $E_A - U_A / E_A$; the fraction of this potential required to sustain the anode region enthalpy rise (Δh_A), $U_A - U_A / E_A$; and the fraction of this potential resulting in energy transfer to the anode surface by the electrons, $U_{A'} / E_A$. According to this subdivision, and retaining the values of T_e and ϕ_A used in Equation IV.21, energy balance considerations require that

$$Q_A = q_a + 26.6\ I\ (5.85 + U_{A'}) \ , \qquad \text{(IV.22)}$$

and that

$$I\ (U_A - U_{A'}) = \dot{m} \Delta h_A \ , \qquad \text{(IV.23)}$$

where, again, Δh_A is the enthalpy acquired by the gas in traversing the anode region. The anode heat flux predictions which result from calculations performed with this modified theoretical model are presented in Table IV.4 along with the experimentally determined values of Δh_A.

Table IV.4. A Comparison Between Experimental Data and Modified Theoretical Predictions for the Total Anode Heat Flux (Argon: p = 1.0 atm, R = 0.5 cm, and $\dot{m}$ = 0.03 lb/min).

I(amp)	Experimental Data		Q_A (Btu/ft^2-min)	
	Δh_A (Btu/lbm)	$U_{A'}$ (volts) (Eq. IV.23)	Calorimetric Measurements	Theory (Eq. IV.22)
35	287	5.88	7,220	13,100
100	628	4.88	24,250	36,800
150	780	2.86	32,700	49,000
200	928	2.66	39,600	68,100
240	1,590	1.41	46,000	77,200

While the values of $U_{A'}$ computed from Equation IV.23 are significantly lower than those given by the linear extrapolation method (U_A), their use in Equation IV.22, along with experimental values of q_a, still result in sizeable overpredictions for the total anode heat flux. It appears then that more appropriate values for T_e and ϕ_A must be determined in order to bring the theoretical predictions into better agreement with experiment. These additional considerations would necessarily require further knowledge of electron temperature distributions in the vicinity of the anode as well as a more rigorous consideration of the plasma-electrode surface interaction. Accordingly, the use of this analytical model to predict the total heat transfer to the anode of a constricted tube arc appears to be of questionable value. This is especially true when the model is compared with existing empirical correlations, such as those appearing in Figure III.15. In connection with these empirical correlations, it is noted that in cases where the anode is not preceded by a fully-developed region, it is necessary to include a dependency on arc length and operating gas flow rate, as is the case, for example, of the Eberhart and Seban[29] anode heat transfer correlation.

CHAPTER V SUMMARY AND CONCLUSIONS

This work provides experimental results for the axial distribution of the electric field intensity and total wall heat flux for the inlet, asymptotic, and anode regions of atmospheric argon, helium, and nitrogen arc plasmas. Whereas data are presented for a wide range of laminar flow rates (0.03-0.11 lb/min) and arc currents (35-240 amp) in argon, the amount of data presented for helium and nitrogen arcs is considerably less extensive. The range of operation for these two gases was restricted by the power supply employed in this study. In addition to the development of the diagnostics required for the electric field intensity and total wall heat flux measurements, considerable effort was given to the development of a unique gage to measure the radiative component of the total wall heat flux. This instrument has been used successfully in providing the radiative wall heat flux data which are presented for the asymptotic region in argon. The accuracy of the experimental measurements, as well as the consistency of the arc facility, is assessed on the basis of the observed precision of local energy balance checks. Further confidence in the experimental

measurements is inferred from the favorable agreement which exists between the data of this study and the experimental results reported by other investigators.

Through comparisons between the experimental data and available equilibrium and nonequilibrium numerical solutions, an attempt is made to ascertain the adequacy of single-fluid models to accurately describe overall arc energetics. On the basis of the measurements themselves and the comparison with theoretical results, the following conclusions were derived.

1. The increase in duct wall potential with current drawn from the segment is primarily a "cold" boundary layer effect and, therefore, the "floating" duct wall potential provides a more accurate measure of the actual plasma potential, at least for the copper wall-argon plasma combination employed in this study.
2. Variations in the duct entrance conditions can have a significant effect on the experimentally determined and numerically predicted electric field intensity and total wall heat flux distributions for the inlet region of the constrictor. As a result, meaningful comparisons between experiment and theory can be made only for the asymptotic region.

3. Closed form analytical solutions which are based upon the use of linearized property relationships and which assume negligible radiation are inadequate for predicting electric field intensity and total wall heat flux. This is particularly evident at the higher current levels in argon and nitrogen.
4. To within the combined experimental and theoretical uncertainties, the numerical solution of a rigorous single-fluid model is suitable for use in predicting the electric field intensity and total wall heat flux for the asymptotic region in argon, at least over the range of conditions investigated in this study. The equilibrium solution does not, however, appear suitable for predicting the asymptotic mean temperature or the radiative wall heat flux over the same range of conditions in argon. There is a small, but discernable, nonequilibrium effect at the lower arc currents in argon, as a result of which the equilibrium solution tends to overpredict both the electric field intensity and total wall heat flux for currents less than 100 amp. Moreover, the tendency of the equilibrium solution to underpredict these two parameters at arc currents in argon greater than

100 amp is believed to be due to a chemical nonequilibrium effect which renders the equilibrium solution deficient in providing for sufficient energy loss to the tube walls by conduction.

5. Solutions which properly account for thermochemical nonequilibrium, as well as for all pertinent transport phenomena, provide predictions for the electric field intensity and the convective and radiative wall heat transfer which are in excellent agreement with the experimental results over the entire range of asymptotic conditions investigated in argon.
6. Atmospheric helium arcs are characterized by a significant departure from local thermodynamic equilibrium (at least for arc currents less than 250 amp) and, as a result of these departures, single-fluid models are totally inadequate in representing their thermal state.

With reference to the last three of the above conclusions, it is presumed that further comparisons between experiment and equilibrium and nonequilibrium solutions, if extended to include arc conditions characterized by higher order nonequilibrium effects, would lead to an

improved understanding of nonequilibrium arc physics. Accordingly, it is recommended that the present arc facility be extended to permit stable, low current ($I < 35$ amp) operation in argon and to permit stable operation over a greater range of operating conditions in helium and nitrogen. It is also recommended that the solution by Bower and Incropera[20] be expanded to provide equilibrium predictions for nitrogen arcs and that the solution by Clark[25] be appropriately extended to afford nonequilibrium arc predictions for helium and nitrogen.

In addition to the above conclusions for the inlet and asymptotic regions, further comparisons between experiment and theory for the anode region indicate that the large (50-100%) overpredictions for the total anode heat flux which result from use of a heat balance model are primarily due to the relatively large uncertainties involved in specifying associated values of the physical parameters (U_A, T_e, and ϕ_A). Consequently, the theoretical model is thought to be ill-suited for providing design estimates for the total heat flux to the anode of the arc constrictor, particularly in comparison with estimates which are based upon empirical correlations. In this respect, further experimental and theoretical study of plasma-electrode surface interactions is recommended.

LIST OF REFERENCES

LIST OF REFERENCES

1. Maecker, H., "Ein zllindrischer Bogen für hohe Leistungen," Zeits. für Physik, Vol. 129, pp. 108-122, 1951.

2. Skifstad, J.G., "Investigation of Energy Transfer in a Tube Arc Heater," ARL 64-112, July 1964.

3. Shepard, C.E. and Watson, V.E., "Performance of a Constricted-Arc Discharge in a Supersonic Nozzle," Fifth Biennial Gas Dynamics Symposium, Northwestern University, Evanston, Ill., August 1963.

4. Stine, H.A., Watson, V.R., and Shepard, C.E., "Effect of Axial Flow on the Behavior of the Wall-Constricted Arc," AGARD-ograph 84, Part 1, Arc Heaters and MHD Accelerators for Aerodynamic Purposes, 1964.

5. Jedlicka, J.R. and Stine, H.A., "Axial Flow Through the Wall-Constricted Direct-Current Arc-Comparison of Theory and Experiment," IEEE Transactions on Nuclear Science, Vol. NS-11, January 1964, pp. 104-108.

6. Pfender, E., Raithby, G.D., and Eckert, E.R.G., "An Anode Comparison Study in a Wall-Stabilized Argon Arc," ARL 65-232, November 1965.

7. Pfender, E., Eckert, E.R.G., and Raithby, G.D., "Energy Transfer Studies in a Wall-Stabilized, Cascaded Arc," Proceedings of the Eighth International Conference on Ionization Phenomena in Gases, Belgrad, Yugoslavia, 1965, 1, 691, Gradevinska Knjiga Publishing House, Belgrad, 1966.

8. Uhlenbush, J., "Theory and Calculation of Stationary and Quasi-Stationary Clyindrical Arcs," ARL 65-109, May 1965.

9. Maecker, H., "Uber die Charakteristiken zylindrischer Bogen," Zeits für Physik, Vol. 157, pp. 1-29, 1959.

10. Runstadler, P.W., Jr., "Laminar and Turbulent Flow of an Argon Arc Plasma," Harvard University, Engineering Sciences Laboratory, Technical Report No. 22, September 1965.

11. Emmons, H.W. and Land, R.I., "Poiseulle Plasma Experiment," The Physics of Fluids, Vol. 5, No. 12, pp. 1489-1500, December 1962.

12. Emmons, H.W., "Arc Measurement of High-Temperature Gas Transport Properties," The Physics of Fluids, Vol. 10, No. 6, pp. 1125-1136, June 1967.

13. Emmons, H.W., "The Arc Measurement of High Temperature Gas Transport Properties," Harvard University, Engineering Sciences Laboratory, Technical Report No. 23, December 1965.

14. Morris, J.C., Rudis, R.P., and Yos, J.M., "Measurements of Electrical and Thermal Conductivity of Hydrogen, Nitrogen, and Argon at High Temperatures," The Physics of Fluids, Vol. 13, No. 3, pp. 608-617, March 1970.

15. Maecker, H., "Transport Properties in High Power Arcs," ARL 69-0031, February 1969.

16. Skifstad, J.G., "Review of Theoretical Analyses of Arc Heating in a Tube," ARL 65-207, October 1965.

17. Bower, W.W., "Correlations for the Wall Parameters in the Asymptotic Region of a Laminar Constricted Arc," M.S. Thesis, Purdue University, January 1969.

18. Stine, H.A. and Watson, V.R., "The Theoretical Enthalpy Distribution of Air in Steady Flow Along the Axis of a Direct-Current Electric Arc," NASA TN D-1331, 1962.

19. Watson, V.R. and Pegot, E.B., "Numerical Calculations for the Characteristics of a Gas Flowing Axially through a Constricted Arc," NASA TN D-4042, 1967.

20. Bower, W.W. and Incropera, F.P., "Heat Transfer, Development Length, and Friction Factor Correlations for the Asymptotic Region of a Laminar Arc Constrictor," Wärme-und Stoffübertragung, Vol. 2, pp. 150-162, 1969.

21. Bott, J.F., "Spectroscopic Measurement of Temperatures in an Argon Arc Plasma," The Physics of Fluids, Vol. 9, No. 8, pp. 1540-1547, 1966.

22. Incropera, F.P. and Giannaris, R.J., "Evidence of Nonequilibrium Effects in an Atmospheric Argon Arc Plasma," Technical Report No. HTGDL-2, High Temperature Gas Dynamics Laboratory, School of Mechanical Engineering, Purdue University, August 1970.

23. Incropera, F.P. and Viegas, J.R., "Nonequilibrium in an Arc Constrictor," AIAA Journal, Vol. 8, No. 9, pp. 1722-1724, September 1970.

24. Pytte, A. and Winsor, N.K., "A Two-Temperature Theory for a Helium Arc Plasma in a Cylindrical Duct," ARL 66-0047, 1965.

25. Clark, K.J., "Thermochemical Nonequilibrium in an Argon Constricted Arc Plasma," Technical Report No. HTGDL-4, High Temperature Gas Dynamics Laboratory, School of Mechanical Engineering, Purdue University, 1971.

26. Shih, K.T., Pfender, E., and Eckert, E.R.G., "Thermal Analysis of Cathode and Anode Regimes of an MPD-Arc," NASA CR-54664, January 1968.

27. Shih, K.T., "Electrode Erosion in High Current Electric Arcs," ARL 70-0077, June 1970.

28. Shih, K.T., Pfender, E., Ibele, W.E., and Eckert, E.R.G., "Experimental Anode Heat Transfer Studies in a Coaxial Arc Configuration," AIAA Journal, Vol. 6, No. 8, pp. 1482-1487, August 1968.

29. Eberhart, R.C. and Seban, R.A., "The Energy Balance for a High Current Argon Arc," International Journal of Heat and Mass Transfer, Vol. 9, No. 9, pp. 939-949, September 1966.

30. Eckert, E.R.G. and Pfender, E., "Advances in Plasma Heat Transfer," Advances in Heat Transfer, Vol. 4, pp. 229-316, Academic Press, New York, 1967.

31. McKee, H.B., Dean, R.C., and Pytte, A., "On Cooled Anodes in Contact with Laminar Arc-Heated Flows," ARL 64-178, October 1964.

32. McKee, H.B., Dean, R.C., and Pytte, A., "On Cooled Anodes in Contact with a Laminar Arc-Heated Flow," IEEE Transactions on Nuclear Science, NS-11, pp. 66-91, January 1964.

33. Runstadler, P.W., Jr., "Electrical Conduction from a Laminar Arc Heated Flow to a Cooled Cylindrical Anode," ARL 67-0142, July 1967.

34. Dean, R.C. and Runstadler, P.W., Jr., "An Arc Plasma Generator for Research," AIAA Plasmadynamics Conference, AIAA Paper No. 66-162, Monterey, California, 1966.

35. Runstadler, P.W., Jr. and Dean, R.C., "Electrical Conduction Behavior of a Laminar Arc Heated Flow in Contact with a Cooled Anode," AIAA Paper No. 66-188, 1966.

36. Kline, S.J. and McClintoc, F.A., "Describing Uncertainties in Single-Sample Experiments," Mechanical Engineering, January 1963.

37. DeVoto, R.S., "Transport Coefficients of Partially Ionized Argon," The Physics of Fluids, Vol. 10, No. 2, pp. 354-364, February 1967.

38. Drellishak, K.S., Knopp, C.F., and Cambel, A.B., "Partition Functions and Thermodynamic Properties of Argon Plasma," AEDC-TDR-63-146, August 1963.

39. Lick, W.J. and Emmons, H.W., Thermodynamic Properties of Helium to 50,000°K, Harvard University Press, 1962.

40. DeVoto, R.S. and Li, C.P., "Transport Coefficients of Partially Ionized Helium," Journal of Plasma Physics, Vol. 2, Part 1, pp. 17-32, 1968.

41. Drellishak, K.S., Aeschliman, D.P., and Cambel, A.B., "Tables of Thermodynamic Properties of Argon, Nitrogen, and Oxygen Plasmas," AEDC-TDR-64-12, January 1964.

42. AVCO, "Transport Properties of Nitrogen, Hydrogen, Oxygen, and Air to 30,000°K," AVCO/RAD-TM-63-7, 1963.

43. Lukens, L.A., "An Experimental Facility for Friction and Heat Transfer Measurements in a High Temperature Plasma," M.S. Thesis, Purdue University, January 1969.

44. Incropera, F.P. and Leppert, G., "Flow Transition Phenomena in a Subsonic Plasmajet," AIAA Journal, Vol. 4, No. 6, p. 1087, 1966.

45. Hoyaux, M.F., Arc Physics, Springer-Verlag New York Inc., 1968.

46. Private Communication, P.W. Schreiber (ARL-ORL) to L.A. Lukens, September 1970.

47. Barzelay, M.E., "Thermal Radiation from an Argon Plasma," Harvard University, Engineering Sciences Laboratory, Technical Report No. 7, June 1964.

48. Pytte, A. and Williams, A.R., "On Electrical Conduction in a Non-Uniform Helium Plasma," ARL 63-166, September 1963.

49. Watson, V.R., "Comparison of Detailed Numerical Solutions with Simplified Theories for the Characteristics of the Constricted-Arc Plasma Generator," Proceedings of the 1965 Heat Transfer and Fluid Mechanics Institute, Stanford University Press, pp. 24-41, 1965.

50. Kruger, C.H., "Nonequilibrium in Confined Arc-Plasmas," The Physics of Fluids. Vol. 13, No. 7, pp. 1737-1746, July 1970.

51. Butler, J.N. and Brokaw, R.S., "Thermal Conductivity of Gas Mixtures in Chemical Equilibrium," The Journal of Chemical Physics, Vol. 26, pp. 1636-1643, 1957.

52. Fay, J.A., "Hypersonic Heat Transfer in the Air Laminar Boundary Layer," The High Temperature Aspects of Hypersonic Flow, W.C. Nelson, Ed., The MacMillan Company, New York, pp. 583-605, 1964.

53. Private Communication, W.W. Bower to L.A. Lukens, July 1970.

54. Private Communication, K.J. Clark to L.A. Lukens, February 1971.

55. Private Communication, W.W. Bower to L.A. Lukens, October 1970.

56. Bott, J.F., "A Spectroscopic Investigation of a Helium Plasma Arc," Harvard University, Engineering Sciences Laboratory, Technical Report No. 25, January 1966.

57. Stockholm, J.F., "Total Radiation Measurements From Plasma Arcs," Harvard University, Engineering Sciences Laboratory, Technical Report No. 6, May 1964.

58. Aleksandrov, V. Ya., Gurevich, D.B., and Podmoshenskii, I.V., "Study of the Mechanism of Spectrum Excitation in a Helium Arc Plasma," Optics and Spectroscopy, Vol. 26, pp. 18-20, 1969.

59. Morris, J.C., Krey, R.U., and Garrison, R.L., "Radiation Studies of Arc Heated Nitrogen, Oxygen, and Argon Plasmas," ARL 68-0103, May 1968.

60. Kingsbury, R.L., "An Analysis of Internal Flow Wall Parameters for an Argon Plasma," M.S. Thesis, Purdue University, August 1968.

61. Reece, W.J. and Theoclitus, G., "A New Technique for Measuring Thermal Radiation", The 1965 Aerospace Conference and Exhibit, Houston, Texas, June 1965.

62. Skinner, G.T., "A New Method of Calibrating Thin-Film Gage Backing Materials", Cornell Aeronautical Laboratory, Report No. Cal 105, June 1962.

63. Cook, W.J. and Felderman, E.J., "Reduction of Data From Thin-Film Heat-Transfer Gages: A Concise Numerical Technique", AIAA Journal, Vol. 4, No. 3, pp. 561-562, March 1966.

64. Hardy, R.G. and Paddock, D.A., "A New Thermal Radiative Flux Gage", ARS Journal, Vol. 6, No. 1, pp. 15-19, January 1967.

65. Sparrow, E.M. and Cess, R.D., Radiation Heat Transfer, Brooks/Cole Publishing Co., Belmont, California, 1967.

66. Yakubov, I.T., "Energy Emitted by Argon Plasma in Spectral Lines", Optics and Spectroscopy, Vol. 19, pp. 277-281, 1965.

67. Horn, K.P., "Radiative Behavior of Shock Heated Argon Plasma Flows", SU-IPR No. 79, Institute for Plasma Research, Stanford University, May 1966.

68. Madden, R.P., "Preparation and Measurement of Reflecting Coatings for the Vacuum Ultraviolet, Physics of Thin Films, Vol. 1, G. Hass, Ed., Academic Press, New York, pp. 123-186, 1963.

69. Hass, G., Hunter, W.R., and Rousey, R., "Influence of Purity, Substrate Temperature, and Aging Conditions on the Extreme Ultraviolet Reflectance of Evaporated Aluminum", Journal of the Optical Society of America, Vol. 47, p. 1070, 1957.

70. Drummeter and Hass, G., "Solar Absorptance and Thermal Emittance of Evaporated Coatings", Physics of Thin Films, Vol. 2, G. Hass, Ed., Academic Press, New York, pp. 305-361, 1964.

APPENDIX

APPENDIX RADIATION GAGE

A.1 General Remarks and Review of Experimental Studies Relating to Radiative Heat Flux Measurements

Since thermal radiation is often a primary mode of energy transfer in a constricted arc plasma, knowledge of the radiative contribution to the total wall heat flux is of concern in both the engineering application and the laboratory use of plasma arc generators. In addition, knowledge of the radiative wall heat flux is of value in obtaining an improved understanding of arc physics and plasma flow modeling. Accordingly, a portion of this study was directed towards the design, fabrication, and use of appropriate instrumentation to measure the radiative component of the total heat flux to the wall of an arc constrictor.

While there are numerous studies in the literature dealing with the measurement of plasma radiative properties, the author knows of no experimental attempt to deal explicitly with the measurement of the radiative and convective components of the total wall heat flux for an arc constrictor. There are described in the literature, however, two diagnostic techniques which would appear

applicable to this particular measurement. The first of these involves a total radiation detector which utilizes a thin-film resistance sensor. This sensor consists of a thin metallic strip (usually platinum) which is deposited on a substrate material (pyrex, quartz, etc.) and has been used primarily for transient, short duration measurements. The metallic strip acts as a passive resistance element in an electrical circuit designed to record the variation of current through the sensor upon its exposure to a step input of radiation. From knowledge of the temperature coefficient of resistance of the metallic element and the thermal conductivity of the substrate, the heat flux to the substrate can be inferred by analyzing the time variation in the surface temperature as indicated by the electrical output from the sensor. Further discussion of this diagnostic technique is provided by Reece and Theoclitus[61]. A major advantage of this method is that the calibration and data reduction procedures are relatively straight forward and well established[62,63].

While the time limit of sensitivity (saturation time) for the thin-film sensor is typically on the order of 100 msec, this technique can be modified for use with steady state radiation sources. As discussed by Hardy and Paddock[64], this feature is made possible by placing

a fast-acting shutter mechanism between the radiation source and the sensor. This modification would, of course, be required if the thin-film detector were to be used for the radiation measurements of this study. However, herein lies the major disadvantage of this method. In particular, the imposition of interface components (shutter mechanism, etc.) would place the sensor sufficiently far from the plasma source to require detailed consideration of the spectral sensitivity of the resulting cavity walls.

A second device has been employed by researchers at Harvard to measure the total radiation from a steady state, constricted tube arc.* This device uses a recessed sensing element, across which a temperature difference is induced which is proportional to the absorbed radiation. The sensing element consists of a blackened constantan shim which is positioned in a circumferential (with respect to the axis of the cylindrical duct) slot. The slot walls are silver coated in order to reflect a greater percentage of radiation to the sensor, and the sensing element is recessed 1.5 inches in an attempt to minimize convective contributions to the measured heat flux. Calibration of the radiation meter was attempted by comparing the detector output against

---

* A comparison is made in Chapter III between the Harvard results and the radiation data obtained in this study.

several radiation standards, which include filament and gas-filled lamps and globar units.

This diagnostic technique is subject to several sources of error for which compensation cannot be entirely made by the calibration procedure. Consequently, accurate use of this device is contingent upon the successful isolation and evaluation of these sources of error and the subsequent introduction of appropriate correction factors. This matter deserves further discussion, for it serves to illustrate the problems associated with radiative heat flux measurements, particularly with techniques which employ recessed sensors.

As discussed by Emmons[12], certain correction factors must be applied to the experimental results obtained by use of the aforementioned device. This is necessary in order to account for the geometrical differences between the conditions of calibration and actual measurement. Specifically, account must be taken of the difference between the relative positions (with respect to the sensor location) of the radiation standard and the arc. In addition the variation in geometry which results from the fact that the calibration standard (globar unit) is a surface emitter, whereas the arc is a volume emitter, must be considered. These correction factors may be

obtained from geometrical considerations relating to the calibration and actual measurement configurations. However, aside from the geometrical effects, there remains a possible source of error due to the spectral sensitivity of the component parts, particularly the slot walls. If the reflectivity of the slot walls varies appreciably over the wavelength range of the incident plasma radiation, and if this variation is to be incorporated within the calibration of the detector, then the radiation standard must, of course, have the same spectral intensity distribution as the plasma. Unfortunately, such calibrated sources are not available.

Another deficiency inherent in this radiation gage is the fact that the higher plasma radiation intensities could only be determined from a linear extropolation of the calibration data[47]. That is, the detector output during actual measurement was a factor of approximately six higher than the maximum calibrated detector output (as limited by the burnout temperature, 1625°C, of the globar unit). Techniques employing recessed sensors are therefore calibration limited in the sense that if the possible variations in the spectral response of the cavity walls (as well as the full output range of the detector) are to be incorporated within the detector calibration, the calibration source must have the same radiation

intensity, in both magnitude and spectral distribution, as the plasma for which measurements are desired.

A.2 Radiative Heat Transfer Gage - General Design and Operation Considerations

From evaluation of the aforementioned measurement techniques, three primary constraints were initially imposed upon the proposed detector design. First, the detecting unit must not alter the geometry of the constrictor and, in particular, the use of recessed sensing elements should be avoided. Secondly, the detector must not be calibration limited in the sense that generation of its output characteristic is dependent upon an initial calibration against a standard radiation source. Thirdly, the presence of the radiation gage should not significantly alter local conditions in the plasma. This is necessary if useful comparisons between theory and measurements are to be realized.

To adhere to the above criteria, it seemed reasonable to attempt to alter the wall surface characteristics to permit isolation and measurement of the radiative heat flux. The use of a transparent "window" affords a convenient means of isolation; however presently available optical materials cannot provide uniform transmission over the entire spectral range of possible plasma radiation. In addition, the window would have to be

thermally isolated from the sensor so as not to contribute to the measured heat flux through conduction.

Further insight into a possible technique for delineating between the radiative and convective components to the total wall heat flux was gained from consideration of the optical characteristics of the duct wall surface. Expressing the radiative component in terms of the monochromatic absorptance (α_λ) and the plasma irradiation (H_λ), the total wall heat flux takes the form

$$q = q_{conv} + q_{rad}$$

$$= q_{conv} + \int_0^\infty \alpha_\lambda H_\lambda d\lambda \qquad \text{(A.1)}$$

The emissive power of the duct wall surface ($\varepsilon\sigma T_w^4$) is neglected, since its magnitude is small in comparison to the other terms of the equation. Assuming, for the moment, that α_λ is known and that q may be determined by calorimetric measurement, there remain two unknowns in Equation A.1, q_{conv} and H_λ. The appearance of these two unknowns suggests the use of two surfaces (which differ in spectral sensitivity), in which case the application of Equation A.1 for surface-1 yields

$$q_1 = q_{conv,1} + \int_0^\infty \alpha_{\lambda,1} H_{\lambda,1} \, d\lambda \qquad (A.2)$$

and, for surface-2,

$$q_2 = q_{conv,2} + \int_0^\infty \alpha_{\lambda,2} H_{\lambda,2} \, d\lambda \qquad (A.3)$$

If both surfaces are located at the same axial location in the duct, it may be assumed that both the incident irradiation and the convective heat transfer to each surface are the same (i.e., $H_{\lambda,1} = H_{\lambda,2} = H_\lambda$ and $q_{conv,1} = q_{conv,2} = q_{conv}$). Under these assumptions, Equations A.2 and A.3 can be equated on the basis of equal convection to give

$$q_1 - q_2 = \int_0^\infty \alpha_{\lambda,1} H_\lambda \, d\lambda - \int_0^\infty \alpha_{\lambda,2} H_\lambda \, d\lambda \; . \qquad (A.4)$$

To achieve the largest possible difference between the calorimetrically measured values of the total wall heat flux ($q_1 - q_2$) and thus to realize the maximum experimental resolution, the difference between the radiation absorption terms in Equation A.4 should be maximized. This suggests the use of a highly absorbing (black) surface in combination with a highly reflecting surface. For the optically black surface, say surface-1, it is assumed that suitable coating materials are available for

which the monochromatic absorptance is independent of wavelength over the entire spectral range of the plasma irradiation. For such a surface, the radiative wall heat flux component reduces to

$$\int_0^\infty \alpha_{\lambda,1} H_\lambda \, d\lambda = \alpha_1 \int_0^\infty H_\lambda \, d\lambda = \alpha_1 H \, . \qquad (A.5)$$

Similarly for the reflecting surface (surface-2),

$$\int_0^\infty \alpha_{\lambda,2} H_\lambda \, d\lambda = \alpha_2 \int_0^\infty H_\lambda \, d\lambda = \alpha_2 H \, . \qquad (A.6)$$

With these additional assumptions, Equation A.4 reduces to

$$q_1 - q_2 = H(\alpha_1 - \alpha_2) \qquad (A.7)$$

Knowledge of the absorptance values, α_1 and α_2, along with the experimentally determined values of q_1 and q_2 will permit evaluation of the plasma irradiation. This value of H can then be employed in either of the following expressions to yield the value of the convective wall heat transfer:

$$q_1 = q_{conv} + \alpha_1 H \qquad (A.8)$$

or,

$$q_2 = q_{conv} + \alpha_2 H \, . \qquad (A.9)$$

To determine the radiative wall heat flux to the standard (copper) duct segments, this value of q_{conv} is subtracted from the total wall heat flux results (obtained at the same operating conditions and axial location) determined from previous calorimetric measurements.

As shown in Figure A.1, the radiation gage consists of two semicylindrical copper segments which are thermally isolated from one another, individually water cooled, and supplied with individual ΔT-transducers. An optical black (Nextel 101-C10 by Minnesota Mining and Manufacturing Company) coating is applied (and then baked) to the interior cylindrical surface of one of the half-segments, while the opposing half-segment is coated with a highly reflecting, thermally evaporated aluminum film.* The overall dimensions of the assembled radiation gage are precisely the same as those of a standard duct segment.

A.3 Discussion of the Parameters and Assumptions Affecting the Operation of the Radiation Gage

While the above radiation gage design appears to satisfy all of the initially posed constraints and specifications, the following two basic assumptions require further discussion:

---

* The fabrication and optical properties of the reflecting surface are discussed in Section A.4.

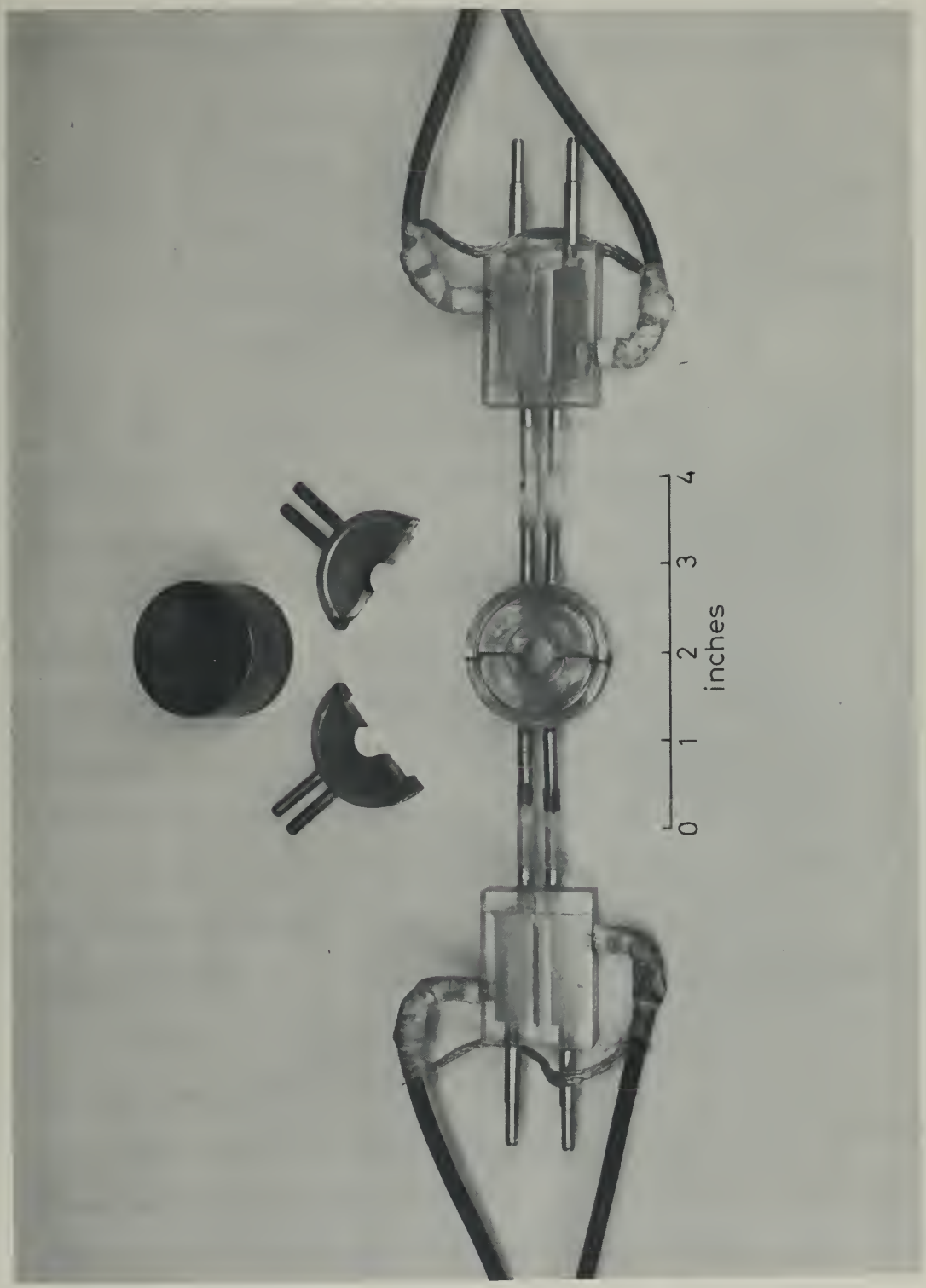

Figure A.1 Radiation Gage Assembly and Thin Film Sample Used For Reflectance Measurements

1. The presence of the radiation gage does not significantly alter the thermal state of the plasma in the vicinity of the gage and,
2. The reflecting surface is characterized by a constant value of absorptance, α_2, over the entire spectral range of the incident plasma irradiation (H_λ).

The validity of the first assumption is critical to the success of this diagnostic technique. That is, if the pressence of the highly absorbing and reflecting surfaces results in a significant change in the local thermal state of the plasma, then the assumptions of equal convection and irradiation required by Equation A.7 would be rendered questionable. Moreover, any such change in the local thermal plasma state would preclude combining the convective wall heat flux (determined from use of the radiation gage) with the total wall heat flux data (obtained from calorimetric measurements employing the standard, copper-wall duct segments) to determine the radiation flux.

Wall heat transfer measurements were made at the radiation gage segment and the eight adjoining standard segments (four upstream and four downstream) in an attempt

to experimentally determine if there existed any effect on the plasma radiosity distribution that could be attributed to the spectral characteristics of the gage surfaces. This experimental investigation in the asymptotic region of an argon arc was performed using both black-versus-reflector and reflector-versus-reflector surface combinations. The results showed no discernable difference between the total wall heat flux to the segments adjoining the radiation gage and the q_a values which were measured in the absence of this gage. Moreover, the total wall heat flux to both of the reflecting surfaces for the case of the reflector-versus-reflector combination compares favorably with the measured total wall heat flux to the reflecting surface of the black-versus-reflector combination.* During the course of these experiments, the duct wall potential distribution was monitored and, as in the case of q_a, there were no discernable variations in this parameter. Accordingly, it is concluded that, to within the experimental uncertainty of q_a ($\pm 6\%$) and $E_{x,a}$ ($\pm 3\%$) measurements, the presence of the radiation gage does not significantly alter the local thermal state of the plasma.

---

* These observations are discussed further in Section A.5.

With respect to the second of the two aforementioned assumptions, consideration must be given to the spectral distribution of the incident plasma irradiation, $H = H(\lambda)$, before a suitable reflecting material, for which $\alpha_2 \neq \alpha_2(\lambda)$ over the spectral range of H_λ, can be selected. The following discussion will be restricted to the case of an argon plasma since the radiative wall heat flux data obtained in this study pertain only to this gas.

On the basis of the theoretical work of Yakubov[66], the emission spectrum from an atmospheric argon plasma is known to cover a wavelength band extending from the vacuum ultraviolet to the infrared. Of particular interest to this discussion is the vacuum ultraviolet ($\lambda < 2000$ Å) portion of the emission spectrum which results from bound- and free-bound transitions to the ground state (resonance lines and ionization continuum, respectively). As indicated by Yakubov, and on the basis of the optical depth and radiative recombination rate calculations performed by Horn[67], the radiation emitted from these transitions is strongly reabsorbed, and, therefore, does not contribute significantly to the balance of energy at the boundary of the plasma. Accordingly, it is assumed that there are no significant contributions to the total plasma radiation incident on the tube wall at wavelengths

less than 2000 Å. This assumption is supported by the theoretical calculations of Maecker[15] and is consistent with the plasma radiation model employed in the non-equilibrium solution by Clark[25] as well as with the experimental radiation source density employed in the equilibrium solution by Bower and Incropera[20]. It remains, however, to select a reflecting surface for which the monochromatic absorptance is invariant for wavelengths greater than 2000 Å.

A.4 Selection, Fabrication, and Optical Characteristics of the Reflecting Surface

While the spectral sensitivity of a metallic surface is enhanced through polishing, the optical characteristics of polished metal surfaces are both difficult to reproduce and to maintain. A possible alternative is to adjust the optical characteristics of the surface by application of a thin metallic coating or thin film. Commonly used methods of thin film preparation include thermal evaporation, sputtering, and electroplating, or chemical deposition. The electroplating process produces films which are relatively porous, rough, and impure. This process is therefore generally ill-suited for applications requiring reproducible, optical quality surfaces. Similarly, film deposition by sputtering is a relatively slow process resulting in impure and low

density coatings which are unsuitable for use as ultraviolet reflectors. Techniques employing thermal evaporation in a vacuum, however, have proven to be most satisfactory for precise deposition of reproducible, optical quality, thin film coatings. The primary control variables for this process are the rate of deposition and the evaporator chamber pressure.

While many metal films (e.g., aluminum, silver, gold, and rhodium) are highly reflecting at wavelengths in the visible and infrared, only aluminum films maintain a high reflectance into the ultraviolet. Through proper preparation and aging, aluminum films will remain better than 90% reflecting at wavelengths greater than 2000 Å. For this reason, the aluminum thin film is particularly suited for the reflecting surface of the radiation gage.

To achieve and to maintain the highest possible reflectance for the aluminum film, precise control is required over the following variables.

1. Film purity.
2. Rate of deposition.
3. Evaporator chamber pressure.
4. Substrate temperature.
5. Film thickness.
6. Aging conditions.

The effect of each of these variables on the reflectance characteristics of evaporated aluminum films has been investigated by Madden[68]. The following discussion provides a summary of this work.

The purity of the aluminum has a slight effect on the optical characteristics of the film at ultraviolet wavelengths, with purer films resulting in a higher percent reflectance. There is little improvement, if any, in the percent reflectance for purities better than 99.95% and, for wavelengths greater than 2200 Å, 99.5% pure aluminum films are sufficient to insure maximum reflectance.

The condition of the oxide layer, which forms naturally on aluminum upon exposure to air, has a direct bearing on the optical properties of the aluminum coating. Generally, the oxide layer will grow (in air) to a thickness of from 30 to 40 Å and will have little effect on the reflectance for wavelengths greater than 2200 Å. At shorter wavelengths, however, the structure of the oxide layer is most critical, with a thinner, tighter layer resulting in higher reflectance characteristics for ultraviolet radiation. This favorable oxide layer structure is obtained by evaporating the aluminum film at high deposition rates (not less than 200 Å/sec) at the lowest possible pressure (preferably lower than 10^{-5} mm Hg).

The substrate temperature during evaporation will affect the crystal size (and thus the surface roughness and reflectance) of the film. The larger the value of the substrate temperature, the lower the value of the reflectance will be, particularly at the shorter wavelengths ($\lambda < 2200$ Å). However, if the substrate temperature is maintained below 150°C during evaporation, the reflectance of the aluminum film will not be affected at wavelengths greater than 2200 Å. A similar effect results from increasing the film thickness beyond that required for maximum reflectance which, for aluminum films, is a thickness between 700-900 Å for wavelengths greater than 1000 Å.

One of the more important factors influencing the performance of thin film aluminum reflectors is their age and the environmental conditions under which aging occurs. While there is a significant decrease in the percent reflectance with increasing film age at the shorter wavelengths, such is not the case for $\lambda > 2000$ Å. As reported by Madden, the reflectance of aluminum films (for $\lambda > 2200$ Å), stored for longer than two years under normal laboratory conditions, remained unchanged. Regardless of the age of the film, however, certain environmental

conditions can cause a change in its optical properties. In particular, the relative humidity and exposure of the film to ultraviolet radiation can produce significant changes in the reflectance characteristics; however, as reported by Hass, et al.[69], these changes are minimal for wavelengths longer than 2000 Å.

In reviewing the previous discussion it is readily apparent that the reflectance characteristics of aluminum films, for $\lambda > 2000$ Å, remain uneffected and, as shown by Hass, et al.[69], relatively constant over a wide range of environmental conditions. On this basis, and subject to the provision that the optical characteristics of the film do not measureably change upon its exposure to the plasma, the thin film aluminum coating was selected for the reflecting surface of the radiation gage.

Since the surface quality of a thin film is dictated by the quality of the substrate surface, special care was taken in the preparation of the cylindrical, copper surfaces prior to the deposition of the aluminum films. Specifically, these surfaces were ground, polished, and cleaned according to the following procedure.

Grinding:

i) 300 grit silicon carbide paper with water lubricant.

ii) 600 grit silicon carbide paper with water lubricant.

Polishing:

i) 6.0 micron diamond paste (Metadi No. 40-6172) with oil lubricant.

ii) 0.25 micron diamond paste (Metadi No. 40-6112) with oil lubricant.

iii) 0.05 micron aluminum oxide powder with water lubricant.

Cleaning:

i) ultrasonic cleaning with detergent agent (ALCONOX).

ii) Ultrasonic cleaning with isopropyl alcohol - blown dry with nitrogen gas.

Subsequent to this procedure, the aluminum films were deposited with the vacuum deposition system (CVE-15 by Consolidated Vacuum Corporation) shown in Figure A.2. In an attempt to gain a uniform deposit over the entire semicylindrical (0.5 cm radius) surface of the half-segment, a special jig was designed to simulate a line source of evaporation. As shown in Figure A.3, this device positions the half-segment such that the filament (or evaporation source) extends along the axis of the segment wall surface. The filament is placed in spring-tension so as to maintain its proper positon upon heating.

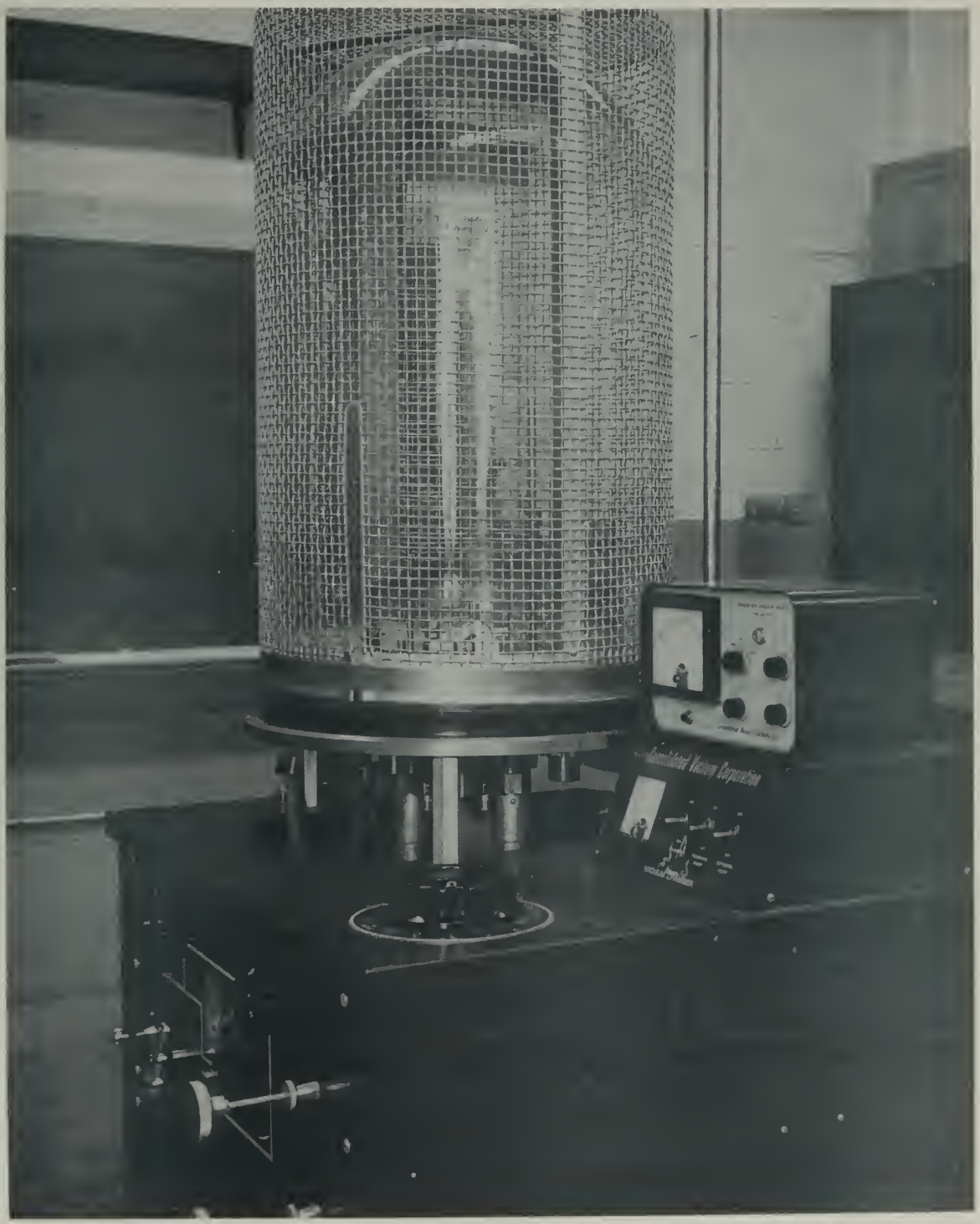

Figure A.2 Vacuum Deposition System

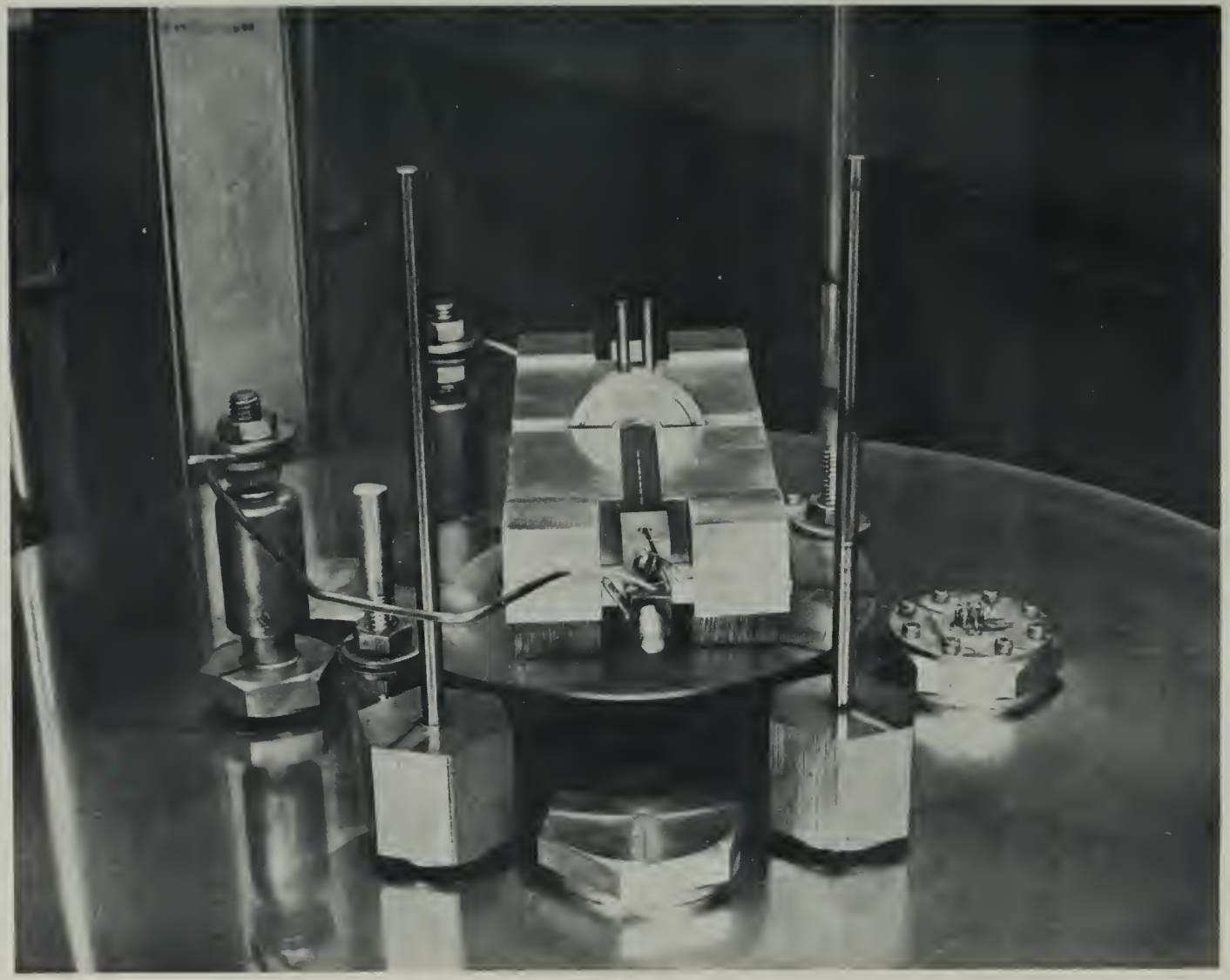

Figure A.3 Line-Source Filament Assembly

Due to the close proximity of the substrate and the filament, there was some difficulty in controlling the thicknesses of the aluminum films. Therefore in order to insure that the desired 700-900 Å film thicknesses were achieved, a glass micro-slide, located at the same position from the filament as the copper substrate surface, was deposited with an aluminum film at the same time that each of the half-segments were film deposited. These glass slides were then used in a Twyman-Green interferometer to determine if the desired film thicknesses were obtained. All of the aluminum films were deposited at a rate of approximately 250 Å/sec at a pressure of $2\text{-}5 \times 10^{-6}$ mm Hg.

While the complete spectral distribution (for $\lambda > 2000$ Å) for the monochromatic reflectance (ρ_λ) of the aluminum film was not measured in this study, ρ_λ was measured at several wavelengths for comparison with the monochromatic reflectance data reported by Drummeter and Hass[70]. An aluminum thin film was deposited on a water-cooled, copper disc (shown in Figure A.1) and this disc was employed for the reflectance measurements of this study. These measurements, which were conducted before and after exposure of the disc to a free argon plasma jet, were made over the combined wavelength range (4880 to 6328 Å) of the argon and helium-neon laser sources employed for these

experiments. The results of these experiments indicate that there is no measureable change in the reflectance of the aluminum film after its exposure to the plasma environment. At each of the wavelengths investigated, the measured reflectance of the aluminum film was 0.98 - a value which is some 6-7% higher than the corresponding values measured by Drummeter and Hass. While the reflectance measurements reported by Drummeter and Hass were averaged (over the wavelength interval, 2200 $\mathring{A} \leq \lambda \leq 70{,}000\ \mathring{A}$) and used to determine the average absorptance of the reflecting surface ($\alpha_2 = 1 - \rho_{ave} = 0.07$), it is noted that use of the reflectance measurements of this study would result in values for the radiative wall heat flux which are within the experimental uncertainties shown in Figure IV.3.

A.5 Presentation and Interpretation of Radiative Wall Heat Flux Measurements

As discussed in Chapter II, it was initially felt that the presence of wall contamination in the arc heating region would preclude any meaningful radiation measurements in this section of the duct. For this reason, the radiation gage was first used in the field-free region (downstream from the anode), since, in this section, wall deposits had not been observed. With reference to Equations A.7 and A.9 and using values of $\alpha_1 = 0.98$ and $\alpha_2 = 0.07$, it was determined from the calorimetric

measurements performed in these experiments that, of the total wall heat flux for the reflecting half-segment (q_2), 2% is contributed by the radiative component.

While attempts to eliminate the wall contamination in the arc heating region had failed, radiation experiments were nonetheless performed in this region in the hope that some meaningful information could be acquired. Upon disassembly of the duct after some four hours of high current ($I > 100$ amp) operation, it was observed that, while the black surface of the radiation gage and the copper surfaces of the adjoining segments were contaminated, the reflecting surface of the radiation gage was completely free of contaminants. Since the deposition of contaminants on the black surface precluded specification of its optical properties, the radiation gage could no longer be used in conjunction with Equation A.7 to provide measurement of the radiative wall heat flux in the arc heating region. In contrast, the absence of contamination on the reflecting surface continues to permit specification of its optical properties, specifically α_2. It was therefore assumed that the radiation gage measurements performed in the field-free region could be used to delineate the radiative and convective wall heat flux components in the arc heating region. That is, of the calorimetrically measured total wall heat flux for the reflecting half-segment, 2% is due to radiation.

On this basis, a series of experiments were conducted with the radiation gage to determine the radiative and convective wall heat flux for the asymptotic region in argon. As indicated in the previous section, these experiments were further used to validate the assumption that the presence of the radiation gage does not significantly alter the local thermal state of the plasma. The results of this experimental investigation are presented in Table A.1.

Prior to an interpretation of the data presented in Table A.1, it is noted that meaningful radiation measurements for arc currents less than 100 amp could not be obtained. This restriction is due to the fact that, at the lower arc currents in argon, the radiative contribution to the total wall heat flux is too small to permit its resolution within the estimated uncertainty of these measurements (± 10%).

The asympotic convective wall heat flux values shown in Table A.1 were obtained by taking 98% of the calorimetrically measured values for the total wall heat flux to the reflecting surface. The first three of the five separate experimental runs that were performed represent an attempt to determine if there exist both anamolies in the ΔT - transducer outputs and asymmetric conditions within the arc. While the data for the first

TABLE A.1 Compilation of Asymptotic Radiative Wall Heat Flux Measurements
(Argon: p = 1.0 atm, R = 0.5 cm)

Run No.	Radiation Gage Surface Combinations (And Ex-* perimental Conditions)	$q_{conv,a}$ Btu/ft^2-min) = 0.98 $q_{2,a}$			
		I(amp)			
		100	150	200	240
1	Black-versus-reflector	7,117	12,013	16,970	-----
2	Black-versus-reflector (Δt transducers interchanged from Run No. 1)	6,558	10,049	16,517	-----
3	Black-versus-reflector (radiation gage rotated 180° from Run No. 2)	7,893	12,142	16,813	23,157
4	Reflector-versus-reflector (research grade gas)	7,558	11,961	18,155	-----
5	Reflector-versus-reflector (commercial grade gas)	7,138	11,733	17,415	22,060
	Average Value of $q_{conv,a}$	7,253	11,580	17,174	22,608
	q_a for copper wall (from Table IV.1)	8,270	14,300	22,800	30,900
	$q_{rad,a}$ $(= q_a - q_{conv,a})$	1,017	2,720	5,626	8,292
	$q_{rad,a}/q_a$	0.123	0.190	0.247	0.268

*Research grade gas was used for Runs no. 1-3.

three runs suggest that these conditions are present, the evidence is not conclusive since, with the exception of the 150 amp value for Run No. 2, all of the $q_{conv,a}$ values agree to within the experimental uncertainty for wall heat transfer measurements (± 6%).

The remaining two experiments (Runs No. 4 and 5) employed a reflector-versus-reflector surface combination for the radiation gage, in which case the $q_{conv,a}$ results were obtained by taking 98% of the combined measured total wall heat flux values for both half-segments. A comparison between the data obtained in these two experiments indicates that the purity of the gas has an effect on the measured results; however, as was the case in the first three runs, the data agree to within the experimental uncertainties.

In comparing the combined results for all five experimental runs, it is noted that, again with the exception of the 150 amp value for Run No. 2, the data agree to within ± 6%. In particular, it is observed that such agreement exists between the data acquired with the black-versus-reflector surface combination and that acquired with the reflector-versus-reflector surface combination. This fact suggests that the presence of the radiation gage does not significantly alter the local thermal state of the plasma. Accordingly, the convective

wall heat flux data obtained with the radiation gage can be compared with the q_a measurements obtained with the standard copper segments in the absence of the radiation gage. For this purpose, the $q_{conv,a}$ values for each arc current condition were algebraically averaged and the resulting values were subtracted from the corresponding q_a values (Table IV.1) to give the radiative wall heat flux results shown in Table A.1. The values for the fraction of radiative to total wall heat flux shown in Table A.1 were used for the comparisons in Chapters III and IV.

wall heat flux data obtained with the radiation gage can be compared with the q_a measurements obtained with the standard copper segments in the absence of the radiation gage. For this purpose, the $q_{conv,a}$ values for each arc current condition were algebraically averaged and the resulting values were subtracted from the corresponding q_a values (Table IV.1) to give the radiative wall heat flux results shown in Table A.1. The values for the fraction of radiative to total wall heat flux shown in Table A.1 were used for the comparisons in Chapters III and IV.

VITA

VITA

Larry Allan Lukens was born on April 16, 1939 in Indianapolis, Indiana where he resided with his parents, Mr. and Mrs. A.H. Lukens, until he was graduated from Arsenal Technical High School in June, 1957.

After attending Purdue University for three years, he entered the United States Navy in September, 1961. In August of 1964, Mr. Lukens was selected to participate in the Naval Enlisted Scientific Education Program (NESEP), whereupon he re-entered Purdue in the School of Mechanical Engineering to pursue completion of his B.S. degree requirements. In the summer of 1967, he was granted permission by the Navy to remain at Purdue to obtain his M.S. and Ph.D. degrees in the School of Mechanical Engineering. He was commissioned an Ensign in the United States Navy in August 1969.

On September 4, 1960, Mr. Lukens was married to Miss Barbara Ann Baker of Indianapolis, Indiana. They have two children; a 3-1/2 year old son, William Earl, and a 7-month old daughter, Rebecca Rayanne.

Thesis 126050
L894 Lukens
An experimental investigation of electric field intensity and wall heat transfer for the heating region of a constricted arc plasma.